

UC Santa Cruz

UC Santa Cruz Previously Published Works

Title

Searches for heavy long-lived sleptons and R-hadrons with the ATLAS detector in pp collisions at $\sqrt{s}=7$ TeV

Permalink

<https://escholarship.org/uc/item/915422kn>

Journal

Physics Letters B, 720(4-5)

ISSN

0370-2693

Authors

Collaboration, ATLAS
Aad, G
Abajyan, T
[et al.](#)

Publication Date

2013-03-01

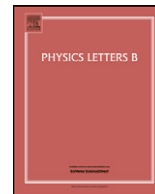
DOI

10.1016/j.physletb.2013.02.015

Copyright Information

This work is made available under the terms of a Creative Commons Attribution License, available at <https://creativecommons.org/licenses/by/4.0/>

Peer reviewed



Searches for heavy long-lived sleptons and R -hadrons with the ATLAS detector in pp collisions at $\sqrt{s} = 7$ TeV

ATLAS Collaboration ^{*}

ARTICLE INFO

Article history:

Received 7 November 2012
 Received in revised form 4 February 2013
 Accepted 5 February 2013
 Available online 13 February 2013
 Editor: H. Weerts

Keywords:

Long-lived
 GMSB
 Slepton
 R -hadron
 ATLAS
 LHC

ABSTRACT

A search for long-lived particles is performed using a data sample of 4.7 fb^{-1} from proton–proton collisions at a centre-of-mass energy $\sqrt{s} = 7$ TeV collected by the ATLAS detector at the LHC. No excess is observed above the estimated background and lower limits, at 95% confidence level, are set on the mass of the long-lived particles in different scenarios, based on their possible interactions in the inner detector, the calorimeters and the muon spectrometer. Long-lived staus in gauge-mediated SUSY-breaking models are excluded up to a mass of 300 GeV for $\tan\beta = 5$ –20. Directly produced long-lived sleptons are excluded up to a mass of 278 GeV. R -hadrons, composites of gluino (stop, sbottom) and light quarks, are excluded up to a mass of 985 GeV (683 GeV, 612 GeV) when using a generic interaction model. Additionally two sets of limits on R -hadrons are obtained that are less sensitive to the interaction model for R -hadrons. One set of limits is obtained using only the inner detector and calorimeter observables, and a second set of limits is obtained based on the inner detector alone.

© 2013 CERN. Published by Elsevier B.V. Open access under [CC BY-NC-ND license](#).

1. Introduction

Heavy long-lived particles (LLP) are predicted in a range of theories which extend the Standard Model (SM). Supersymmetry (SUSY) [1–9] models allow long-lived charged sleptons ($\tilde{\ell}$), squarks (\tilde{q}) and gluinos (\tilde{g}). Heavy LLPs produced at the Large Hadron Collider (LHC) could travel with speed measurably lower than the speed of light. These particles can be identified and their mass, m , determined from their speed, β , and momentum, p , using the relation $m = p/\gamma\beta$, with γ being the relativistic Lorentz factor. Four different searches are presented in this Letter, using time-of-flight to measure β and specific ionisation energy loss, dE/dx , to measure $\beta\gamma$. The searches are optimised for the different experimental signatures of sleptons and composite colourless states of a squark or gluino together with SM quarks and gluons, called R -hadrons.

Long-lived charged sleptons would interact like muons, releasing energy by ionisation as they pass through the ATLAS detector. A search for long-lived sleptons identified in both the inner detector (ID) and in the muon spectrometer (MS) is therefore performed (“slepton search”). The results are interpreted in the framework of gauge-mediated SUSY breaking (GMSB) [10–16] with the light stau ($\tilde{\tau}$) as the LLP. In these models a substantial fraction of the events would contain two LLP candidates, and this feature is also utilised

in discriminating signal from background. Direct pair production of sleptons is also used to interpret the data independently of the mass spectrum of the other SUSY particles.

Coloured LLPs (\tilde{q} and \tilde{g}) would hadronise forming R -hadrons, bound states composed of the LLP and light SM quarks or gluons. They may emerge as charged or neutral states from the pp collision and be converted to a state with a different charge by interactions with the detector material, and thus arrive as neutral, charged or doubly charged particles in the muon spectrometer.

In ATLAS, LLPs can be identified via the timing information in the muon spectrometer or calorimeters and via the measurement of the energy loss in the silicon pixel detector. All of these techniques are combined in this analysis to achieve optimal sensitivity for the “full-detector R -hadron search”. In addition, searches based on only the calorimeter and the inner detector information (“MS-agnostic R -hadron search”), and based solely on the inner detector (“ID-only R -hadron search”) are performed. The latter two cases are motivated by the limited understanding of R -hadron interactions in matter, in particular the possibility that R -hadrons are electrically neutral in the MS. Furthermore, these searches are sensitive to scenarios in which the R -hadrons decay before reaching the MS. In all searches the signal particles are assumed to be stable within the ATLAS detector, at least to the point it hits the last relevant component of the subdetector used for detecting it.

Previous collider searches for LLPs have been performed at LEP [17–20], HERA [21], the Tevatron [22–28], and the LHC [29–35].

^{*} E-mail address: atlas.publications@cern.ch.

2. Data and simulated samples

The work presented in this Letter is based on 4.7 fb^{-1} of pp collision data collected at a centre-of-mass energy $\sqrt{s} = 7 \text{ TeV}$ in 2011. The events are selected online by muon triggers for the slepton search and by missing transverse momentum and muon triggers for the R -hadron searches. Data and Monte Carlo $Z \rightarrow \mu\mu$ samples are used for timing resolution studies. Monte Carlo signal samples are used to study the expected signal behaviour and to set limits.

The GMSB samples are generated with the following model parameters: number of super-multiplets in the messenger sector, $N_5 = 3$, messenger mass scale, $m_{\text{messenger}} = 250 \text{ TeV}$, sign of the Higgsino mass parameter, $\text{sign}(\mu) = 1$, and C_{grav} , the scale factor for the gravitino mass which determines the $\tilde{\tau}$ lifetime was set to 5000 to ensure that the $\tilde{\tau}$ does not decay in the detector. The ratio of the vacuum expectation values of the two Higgs doublets, $\tan\beta$, is varied between 5 and 40 and the SUSY-breaking mass scale Λ is varied from 50 to 150 TeV, corresponding to light $\tilde{\tau}$ masses varying from 122.2 to 465 GeV. The mass spectra of the GMSB models are obtained from the SPICE program [36] and the events are generated using HERWIG [37].

The R -hadron samples are generated with gluino (squark) masses from 300–1500 GeV (200–1000 GeV). The pair production of gluinos and squarks is simulated in PYTHIA [38], incorporating specialised hadronisation routines [39–41] to produce final states containing R -hadrons. A 10% gluino-ball fraction is assumed in the gluino sample production. The simulation of R -hadron interactions with matter is handled by dedicated GEANT4 [42,43] routines based on a generic model [44]. All Monte Carlo events pass the full ATLAS detector simulation [42,45] and are reconstructed with the same programs as the data. All signal Monte Carlo samples are normalised to the integrated luminosity of the data.

3. The ATLAS detector

The ATLAS detector [46] is a multipurpose particle physics detector with a forward–backward symmetric cylindrical geometry and near 4π coverage in solid angle.¹ The ID consists of a silicon pixel detector, a silicon micro-strip detector, and a transition radiation tracker. The ID is surrounded by a thin superconducting solenoid providing a 2 T magnetic field, and by high-granularity liquid-argon sampling electromagnetic calorimeters (LAr). An iron/scintillator-tile calorimeter provides coverage for hadrons in the central rapidity range. The end-cap and forward regions are instrumented with liquid-argon calorimeters for both electromagnetic and hadronic measurements. The MS surrounds the calorimeters and consists of three large superconducting air-core toroids each with eight coils, a system of precision tracking chambers, and detectors for triggering.

The ATLAS trigger system is designed to select the events of most interest with a data-taking rate of about 400 Hz from a beam bunch crossing rate as high as 40 MHz. The first-level trigger (level-1) selection is carried out by custom hardware and identifies detector regions and the bunch crossing for which a trigger element is found. The high-level trigger is performed by dedicated software, seeded by data acquired from the bunch crossing and re-

gions found at level-1. The components of particular importance to this analysis are described in more detail below.

3.1. The pixel detector

As the innermost detector system in ATLAS, the silicon pixel detector provides at least three precision measurements for each track in the region $|\eta| < 2.5$ at radial distances from the LHC beam line $r < 15 \text{ cm}$. The sensors in the pixel barrel (covering the central $|\eta|$ -region) are placed on three concentric cylinders around the beam-line, whereas sensors in the end-cap (covering the high- $|\eta|$ region) are located on three disks perpendicular to the beam axis on each side of the barrel. In the barrel (end-cap) the intrinsic accuracy is $10 \mu\text{m}$ in the $r\phi$ -plane and $115 \mu\text{m}$ in the $z(r)$ -direction. The data are only read out if the signal is larger than a set threshold. The time for which the signal exceeds that threshold, ToT, is recorded. The larger the initial signal is the longer this time.

3.1.1. Pixel detector specific ionisation (dE/dx) measurement

The relation between the ToT and the charge deposition in each pixel is measured in dedicated calibration scans and shows a good linearity. Therefore, the ToT measurement is well correlated with the energy loss of a charged particle in the pixel detector. The maximum ToT value corresponds to 8.5 times the average charge released by a minimum ionising particle (MIP) for a track perpendicular to the silicon detectors and leaving all its ionisation charge on a single pixel. If this value is exceeded, the ToT (and therefore the charge) is not correctly measured. In LHC collisions the charge generated by one track crossing the pixel detector is rarely contained in just one pixel. Neighbouring pixels are joined together to form clusters and the charge of a cluster is calculated by summing up the charges of all pixels after calibration correction. The specific energy loss dE/dx is defined as the average of all individual cluster charge measurements for the clusters associated with the track. To reduce the Landau tails, the average is evaluated after having removed the cluster with the highest charge (the two clusters with the highest charge are removed for tracks having five or more clusters).

3.1.2. Mass measurement with the pixel detector

The masses of slow charged particles can be measured using solely the ID information by fitting each dE/dx and momentum measurement to an empirical Bethe–Bloch function and deducing their $\beta\gamma$ value. The measurable $\beta\gamma$ range lies between 0.2 and 1.5, the lower bound being defined by the overflow in the ToT spectrum, and the upper bound by the overlapping distributions in the relativistic rise branch of the curve. This particle identification method [47] uses a five-parameter function to describe how the most probable value of the specific energy loss ($\mathcal{M}_{\frac{dE}{dx}}$) depends on $\beta\gamma$:

$$\mathcal{M}_{\frac{dE}{dx}}(\beta\gamma) = \frac{p_1}{\beta p_3} \ln(1 + (p_2\beta\gamma)^{p_5}) - p_4. \quad (1)$$

Fig. 1(left) shows how this function describes data for low momentum tracks. Fig. 1(right) shows the simulated pixel dE/dx spectra for singly-charged hypothetical R -hadrons of masses 100, 300, 500 and 700 GeV. As expected, these distributions extend into the high pixel dE/dx region even for high momentum tracks. The most probable value of dE/dx for MIPs is about $1.2 \text{ MeV g}^{-1} \text{ cm}^2$ with a spread of about $0.2 \text{ MeV g}^{-1} \text{ cm}^2$ and a slight η dependence, increasing by about 10% from low- η to high- η regions.

For all tracks having a reconstructed momentum p and a measured specific energy loss dE/dx above the value for MIPs, a mass estimate $m_{\beta\gamma} = p/\beta\gamma$ is obtained by inverting Eq. (1). The procedure is continuously monitored through precise ($< 1\%$)

¹ ATLAS uses a right-handed coordinate system with its origin at the nominal interaction point in the centre of the detector and the z -axis coinciding with the axis of the beam pipe. The x -axis points from the interaction point to the centre of the LHC ring, and the y -axis points upward. Cylindrical coordinates (r, ϕ) are used in the transverse plane, ϕ being the azimuthal angle around the beam pipe. The pseudorapidity is defined in terms of the polar angle θ as $\eta = -\ln(\tan(\theta/2))$.

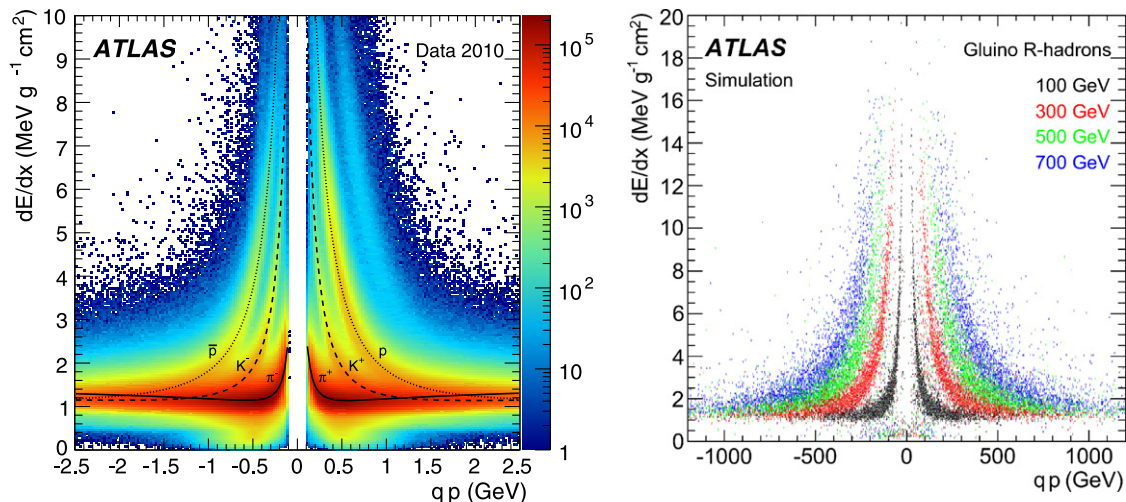


Fig. 1. Left: Distribution of dE/dx versus charge times momentum for minimum bias collisions in a data sample from 2010. With tracks reconstructed for $p_T > 100$ MeV this sample is more suitable for the calibration of the Bethe–Bloch function than 2011 data in which tracks had a cutoff of $p_T = 400$ MeV. The distribution of the most probable value for pions (solid), kaons (dashed) and protons (dotted) are superimposed. The band due to deuterons is clearly visible. Right: Simulated distribution of specific energy loss versus momentum for singly-charged hypothetical R -hadrons of various masses.

measurements of the mass of known particles (kaons and protons). For LLPs the expected dE/dx values are much larger than those of SM particles, allowing for identifying them based on this information.

3.2. Calorimeters

Liquid argon is used as the active detector medium in the electromagnetic (EM) barrel and end-cap calorimeters, as well as in the hadronic end-cap (HEC) calorimeter. All are sampling calorimeters, using lead plates for the EM calorimeters and copper plates for the HEC calorimeter. The barrel EM calorimeter covers the region $|\eta| < 1.475$ and consists of three layers and a pre-sampler. The EM end-cap calorimeter consists of three layers in the region $1.375 < |\eta| < 2.5$ (two for $2.5 < |\eta| < 3.2$) and a pre-sampler for $1.5 < |\eta| < 1.8$. The four layers of the HEC calorimeter cover the range $1.5 < |\eta| < 3.2$.

The ATLAS tile calorimeter is a cylindrical hadronic sampling calorimeter. It uses steel as the absorber material and plastic scintillators as the active layers. It covers radii from 2280 to 4230 mm and the η coverage extends to $|\eta| \lesssim 1.7$. The calorimeter is subdivided into a central barrel covering $|\eta| \lesssim 1.0$ and an extended barrel covering $0.8 \lesssim |\eta| \lesssim 1.7$. Both barrel parts are divided into 64 modules and the cells in each module are divided into three layers.

3.2.1. Calorimeter β measurement

The ATLAS tile and LAr calorimeters have sufficiently good timing resolutions to distinguish highly relativistic SM particles from the slower moving LLPs. The time resolution depends on the energy deposited in the cell and also the layer type and thickness, but typical resolutions are 2 ns for an energy deposit of 1 GeV and generally better for the tile calorimeter.

To ensure the highest possible timing accuracy, it is necessary to calibrate the data using particles with known speed. This calibration applies a common shift for each run, and is then performed as a function of calorimeter layer and cell energy. The reliability of such a calibration for this analysis depends on the assumption that the particles used for calibration have similar characteristics to the LLPs in question when depositing energy in the calorimeters. The analysis uses muons for this purpose and it is cross-checked that jets give a consistent result. The effect of a possible bias in the

measured time for late-arriving signals was tested by applying an arrival-time-dependent resolution function and found negligible. The β measurements from all cells assigned to the extrapolated track are combined in a cell-energy-weighted average, typically using timing measurements from three or four calorimeter cells. The resolution of the resulting β measurement can be seen in Fig. 2(left). For data (MC) the mean β -value is 0.983 (0.986) and the resolution is 0.090 (0.092).

3.3. The muon detectors

The MS forms the outer part of the ATLAS detector and detects charged particles exiting the calorimeters and measures their momenta in the pseudorapidity range $|\eta| < 2.7$. It is also designed to trigger on these particles in the region $|\eta| < 2.4$. In the barrel the chambers are arranged in three concentric cylindrical shells around the beam axis, while in the two end-caps the muon chambers are arranged in three wheels that are perpendicular to the beam axis.

The precision momentum measurement is performed by monitored drift tube (MDT) chambers, using the η coordinate. These chambers consist of three to eight layers of drift tubes. In the forward region ($2.0 < |\eta| < 2.7$), cathode strip chambers are used in the innermost tracking layer. Resistive plate chambers (RPC) in the barrel region ($|\eta| < 1.05$) and thin gap chambers in the end-cap ($1.05 < |\eta| < 2.4$) provide a fast level-1 trigger and measure both the η and ϕ coordinates of the track.

3.3.1. β measurement in the MS

The default reconstruction of particles in the MDT chambers [48] relies on the assumption that they travel with the speed of light ($\beta = 1$). To improve the track quality for slow LLPs, the individual track segments can be reconstructed with different values for β . The actual β of the particle is estimated from the set of segments with the lowest χ^2 . In a successive combined track re-fit, including ID and MS hits, the particle trajectory is estimated more accurately. The time-of-flight to each tube is then obtained using the difference between the time-of-flight corresponding to the re-fitted track position in each tube and the time actually measured. By averaging the β values estimated from the time-of-flight in the different tubes an improved MDT β estimation can be achieved.

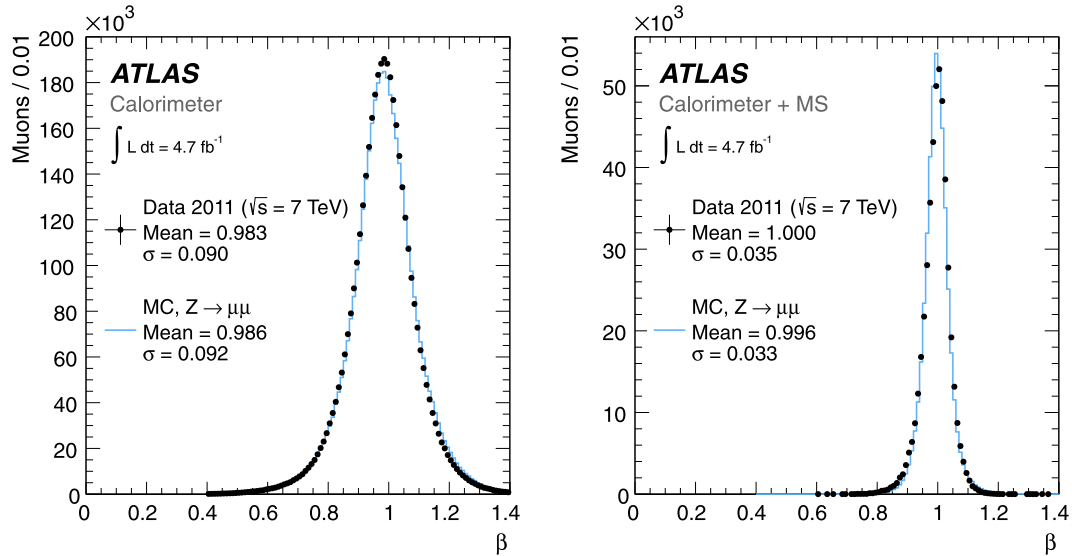


Fig. 2. Distribution of β for the calorimeter (left) and combined calorimeter + MS measurements (right) obtained for selected $Z \rightarrow \mu\mu$ decays in data and MC simulation. The typical resolutions are quoted in the figures.

The RPCs have an intrinsic time resolution of ~ 1 ns while the digitised signal is sampled with a 3.12 ns granularity, allowing a measurement of the time-of-flight. In the RPCs, β is first calculated separately for each hit from the independent position and time measurements. A single β estimate is obtained by averaging the β values from all the hits.

By definition, in a perfectly calibrated detector, any energetic muon coming from a collision at the interaction point will pass the detector at $t_0 = 0$. The t_0 distributions in the different detector systems are measured and their means used to correct the calibration. The observed width of these distributions after correction is used as the error on the time measurement in the β fit and to smear times in the simulated samples. The time resolution in the MS (about 3 ns) does not depend on the arrival time.

3.4. Combining β measurements

There are three possible β measurements per track, from the RPCs, the MDTs and the calorimeters. The β measurements from the different detectors are only used if $\beta > 0.2$ (the limit of the sensitivity) and if they are consistent internally, i.e. the χ^2 probability of the average between hits is reasonable (calorimeter) or the RMS of the measurement is consistent with the expected errors (MS). Measurements that are accepted are combined in a weighted average. The weights are obtained from the calculated error of each measurement multiplied by the pulls of the β distributions for muons from Z boson decays.

Since β is estimated from the measured time-of-flight, for a given resolution on the time measurement, a slower particle has a better β resolution. Prior to the β estimation, the timing values of the hits in the MC samples are smeared to reproduce the resolution measured in the data. Fig. 2(right) shows the β distribution for selected $Z \rightarrow \mu\mu$ candidate events in data compared to simulation after having smeared the hit times in simulation as described above. The data are well reproduced by the smeared MC distribution: the mean values are 1.000 and 0.996 and the resolution values are 0.035 and 0.033 for data and MC, respectively. The smearing mechanism reproduces the measured muon β distribution. The same time-smearing mechanism is applied to the signal Monte Carlo samples.

4. LLP candidate and event selection

4.1. Trigger selection

This analysis is based on events collected by two main trigger types: single-muon and missing transverse momentum triggers.

4.1.1. Single-muon trigger

The muon trigger and its performance in 2011 data are described in detail in Refs. [49,50]. This analysis uses un-prescaled muon triggers with a p_T threshold of 18 GeV. Offline muons are selected with $p_T > 50$ GeV, well above the trigger threshold.

Level-1 muon triggers are accepted and passed to the high-level trigger only if assigned to the collision bunch crossing. Late triggers due to late arrival of the particles are thus lost. The trigger efficiency for particles arriving late at the muon spectrometer is difficult to assess from data, where the majority of candidates are in-time muons. This efficiency is obtained from simulated R -hadron and GMSB events passing the level-1 trigger simulation. The muon triggers are found to be efficient for GMSB signatures, which contain two typically high- β LLPs that reach the MS, and additional muons stemming from neutralino decays. The trigger efficiency increases roughly linearly from zero at $\beta = 0.62$ to its full potential of about 90% at $\beta = 0.82$ for sleptons and R -hadrons that reach the MS. The estimated trigger efficiency for GMSB slepton events is between 70% and 85%. Muon triggers are less efficient for R -hadron events, where one or both of the R -hadrons may be uncharged as they enter the MS and β is typically low.

4.1.2. Missing transverse momentum trigger

Since gluinos and squarks are produced via the strong interaction, R -hadron events often contain high- p_T jets from QCD radiation. The modest energy depositions of the R -hadrons themselves combined with these jets naturally give rise to missing transverse momentum (magnitude denoted as E_T^{miss}).

The R -hadron analyses use missing transverse momentum triggers utilising only calorimeter information [51,50] with thresholds between 60 and 70 GeV (a full description of the ATLAS trigger system is given in [46]). For the full-detector search the single-muon trigger described in the previous section is used in addition to the E_T^{miss} trigger. Unlike the muon trigger, there is no loss

of efficiency for the E_T^{miss} triggers when R -hadrons arrive late. The efficiency of the E_T^{miss} triggers decreases with increasing R -hadron mass as the relative contribution of gg -initiated processes decreases, though it remains between 15% and 20% for heavy R -hadrons.

4.2. Offline selection

Two different signal types are studied: sleptons and R -hadrons. Given their different expected interactions with the ATLAS detector, two dedicated LLP candidate and event selections are used as described in the following sections.

4.2.1. Common event selection

Collision events are selected by requiring a good primary vertex, with at least three ID tracks, and with requirements on the position of the reconstructed primary vertex. The primary vertex is defined as the reconstructed vertex with the highest $\sum p_T^2$ of associated tracks. Events recorded during a time where a problem was present in one of the relevant subdetectors are rejected. Cosmic-ray background is rejected by removing tracks that do not pass close to the primary vertex in z . Candidates with an ID track with $|z_0^{\text{trk}} - z_0^{\text{vtx}}| > 10$ mm or $|d_0^{\text{trk}}| > 2$ mm are removed, where z_0^{trk} is the coordinate along the beam direction and d_0^{trk} is the transverse impact parameter at the distance of closest approach of the track to the primary vertex. Both requirements are tightened to 1.5 mm for the ID-only analysis. For the analyses involving the muon spectrometer, events with cosmic rays are also rejected by a topological cut on any two candidates with opposite η and ϕ ($|\eta_1 + \eta_2| < 0.005$ and $|\phi_1 - \phi_2 - \pi| < 0.005$).

4.2.2. Slepton candidate selection

The analysis searching for sleptons requires two muon candidates in each event, because two sleptons are produced, and both have a high probability of being observed in the MS. Two sets of selection criteria are applied. A loose selection with high efficiency is used to select candidates in events where there are two LLP candidates. In events where only one candidate passes the loose selection, that candidate is required to pass a tight selection.

Candidates in the loose slepton selection are required to have $p_T > 50$ GeV. The p_T measurements in the ID and MS are required to be consistent, so that the difference between the ID p_T and the combined fit p_T does not exceed a half of their average. Each candidate is required to have $|\eta| < 2.5$. Any two candidates that combine to give an invariant mass close to the Z boson mass (± 10 GeV) are both rejected. Candidates are also required to have associated hits in at least two of the three super-layers of precision measurement chambers in the MS.

The number of calorimeter cells plus MS hits contributing to the β measurement must exceed the number of detector (sub)systems used by three. For signal LLPs, the β values are expected to be consistent between the individual measurements, whereas for muons a low β -value is typically due to a poor measurement in one detector component and thus not consistent between different components. Therefore the estimated β is required to be consistent for measurements in the same detector system, based on the hit time resolutions, and the β measurements from the different detector systems are required to be consistent with each other. The different detector system measurements of β are required to be pair-wise consistent at the 3σ level, and the combined β to be consistent with the $\beta\gamma$ estimated in the pixel detector within 3σ . Finally, in order to reduce the muon background, the combined β measurement is required to be less than 0.95.

To pass the tight selection, a candidate is required in addition to have $p_T > 70$ GeV, at least two separate detector systems measuring β , the number of hits minus the number of detector systems participating in the measurement be at least twelve, and the consistency between β estimates in different detector systems be within 2σ . These cuts are optimised to give better background rejection.

Finally, a mass cut is applied on the candidate mass, $m_\beta = p/\gamma\beta$, calculated from the candidate's measured momentum and β . This cut depends on the hypothetical $\tilde{\tau}$ mass and is different for different points in the GMSB model parameters space, determined by the expected significance of the signal. For the two-candidate sample, both masses are required to be above the cut.

The number of background and expected signal events above the mass cut in the two-candidate and one-candidate signal regions is used to search for the presence of sleptons and R -hadrons.

Typical efficiencies for signal events to pass all cuts including the mass cut are 20% for each of the one and two candidate event categories, giving 40% efficiency in total.

4.2.3. R -hadron candidate selection

Since the R -hadron contains light quarks and gluons in addition to the squark or gluino, the charge of the R -hadron can change following nuclear interactions with the detector material. This possibility makes it difficult to rely on a single detection mechanism without some loss of detection efficiency, as a neutral state would go undetected until the next nuclear interaction occurs. Some of the main hadronic states regarded in the models considered are neutral, and it is thus natural to take an inside-out approach, starting from the ID track and adding discriminators from outer detector systems if a signal is seen along the extrapolated track. This is reflected in the three different R -hadron searches; “full-detector”, “MS-agnostic” (not considering the MS) and “ID-only” (relying solely on the ID); making successively fewer assumptions about the R -hadron scattering model and lifetime. While the first two differ only in their estimate of β (the “MS-agnostic” uses only the calorimeters) and the utilised triggers, the ID-only selection is generally more restrictive in order to reject the larger backgrounds.

In the full-detector and MS-agnostic analyses, R -hadron candidates are required to have a good quality ID track with $p > 140$ GeV and $|\eta| < 2.5$. The track must not be within an η - ϕ distance $\Delta R = \sqrt{(\Delta\eta)^2 + (\Delta\phi)^2} = 0.3$ of any jet with $p_T > 40$ GeV, reconstructed using the anti- k_t jet algorithm [52] with distance parameter set to 0.4. Furthermore, the track must not have any nearby ($\Delta R < 0.25$) tracks with $p_T > 10$ GeV nor pixel hits shared with another track. Tracks with momenta greater than 3.5 TeV are rejected as unphysical. The candidate must have a good dE/dx measurement and a good estimate of β . The uncertainty on β is required to be less than 10% when measured with the calorimeter only, and less than 4% when the result of a combination.

In the ID-only analysis, selection requirements are further tightened. Vertices must have more than four associated tracks and the E_T^{miss} trigger must be confirmed off-line ($E_T^{\text{miss}} > 85$ GeV, including MS contributions) to ensure better background rejection. Candidate R -hadron tracks must have more than two (six) pixel (silicon micro-strip) hits, impact parameters compatible with the primary vertex, $p_T > 50$ GeV and $p > 100$ GeV. The isolation cut is also more severe, rejecting events that have a track of $p_T > 1$ GeV within $\Delta R = 0.25$ of the R -hadron candidate. Additionally, tracks are discarded if their momentum resolution exceeds 50%, or if they are identified as an electron.

In events with multiple R -hadron candidates, only one – randomly chosen – candidate is used.

The final signal selection in the full-detector and MS-agnostic analyses, optimised for each mass hypothesis, is based on $\beta\gamma$ and β requiring $\beta\gamma < 1.5\text{--}2.0$ and $\beta < 0.8\text{--}0.9$, with lower values for higher masses. A signal region is defined in the $m_{\beta\gamma}\text{--}m_{\beta}$ plane for each mass point. The lower value of the mass cut is set such that it corresponds to being 2σ of the mass resolution below the nominal mass value. The upper value is set to 2.5 TeV. For the ID-only analysis the final selection requires the measured dE/dx value to exceed a certain threshold, which has been set as function of η such that the rejection of MIPs is independent of η . The selection efficiency for gluino R -hadrons of 900 GeV mass is about 11% and 7% in the full-detector and MS-agnostic analyses, respectively. It is about 6% in the ID-only analysis.

An alternative R -hadron model, which is an extension of the triple-Regge model used to describe squark R -hadrons [44] has also been considered. In this model, the signal efficiency is 40% lower at 300 GeV and increasing to the same level at 900 GeV above which it is higher, compared to the model used throughout this analysis.

5. Background estimation

The background for both the slepton and the R -hadron searches is mostly composed of high- p_T muons with mis-measured β or large ionisation. The background estimation is derived from data in all cases. The background mass spectrum is estimated by calculating a mass from the p_T spectrum of candidates and the measured β distribution of the background obtained from control samples.

The estimation of the background mass distributions relies on two assumptions: that the signal-to-background ratio before applying cuts on β is small, and that the β distribution for background candidates is due to the finite resolution of the measurement and is therefore independent of the source of the candidate and its momentum. Checks of the validity of these assumptions are discussed in Section 6.3.

The detector is divided into η regions so that the β resolution within each region is similar. The muon β probability density function (pdf) in each η region is the distribution of the measured β of all muons in the region normalised to one. The sample used in producing the β pdf is enlarged with respect to the main selection of the analysis by lowering the p_T cut to 30 GeV and removing the Z veto, in order to increase the acceptance and reduce possible signal contamination. Similarly, a $\beta\gamma$ pdf is constructed from tracks in a background dominated region.

The reconstructed mass distribution of muons in different regions of the detector depends on both β and momentum distributions through $m = p/\gamma\beta$. The regions also differ in the muon momentum distribution; therefore the combination of momentum with random β (see below) is done separately in each region and the resulting mass distributions are added together.

5.1. Slepton search

The background is determined by convoluting the β -distribution of muons with the expected muon momentum spectrum. The momentum spectrum is determined by selecting candidates that pass all selection requirements listed in Section 4.2.2 apart from the requirements on β and m . Each candidate then gets assigned a β -value by drawing it randomly from the muon β distribution. If the assigned β -value is below the cut value it is used (together with the measured momentum) to assign a mass to the candidate. The statistical uncertainty is reduced by using each muon candidate multiple times. The distribution of mass values obtained this way gives the background estimate.

5.2. R -hadron searches

For the R -hadron full-detector and MS-agnostic analyses, the momentum, $\beta\gamma$ and β are obtained by taking a p_T -spectrum of charged particle tracks from the data and assigning randomly $\beta\gamma$ and β values to these tracks. The mass is then calculated from the measured p value and the assigned value of $\beta\gamma$ or β . The mass distributions are then normalised to data by scaling to a sideband outside the signal region.

For the ID-only analysis the choice of the control sample takes into account the non-negligible correlations between p , dE/dx and η . The ionisation dependence on the path length in the sensor is not linear [53], so the pixel dE/dx depends on η ; the ionisation also depends on the particle $\beta\gamma$ via the Bethe–Bloch formula, and therefore on its momentum, until the Fermi plateau is reached; finally p and η are not uncorrelated. The distributions used for the random-sampling are derived from two categories of background events. They are obtained by applying modified selections which ensure that signal contamination is minimised.

- A first sample (“low-ionisation”) is used to generate the η and p distributions. This is selected in the same way as the event candidates, but without the requirement on high ionisation. Instead, an upper bound is placed on the dE/dx (at $(1.8 \text{ MeV g}^{-1} \text{ cm}^2)$), ensuring orthogonality with the signal selection.
- A second background sample (“low-momentum”) is used to generate the dE/dx templates. A background sample free of signal but with no upper bound on the dE/dx is obtained by considering tracks that have a maximum momentum of 100 GeV. Specifically, tracks in the “low-momentum” background sample satisfy all the event candidate requirements except that the transverse momentum cut is looser, $p_T > 10$ GeV, and the momentum p is required to be between 40 and 100 GeV (where the Fermi plateau has already been reached).

A large background sample consisting of two million p , η , dE/dx triplets is randomly generated. The momentum is first generated according to a binned function based on “low-ionisation” events. Then the pseudorapidity is generated according to the $\eta(p)$ binned functions based on “low-ionisation” events. Finally the ionisation is generated according to $dE/dx(\eta)$ binned functions based on “low-momentum” events. The normalisation of the generated background to the selected data is obtained by scaling the background to the data before the high dE/dx cut and in the region of the mass distribution where no signal is expected (mass below 140 GeV).

6. Systematic uncertainties

Several possible sources of systematic effects are studied. The resulting systematic uncertainties are summarised in Table 1. The errors given are those on the expected yields in the signal region.

6.1. Theoretical cross-sections

Signal cross-sections are calculated to next-to-leading order in the strong coupling constant, adding the resummation of soft gluon emission at next-to-leading-logarithmic accuracy (NLO + NLL) [54–60]. The nominal cross-section and the uncertainty are taken from an envelope of cross-section predictions using different PDF sets and factorisation and renormalisation scales, as described in Ref. [61]. This prescription leads to a 5% relative uncertainty on the expected signal normalisation in the slepton search, and a

Table 1

Summary of systematic uncertainties (given in percent). Ranges indicate a mass dependence for the given uncertainty (low mass–high mass).

Source	GMSB sleptons		R-hadrons	
	one-cand.	two-cand.	ID-only	other
Theoretical uncertainty on signal acceptance	5	5	15–30	
Uncertainty on signal efficiency				
Signal trigger efficiency	1.8	1.8	4.5	4.5
QCD uncertainties (ISR, FSR)	–	–	8.5	8.5
Signal pre-selection efficiency	–	–	–	1.5
Momentum resolution	0.5	0.5	1.3	1.3
Pixel dE/dx calibration	–	–	5.8–0.2	5
Combined β timing calibration	4	6	–	–
Calorimeter β timing calibration	–	–	–	1.0
MS β timing calibration	–	–	–	3.6
Offline E_T^{miss} scale	–	–	7.3–4.5	–
Total uncertainty on signal efficiency	4.4	6.3	13.4–10.6	11.6
Luminosity	3.9	3.9	3.9	3.9
Experimental uncertainty on background estimate	11	13	3–20	15

15% to 30% uncertainty for the R -hadron search, increasing with R -hadron mass.

6.2. Expected signal

The muon trigger efficiency is calculated using the tag-and-probe technique on $Z \rightarrow \mu\mu$ events as described in Refs. [49,50]. The uncertainty on the single muon trigger efficiency is estimated to be 1%. The reduction in the muon trigger efficiency due to late arrival of particles is estimated from simulation. The effect of the difference between data and MC simulation in time alignment of hits in the muon trigger system relative to the LHC clock is estimated by shifting the hit time of the highest β candidate in each simulated event by 4 ns. The difference in trigger efficiency when this change is applied is between 0.5% and 1.5% for the different GMSB samples, and a systematic uncertainty of 1.5% is assigned. For R -hadrons the systematic uncertainty is estimated in the same way and found to be 2%.

The E_T^{miss} trigger used for the R -hadrons relies on the emission of jets. Therefore, the trigger efficiency depends on the amount of initial and final state radiation (ISR and FSR). To evaluate the associated uncertainty, 1 TeV gluino pair-production samples are simulated in PYTHIA 6.4.26 using the Perugia 2011 tune [62], setting the radiation level low and high. A simple threshold curve modelling of the trigger is applied to all three samples. The largest variation from the central sample is found to be 8.5%.

The E_T^{miss} triggers use calorimeter energy deposits to calculate the transverse energy, and are thus blind to muons, which therefore can be used for calibration and to study systematic errors. To evaluate the trigger efficiency, the trigger turn-on curve is obtained by fitting the measured efficiency vs. E_T^{miss} in $Z \rightarrow \mu\mu$ events where the Z has a high p_T , both in data and simulation. Simulated events are re-weighted so the distribution of collisions per bunch-crossing match the running conditions of the 2011 data. These efficiency turn-on curves are then applied to the expected E_T^{miss} spectrum from simulated R -hadron events. The total uncertainty is estimated from three contributions: the relative difference between the efficiencies obtained using the fitted threshold curves from $Z \rightarrow \mu\mu$ data and simulation and the differences in efficiency obtained from independent $\pm 1\sigma$ variations in fit parameters relative to the unchanged turn-on curve fit for both $Z \rightarrow \mu\mu$ data and MC simulation. The total estimated E_T^{miss} trigger uncertainty, including effects of a 10% variation of the E_T^{miss} scale, is a 4.5% relative error on the efficiency for the signal.

In the ID-only analysis, the effect of the offline E_T^{miss} measurement uncertainty on the total efficiency is evaluated by applying a scale factor of $\pm 10\%$ and a smearing of up to 20% to the missing transverse momentum [63]. The resulting uncertainty depends on the R -hadron mass and is between 7.3% (200 GeV) and 4.5% (1500 GeV) of the central value.

Differences in the selection efficiency between data and MC simulation for the R -hadron full-detector and MS-agnostic searches (excluding the final selection on $\beta\gamma$, β , momentum and mass selection) are evaluated using $Z \rightarrow \mu\mu$ events. The overall relative uncertainty is found to be below 1.5%. The effect of the jet energy scale (JES) uncertainty on the requirement for signal candidates in the R -hadron full-detector and MS-agnostic searches to be separated by $\Delta R = 0.3$ from jets with $p_T > 40$ GeV is found to be negligible.

To verify that the signal efficiency is insensitive to the pile-up re-weighting, a 900 GeV gluino sample is divided into samples of high ($N_{\text{vtx}} \geq 8$) and low ($N_{\text{vtx}} < 8$) number of reconstructed primary vertices. The relative difference in reconstruction efficiency is found to be negligible.

The systematic uncertainty due to the track reconstruction efficiency and momentum resolution differences between data and simulation is estimated [64] to be 0.5% on the acceptance for GMSB events. For analyses relying solely on the ID for tracking, the resulting relative uncertainty on the signal efficiency is 1.3%.

Differences in the pixel dE/dx and the subsequent measurement of $\beta\gamma$ between data and simulation are considered by comparing the pixel dE/dx distribution for high- p_T muons from $Z \rightarrow \mu\mu$ events in data and MC simulation. This uncertainty is estimated to be 5%. In the ID-only analysis, this effect is evaluated by comparing the ionisation in data and simulation for MIPs and for particles with low $\beta\gamma$. Scale factors are measured in the two cases and found to be consistent. The uncertainty on the signal efficiency derived by applying these scale factors varies between 0.2% and 5.8% in the studied mass range, decreasing with the particle's mass.

The signal β resolution is estimated by smearing the measured time of hits in the MS and calorimeter according to the spread observed in the time calibration. The systematic uncertainty due to the smearing process is estimated by scaling the smearing factor up and down, so as to bracket the distribution obtained in data. A 4% (6%) systematic uncertainty is found in the one-candidate (two-candidate) GMSB signal region. The corresponding uncertainty for R -hadrons is 3.6%. The uncertainty due to the timing calibration of the calorimeter hits is further tested by comparing a

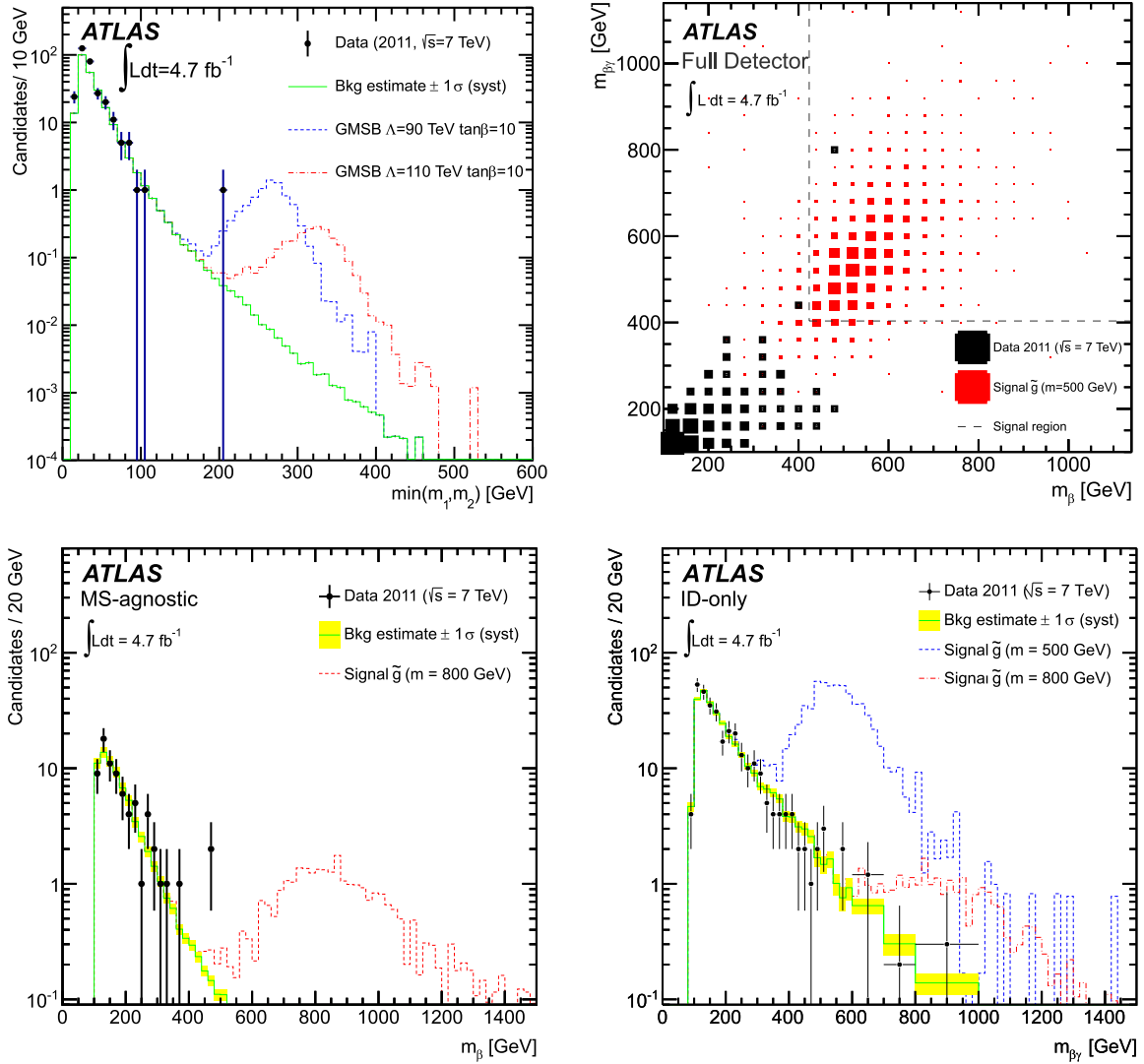


Fig. 3. Observed data, background estimate and expected signal in the two-candidate signal region in the slepton search (top-left), full-detector R -hadron search (top-right), MS-agnostic R -hadron search (bottom-left) and in the ID-only R -hadron search (bottom-right). For the slepton search only the lower of the two masses is plotted and for the full-detector R -hadron search there is one candidate in the $m_{\beta\gamma}$ overflow bin not shown in the figure. The dashed lines in the upper-right plot mark the lower edges of the signal region chosen for this R -hadron mass point.

calibration obtained from jet events to that obtained from muons. This results in a 1% relative systematic uncertainty on the signal yield.

An uncertainty of 3.9% [65,66] is assigned to the integrated luminosity corresponding to this data set.

6.3. Background estimation

The assumption that the β -pdf is independent of p is tested by constructing the β -pdf separately in each η -region using a low and a high-momentum sample. This results in differences of up to 10% on the background estimate. To quantify the variability of the β and momentum distributions within a region and its effect on the background estimation for sleptons, the detector is sub-divided into 25 η regions instead of the eight used in the analysis and the background estimated with this division. The resulting systematic uncertainty is 6.5% for the two-candidate events and 3.1% for one-candidate events. The uncertainty on the background distribution due to the limited numbers of data events used to estimate the momentum distribution was calcu-

lated by dividing the candidate sample randomly into two samples and estimating the background from each sub-sample separately. The resulting error in the slepton search is negligible. A comparison of the muon β distribution in inclusive muon events to that from $Z \rightarrow \mu\mu$ decays also exhibited negligible differences. The total uncertainty on the background estimate for the slepton search is 13% for two-candidate events and 11% for one-candidate events.

The total uncertainty in the background estimation for the full-detector R -hadron analysis is estimated as follows. The $\beta\gamma$ and β pdfs are obtained by considering sidebands (lower momenta, for R -hadrons 40–100 GeV). Similarly, the momentum pdf is obtained from sidebands in $\beta\gamma$ and/or β . Several variations of the size of the sidebands (and also inclusion of the signal region) result in 8–10% uncertainty estimates for each of the two variables. To test the momentum dependence of the β pdf, the number of η bins is varied. The resulting systematic uncertainty is 2%. To estimate the uncertainty on the background distribution coming from the limited statistics of the data samples used to estimate the momentum distribution, the candidate sample is divided randomly into two

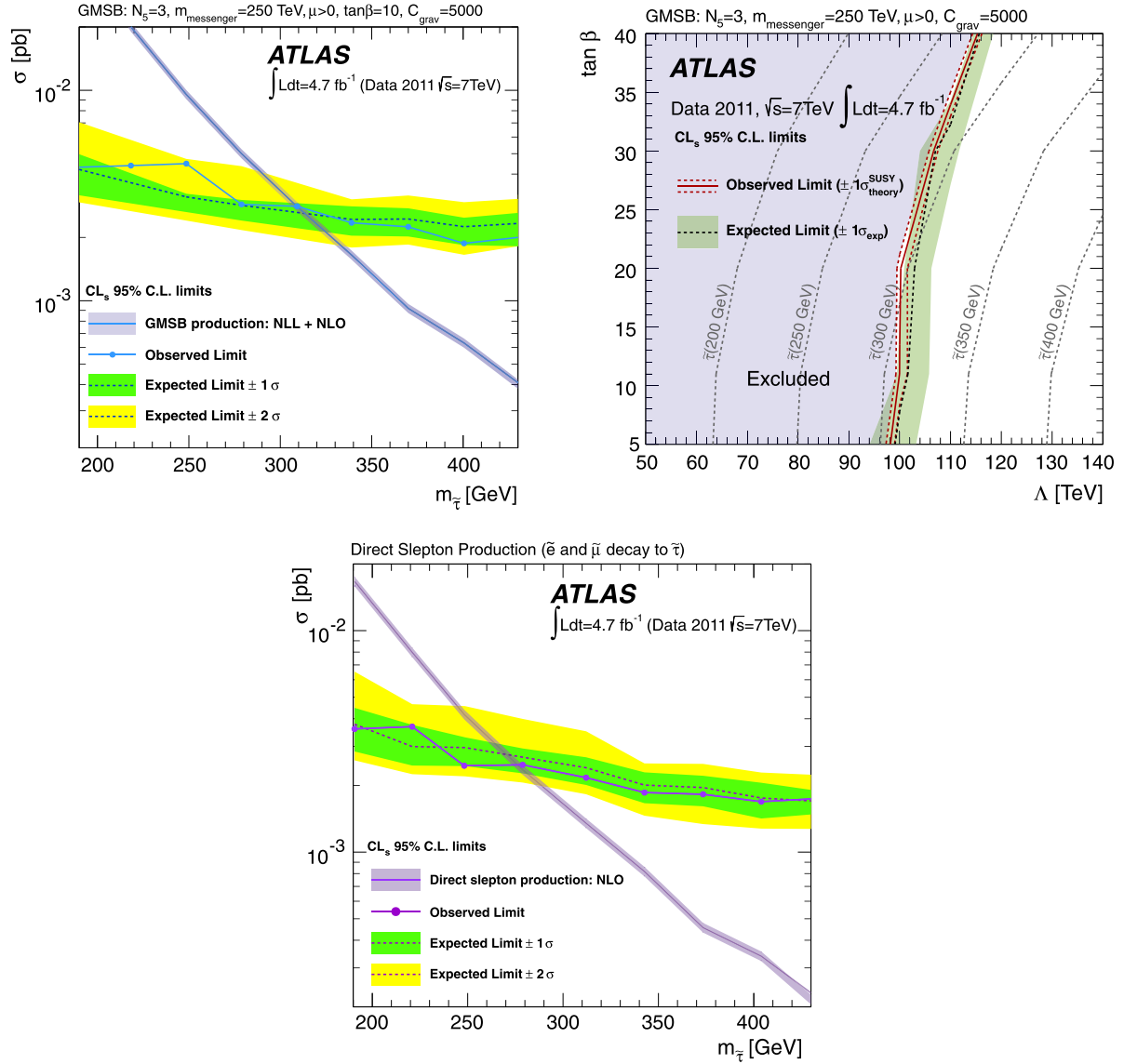


Fig. 4. Cross-section limits as a function of the $\tilde{\tau}$ mass in GMSB models (top-left), limits on Λ and $\tan\beta$ in GMSB models (top-right) and the cross-section limits as a function of mass on directly produced sleptons (bottom). The top-left and bottom plots show observed and expected limits with $\pm 1\sigma$ and $\pm 2\sigma$ uncertainty bands, as well as the theoretical prediction for the cross-section is shown with a 1σ band. In the top-right plot, the observed and expected limits are shown, with the 1σ theoretical uncertainty and the 1σ band, respectively.

samples and the background estimate is derived from each sub-sample separately. The resulting uncertainty on the full-detector R -hadron search is 2% for low mass and 5% for high mass. The total uncertainty on the background estimate from the above tests is 15%.

For the ID-only analysis, the statistical uncertainty in the background estimate dominates for most of the mass range, and is up to 20%. Other effects contribute at most a few percent. These include variations from different binning choices for p , η and dE/dx in the two background samples, and a contribution from pile-up effects.

7. Results

The mass distributions observed in data together with the background estimate, its systematic error and examples of signal are shown in Fig. 3, for the two-candidate signal region in the slepton search (top-left), the full-detector R -hadron search (top-right),

the MS-agnostic R -hadron search (bottom-left) and the ID-only R -hadron search (bottom-right).

No indication of signal above the expected background is observed. Upper cross-section limits on new particles are set by counting the number of events passing a set of mass cuts optimised for a given mass point and model. For the ID-only analysis the full mass spectrum of the background and the hypothetical signal is considered. Cross-section limits are obtained using the CL_s prescription [67]. Mass limits are derived by comparing the obtained cross-section limits to the lower edge of the 1σ band around the theoretically predicted cross-section for each process. A Poisson likelihood function is used for the R -hadron limit-setting while a likelihood combining two Poisson functions is used for the slepton search to benefit from the separation into one-candidate and two-candidate signal regions.

The resulting production cross-section limits in the GMSB scenario as a function of the stau mass are presented in Fig. 4 and compared to theoretical predictions. Long-lived staus in GMSB

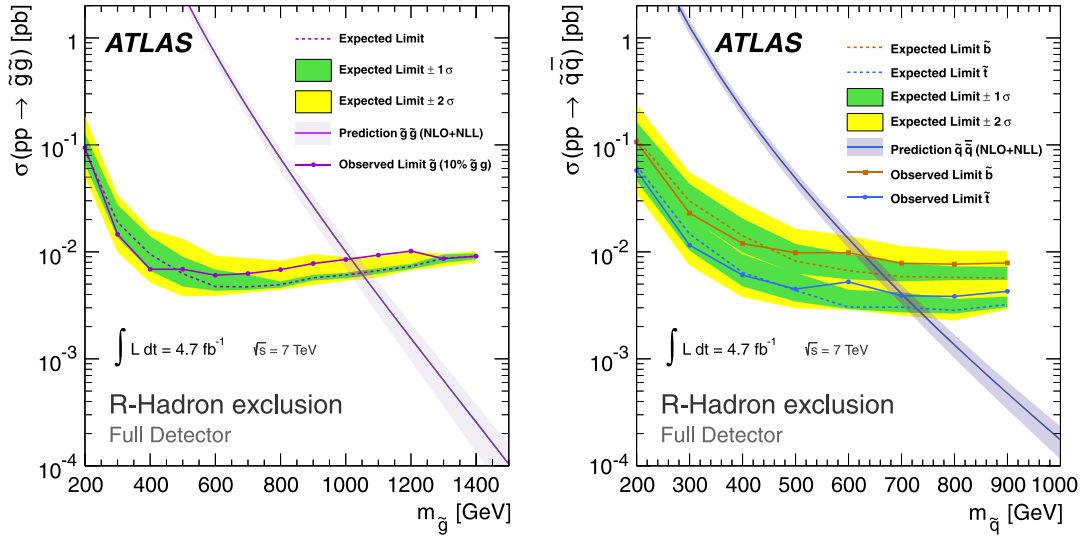


Fig. 5. Cross-section upper limits at 95% CL for gluino (left) and squark (right) R -hadrons in the full-detector search are shown. Both the expected limit with $\pm 1\sigma$ and $\pm 2\sigma$ uncertainty bands and the observed upper limit are given. In addition the theoretical prediction for the production cross-section calculated at NLO + NLL and its uncertainty are drawn.

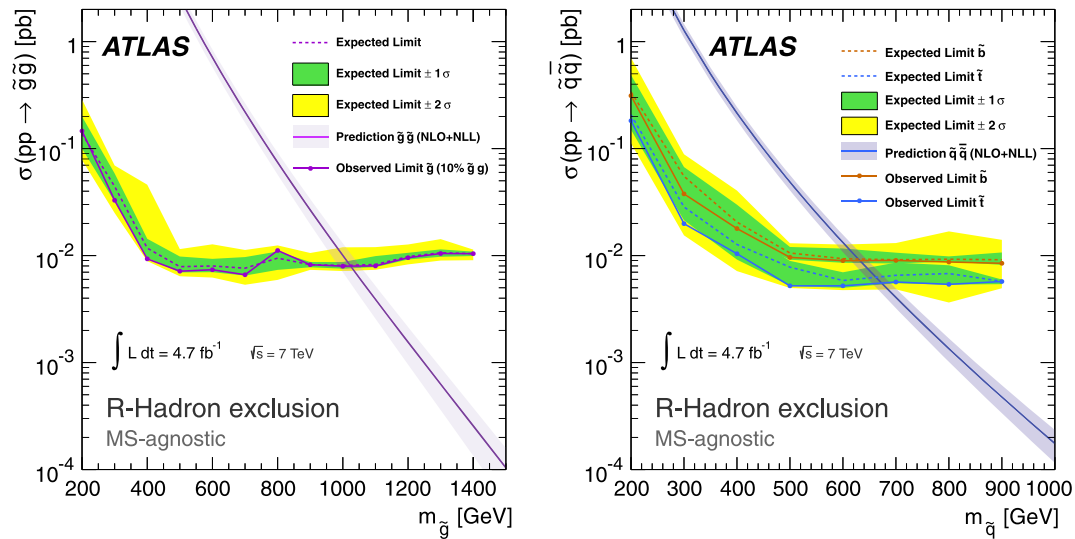


Fig. 6. Cross-section upper limits at 95% CL for gluino (left) and squark (right) R -hadrons in the MS-agnostic search, which is independent of the fraction of R -hadrons that are charged in the MS. Both the expected limit with $\pm 1\sigma$ and $\pm 2\sigma$ uncertainty bands and the observed upper limit are given. In addition the theoretical prediction for the production cross-section calculated at NLO + NLL and its uncertainty are drawn.

models with $N_5 = 3$, $m_{\text{messenger}} = 250 \text{ TeV}$ and $\text{sign}(\mu) = 1$ are excluded at 95% confidence level (CL) up to a stau mass of 300 GeV for $\tan\beta = 5\text{--}20$, and up to stau masses of 285 GeV and 268 GeV for $\tan\beta = 30$ and $\tan\beta = 40$, with expected limits of 305 GeV, 287 GeV and 270 GeV respectively. The lower limit on Λ is 99–110 TeV for values of $\tan\beta$ from 5 to 40. For Λ values around this limit, strong production of squarks and gluinos is suppressed due to their large masses. Directly produced sleptons comprise 38–64% of the GMSB cross-section, and depend only on the slepton mass. Using the same analysis, directly produced long-lived sleptons, or sleptons decaying to long-lived ones, are excluded at 95% CL up to a $\tilde{\tau}$ mass of 278 GeV (273 GeV expected) for models with slepton mass splittings smaller than 50 GeV.

The resulting limits on R -hadrons are shown in Figs. 5 and 6 compared to the theoretical cross-sections. Gluino R -hadrons in a

generic interaction model are excluded up to a mass of 985 GeV. Stop R -hadrons are excluded up to a mass of 683 GeV, and sbottom R -hadrons are excluded up to a mass of 612 GeV. The according expected limits are 1012 GeV, 707 GeV and 645 GeV respectively. The MS-agnostic search yields a lower mass limit of 989 GeV for gluinos, 657 GeV for stops and 618 GeV for sbottoms, with expected limits of 988 GeV, 647 GeV and 615 GeV respectively. The MS-agnostic limits are independent of the fraction of R -hadrons that arrive charged in the MS.

The limits from the ID-only search are shown in Fig. 7 compared to the theoretical cross-sections. Gluino R -hadrons with $m < 940 \text{ GeV}$, stop R -hadrons with $m < 604 \text{ GeV}$ and sbottom R -hadrons with $m < 576 \text{ GeV}$ are excluded at 95% CL, with expected limits of 952 GeV, 620 GeV and 571 GeV respectively. The ID-only search has similar sensitivity also to R -hadrons with lifetimes as short as a few ns.

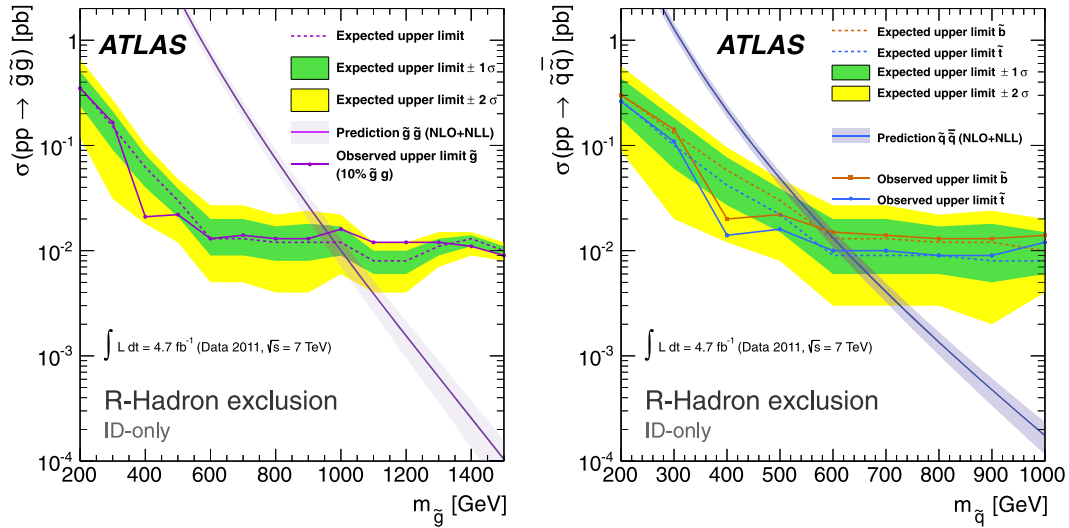


Fig. 7. Cross-section upper limits at 95% CL for gluino (left) and squark (right) R -hadrons in the ID-only search. Both the expected limit with $\pm 1\sigma$ and $\pm 2\sigma$ uncertainty bands and the observed upper limit are given. In addition the theoretical prediction for the production cross-section calculated at NLO + NLL and its uncertainty are drawn.

8. Conclusion

Searches for long-lived massive particles were performed using data from pp collisions at $\sqrt{s} = 7$ TeV collected by the ATLAS detector in 2011, corresponding to an integrated luminosity of 4.7 fb^{-1} . Several different signatures are considered. The data are found to match the Standard Model background expectation in all signal regions. The exclusion limits placed for various models impose new constraints on non-SM cross-sections. Long-lived $\tilde{\tau}$'s in the GMSB model considered, for $\tan\beta = 5\text{--}20$, are excluded at 95% CL for masses up to 300 GeV, while directly produced long-lived sleptons, or sleptons decaying to long-lived ones, are excluded at 95% CL up to a $\tilde{\tau}$ mass of 278 GeV for models with slepton mass splittings smaller than 50 GeV.

Long-lived R -hadrons containing a gluino (stop, sbottom) are excluded for masses up to 985 GeV (683 GeV, 612 GeV) at 95% CL, for a generic interaction model. Limits obtained independently of the fraction of R -hadrons that arrive charged in the MS exclude masses up to 989 GeV (657 GeV, 618 GeV). Furthermore, using only the inner detector, R -hadrons are excluded up to 940 GeV (604 GeV, 576 GeV).

These results substantially extend previous ATLAS limits [32,33], and are complementary to the searches for SUSY particles which decay promptly.

Acknowledgements

We thank CERN for the very successful operation of the LHC, as well as the support staff from our institutions without whom ATLAS could not be operated efficiently.

We acknowledge the support of ANPCyT, Argentina; YerPhI, Armenia; ARC, Australia; BMWF and FWF, Austria; ANAS, Azerbaijan; SSTC, Belarus; CNPq and FAPESP, Brazil; NSERC, NRC and CFI, Canada; CERN; CONICYT, Chile; CAS, MOST and NSFC, China; COLCIENCIAS, Colombia; MSMT CR, MPO CR and VSC CR, Czech Republic; DNRF, DNSRC and Lundbeck Foundation, Denmark; EPLANET, ERC and NSRF, European Union; IN2P3-CNRS, CEA-DSM/IRFU, France; GNSF, Georgia; BMBF, DFG, HGF, MPG and AvH Foundation, Germany; GSRT and NSRF, Greece; ISF, MINERVA, GIF, DIP and Benoziyo Center, Israel; INFN, Italy; MEXT and JSPS, Japan; CNRST, Morocco; FOM and NWO, Netherlands; BRF and RCN, Norway; MNiSW, Poland; GRICES and FCT, Portugal; MERYS (MECTS), Roma-

nia; MES of Russia and ROSATOM, Russian Federation; JINR; MSTD, Serbia; MSSR, Slovakia; ARRS and MVZT, Slovenia; DST/NRF, South Africa; MICINN, Spain; SRC and Wallenberg Foundation, Sweden; SER, SNSF and Cantons of Bern and Geneva, Switzerland; NSC, Taiwan; TAEK, Turkey; STFC, the Royal Society and Leverhulme Trust, United Kingdom; DOE and NSF, United States of America.

The crucial computing support from all WLCG partners is acknowledged gratefully, in particular from CERN and the ATLAS Tier-1 facilities at TRIUMF (Canada), NDGF (Denmark, Norway, Sweden), CC-IN2P3 (France), KIT/GridKA (Germany), INFN-CNAF (Italy), NL-T1 (Netherlands), PIC (Spain), ASGC (Taiwan), RAL (UK) and BNL (USA) and in the Tier-2 facilities worldwide.

Appendix A. Auxiliary material

Appendix consists of Figs. A.8–A.18 and Tables A.2–A.9.

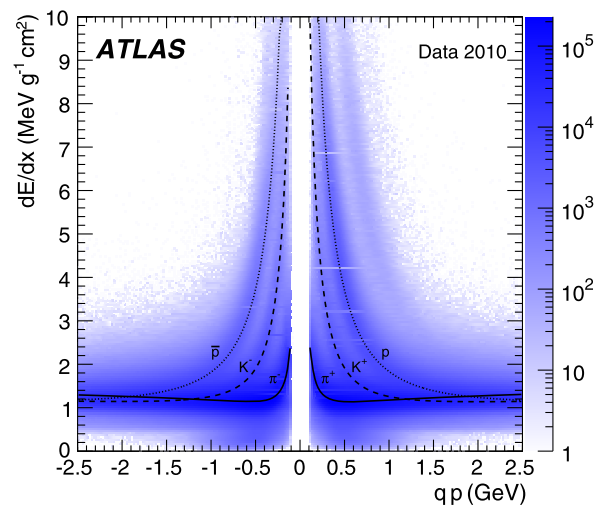


Fig. A.8. Greyscale-printing version of Fig. 1(left): Distribution of dE/dx versus charge times momentum for minimum bias collisions in a data sample from 2010. With tracks reconstructed for $p_T > 100$ MeV this sample is more suitable for the calibration of the Bethe-Bloch function than 2011 data in which tracks had a cut-off of $p_T = 400$ MeV. The distribution of the most probable value for pions (solid), kaons (dashed) and protons (dotted) are superimposed. The band due to deuterons is clearly visible.

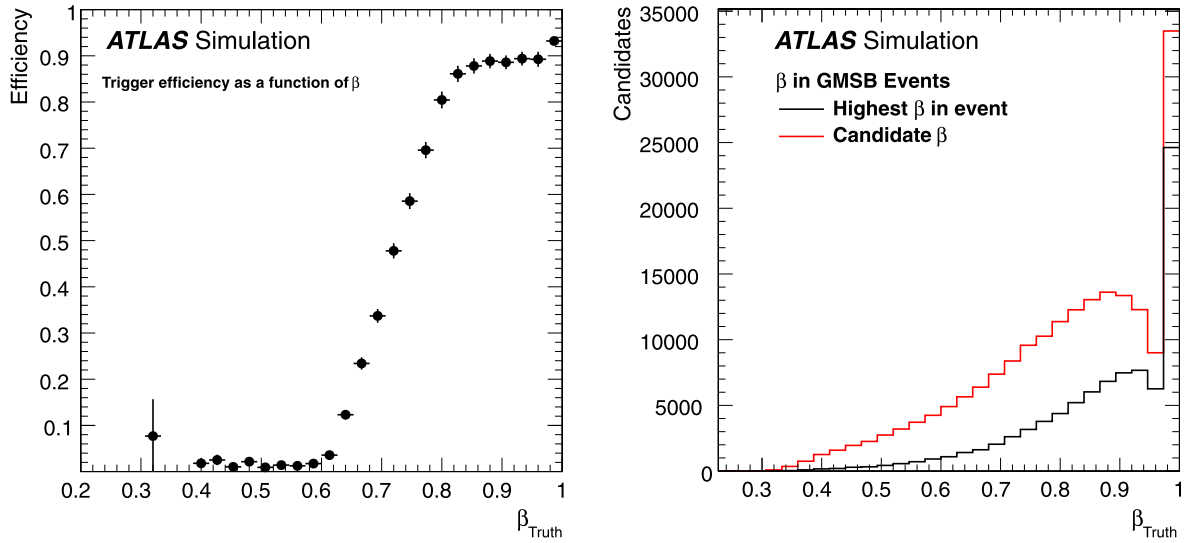


Fig. A.9. Left: Muon trigger efficiency in simulated GMSB events as a function of the highest β candidate in the event. Right: Distribution of β for candidates with the highest β (black) and for all candidates in the events (red). Low- β candidates are found in triggered events because there is a high- β slepton or muon in the event that could trigger. (For interpretation of the references to colour in this figure legend, the reader is referred to the web version of this Letter.)

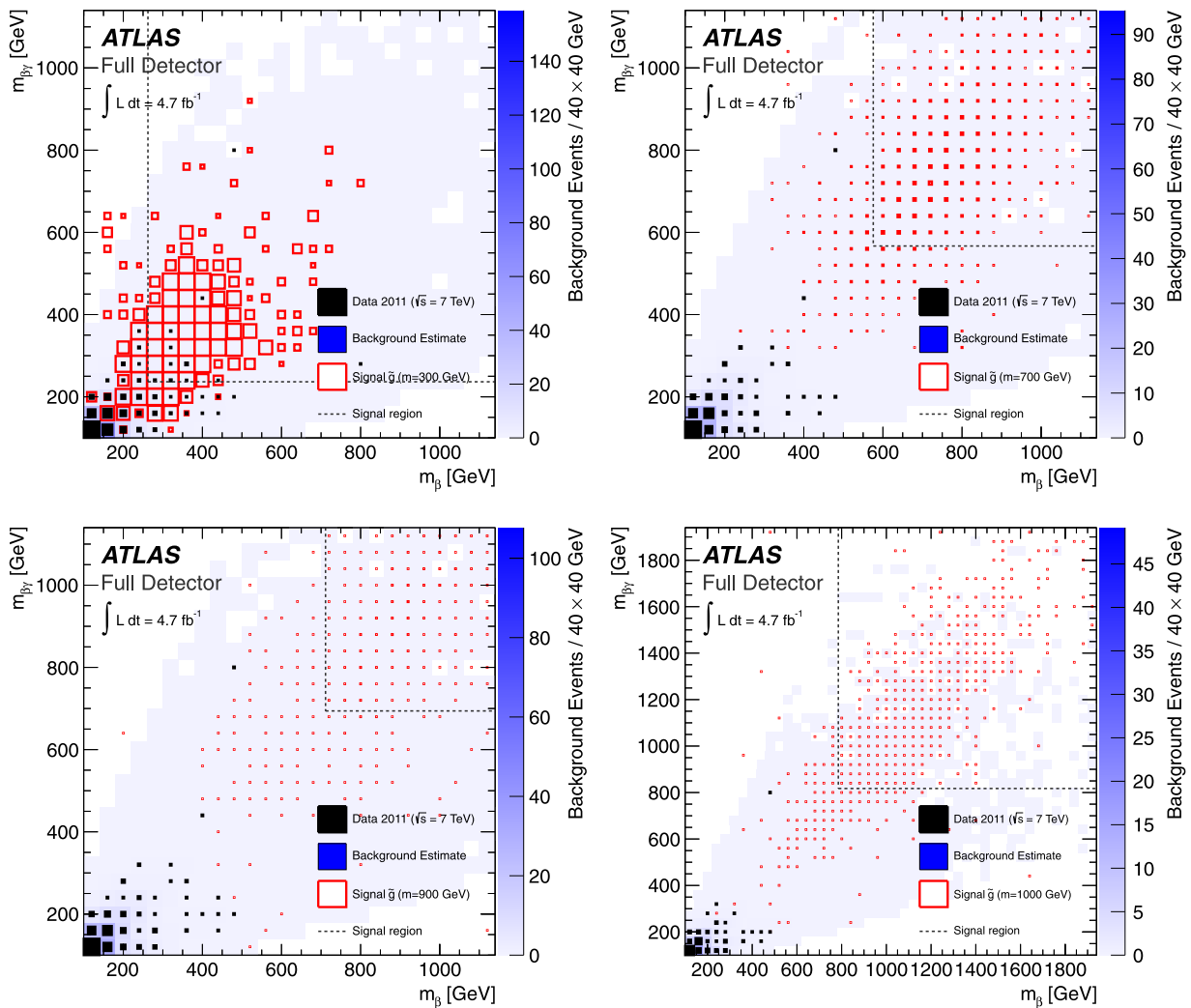


Fig. A.10. Examples of the $m_{\beta\gamma}$ vs. m_{β} distributions for gluino R -hadrons with masses of 300, 700, 900 and 1000 GeV, with the full-detector search. The figures show data, background and signal after β , $\beta\gamma$ and p cuts. The dashed grey line highlights the counting window for each specific hypothesis, and is defined by requiring 90% of the signal to be within the window. There is one candidate in the $m_{\beta\gamma}$ overflow.

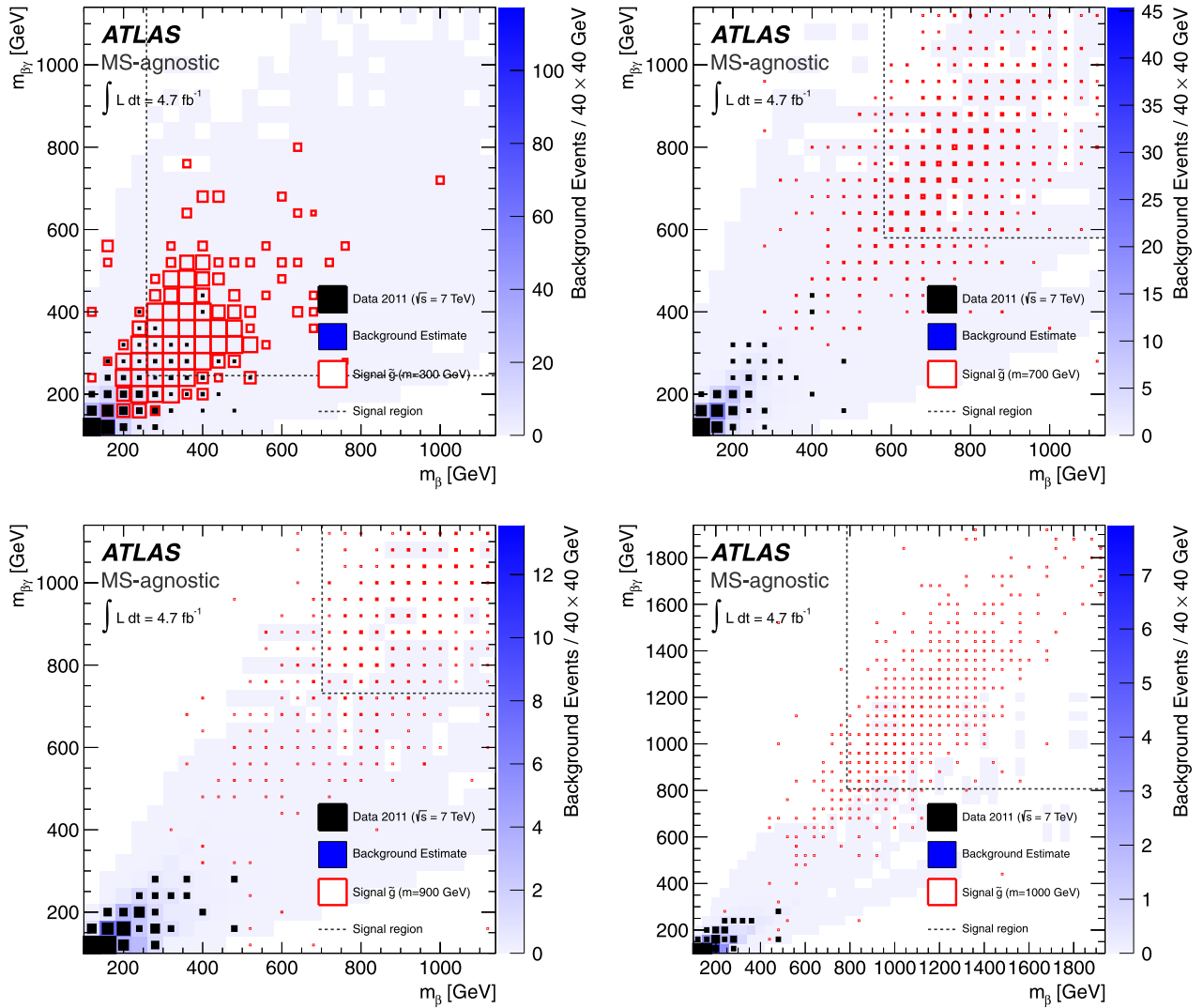


Fig. A.11. Examples of the $m_{\beta\gamma}$ vs. m_{β} distributions for gluino R-hadrons with masses of 300, 700, 900 and 1000 GeV, with the MS-agnostic search. The figures show data, background and signal after β , $\beta\gamma$ and p cuts. The dashed grey line highlights the counting window for each specific hypothesis, and is defined by requiring 90% of the signal to be within the window.

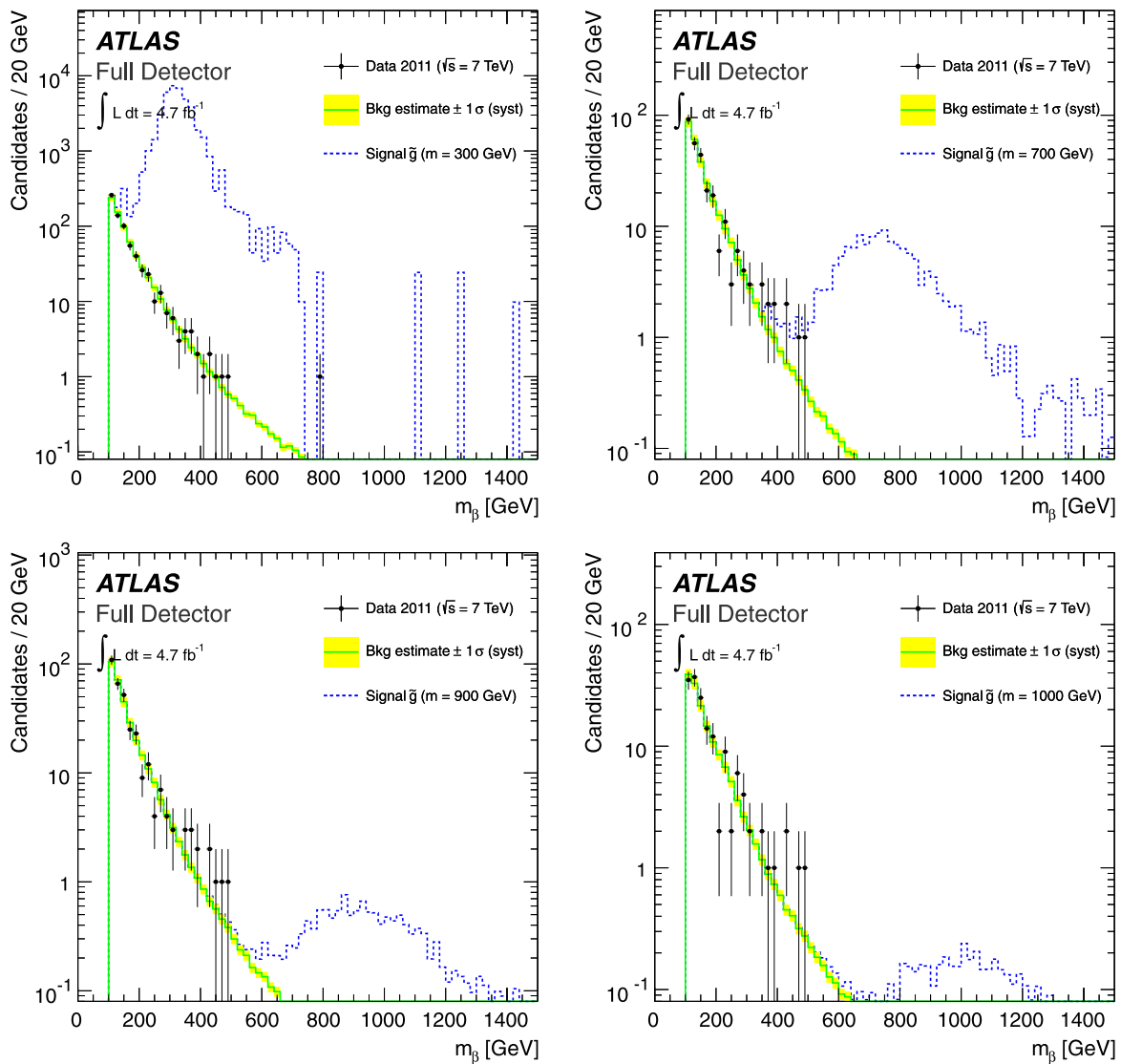


Fig. A.12. Observed data, background estimate and expected signal in the full-detector R -hadron search, for various mass hypotheses (300, 700, 900 and 1000 GeV). The 1D histograms are projections of the 2D signal range with unconstrained $m_{\beta\gamma}$.

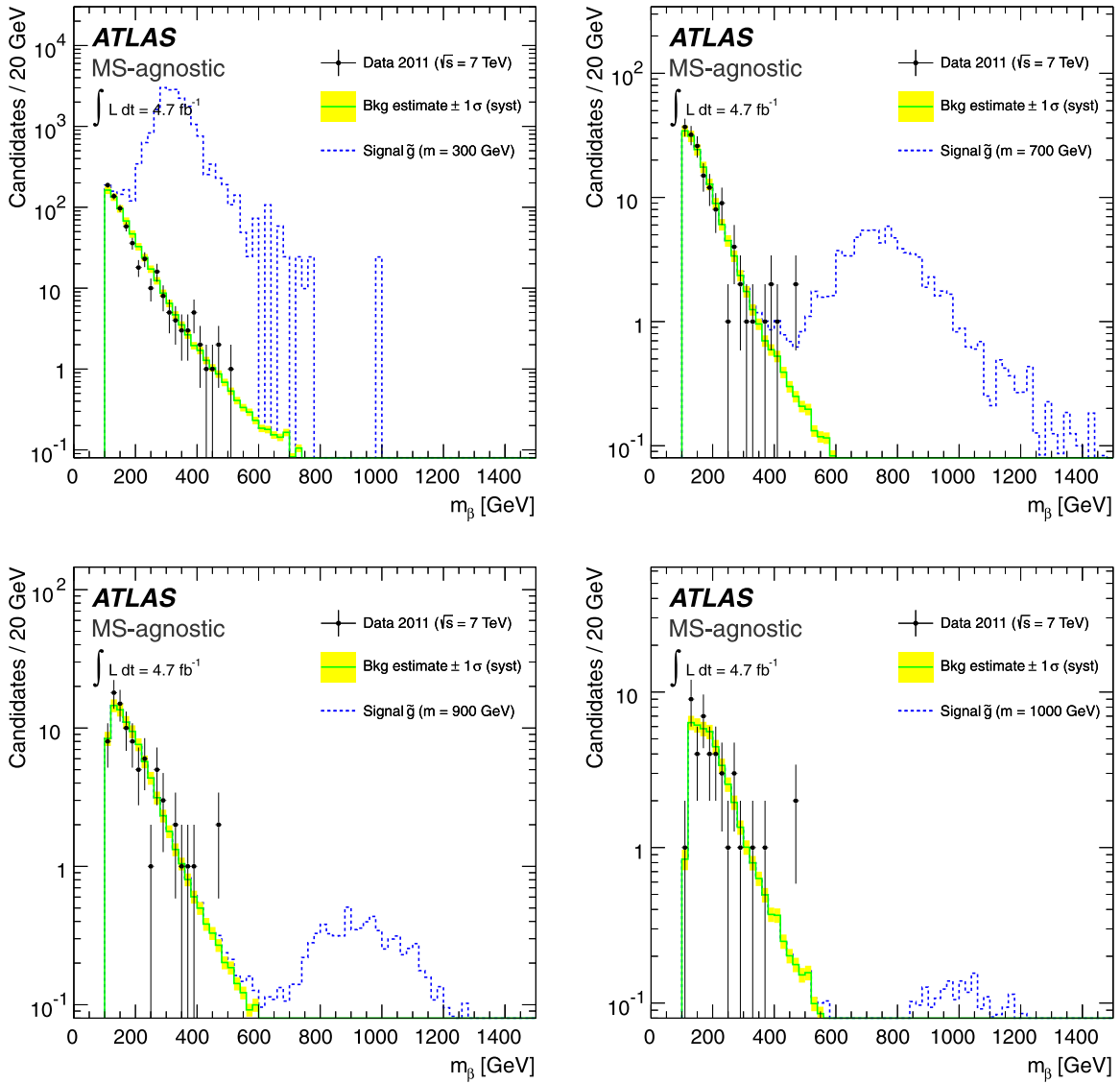


Fig. A.13. Observed data, background estimate and expected signal in the MS-agnostic R -hadron search, for various mass hypotheses (300, 700, 900 and 1000 GeV). The 1D histograms are projections of the 2D signal range with unconstrained $m_{\beta\gamma}$.

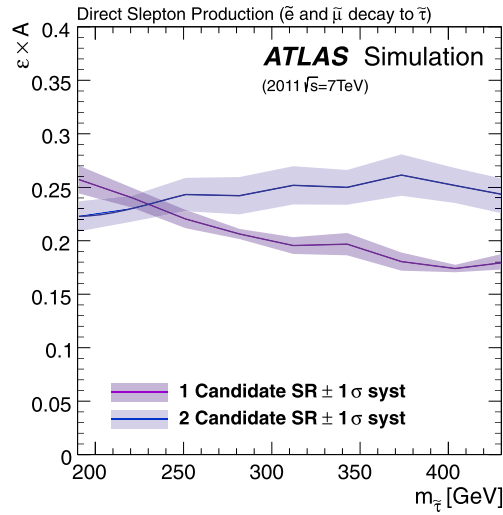


Fig. A.14. Efficiency times acceptance for directly produced slepton events in the one-candidate and two-candidate signal regions as a function of the stau mass.

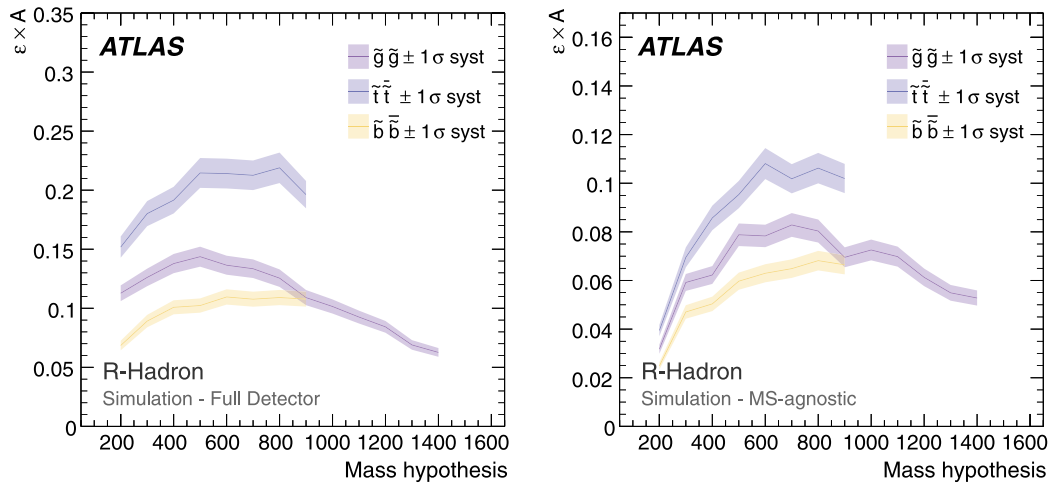


Fig. A.15. Efficiency times acceptance for the tested R -hadron mass hypotheses. Each point on the x -axis represent a hypothesis mass, the efficiency for a given hypothesis is based on the number of signal events in the counting region after cuts, divided by the number of generated events. The band represents the 11.4% systematic uncertainty on the efficiency.

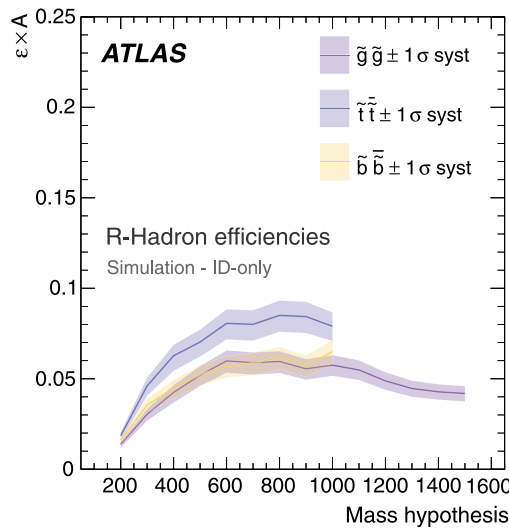


Fig. A.16. Efficiency times acceptance for the tested R -hadron mass hypotheses. Each point on the x -axis represent a hypothesis mass, the efficiency for a given hypothesis is based on the number of signal events in the counting region after cuts, divided by the number of generated events. The band represents the systematic uncertainty on the efficiency, varying with mass as specified in Table 1.

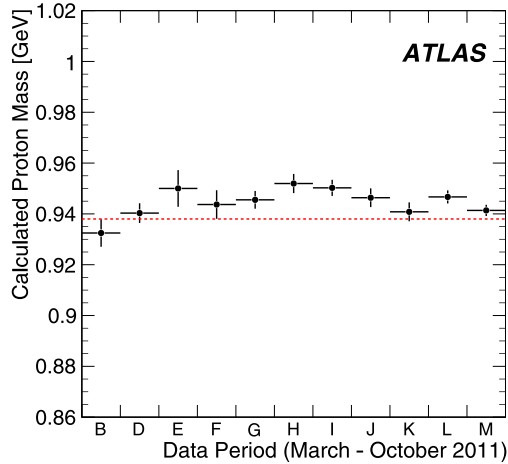


Fig. A.17. Proton mass calculated from the momentum measured in the inner detector and the specific energy loss measured in the pixel detector. The data, covering the 2011 statistics considered for this analysis, are subdivided in periods of similar data-taking conditions to illustrate the stability of the method. The red horizontal line represents the nominal proton mass value.

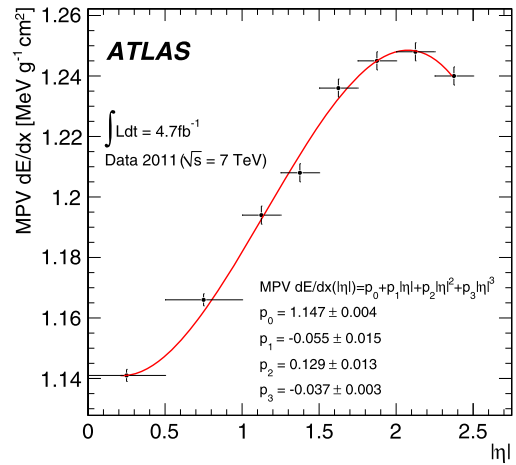


Fig. A.18. Plot of the dE/dx most probable values (MPVs) obtained from data, selected as in the “low-ionisation” sample (see Section 5.2), as a function of η overlapped with a fit obtained using a third order polynomial.

Table A.2

Signal efficiency, number of expected background events, events observed in data, expected and observed limit for the one candidate (SR_1) and two candidates (SR_2) signal regions in various GMSB scenarios.

Λ [TeV]	$\tan \beta$	m [GeV]	σ [fb]	$SR_1 : \varepsilon \times A$ [%]	$SR_1 : Bkg$	$SR_1 : Obs$	$SR_2 : \varepsilon \times A$ [%]	$SR_2 : Bkg$	$SR_2 : Obs$	σ_{95CLS}^{exp}	σ_{95CLS}^{obs}
60	5	191	43.8	22.4 ± 1.1	131 ± 17	115	17.2 ± 1.2	0.62 ± 0.13	1	4.21	4.35
70	5	221	18.4	20.7 ± 0.8	61 ± 8	61	18.6 ± 1.0	0.28 ± 0.05	1	3.44	4.51
80	5	251	8.65	20.4 ± 1.0	31 ± 4	35	19.0 ± 1.0	0.17 ± 0.02	1	3.20	4.61
90	5	281	4.47	21.1 ± 1.1	20 ± 2	24	18.7 ± 1.2	0.077 ± 0.008	0	2.95	3.09
100	5	312	2.48	19.5 ± 0.6	11.3 ± 1.2	14	19.8 ± 1.3	0.045 ± 0.005	0	2.70	2.86
110	5	343	1.43	19.6 ± 0.9	6.7 ± 0.7	6	20.2 ± 1.3	0.022 ± 0.003	0	2.46	2.35
120	5	373	0.86	17.3 ± 0.4	4 ± 0.4	3	20.4 ± 1.3	0.014 ± 0.003	0	2.33	2.19
130	5	404	0.53	18.3 ± 0.7	2.9 ± 0.3	1	20.5 ± 1.3	0.0092 ± 0.0018	0	2.23	1.84
140	5	435	0.34	18.2 ± 0.7	1.9 ± 0.2	1	17.9 ± 1.2	0.0038 ± 0.0008	0	2.33	2.07
60	10	189	47.7	21.1 ± 1.0	131 ± 17	115	17.6 ± 1.1	0.62 ± 0.13	1	4.23	4.31
70	10	218	20.0	20.4 ± 1.0	61 ± 8	61	17.3 ± 0.4	0.36 ± 0.06	1	3.68	4.39
80	10	249	9.55	21.1 ± 1.0	39 ± 5	41	19.2 ± 1.0	0.17 ± 0.02	1	3.11	4.48
90	10	279	5.00	20.1 ± 0.6	20 ± 2	24	20.4 ± 1.3	0.1 ± 0.01	0	2.84	2.87
100	10	309	2.80	19.7 ± 0.6	11.3 ± 1.2	14	20.2 ± 1.2	0.045 ± 0.005	0	2.64	2.81
110	10	339	1.65	19.6 ± 0.9	6.7 ± 0.7	6	20.2 ± 1.3	0.022 ± 0.003	0	2.45	2.35
120	10	370	0.92	17.5 ± 0.5	4 ± 0.4	3	19.6 ± 1.3	0.014 ± 0.003	0	2.25	2.24
130	10	401	0.63	17.9 ± 0.7	2.9 ± 0.3	1	20.3 ± 1.3	0.0092 ± 0.0018	0	2.25	1.87
140	10	431	0.40	17.4 ± 0.9	1.9 ± 0.2	1	19.5 ± 1.1	0.0049 ± 0.0012	0	2.23	2.00
60	20	176	51.6	22.3 ± 0.8	171 ± 22	141	16.6 ± 1.0	0.81 ± 0.19	1	4.74	4.35
70	20	206	21.2	22.7 ± 1.3	101 ± 13	89	18.3 ± 1.1	0.48 ± 0.09	1	3.78	4.14
90	20	266	5.60	20.6 ± 0.7	25 ± 3	29	20.3 ± 1.5	0.132 ± 0.014	0	2.82	3.07
100	20	295	3.14	18.8 ± 0.7	13.7 ± 1.5	19	19.4 ± 1.5	0.059 ± 0.006	0	2.77	3.12
110	20	325	1.87	17.7 ± 0.6	7.9 ± 0.8	9	18.0 ± 1.2	0.028 ± 0.003	0	2.78	2.91
120	20	355	0.96	19.5 ± 0.7	5.5 ± 0.6	4	20.4 ± 1.2	0.018 ± 0.003	0	2.38	2.39
60	30	153	61.8	21.1 ± 1.1	302 ± 38	237	17.6 ± 0.9	1.57 ± 0.38	1	5.01	3.73
70	30	183	26.4	22.9 ± 1.4	171 ± 22	141	19.1 ± 1.1	0.81 ± 0.19	1	4.11	3.74
90	30	241	6.80	20.6 ± 0.6	39 ± 5	41	20.5 ± 1.5	0.21 ± 0.03	1	3.06	4.23
100	30	269	3.84	19.4 ± 1.0	25 ± 3	29	17.3 ± 1.1	0.1 ± 0.01	0	2.51	2.77
110	30	298	2.30	20.9 ± 0.7	13.7 ± 1.5	19	21.2 ± 1.5	0.059 ± 0.006	0	2.18	2.84
130	30	355	0.89	20.1 ± 0.7	5.5 ± 0.6	4	22.7 ± 1.5	0.018 ± 0.003	0	2.21	1.97
140	30	383	0.58	19.5 ± 0.7	3.4 ± 0.4	2	20.7 ± 1.5	0.0092 ± 0.0019	0	2.20	1.95
60	40	113	111	21.0 ± 0.8	1057 ± 140	895	12.8 ± 0.7	4.9 ± 1.1	3	4.01	6.30
100	40	228	6.34	20.5 ± 0.8	49 ± 6	51	21.5 ± 1.5	0.28 ± 0.05	1	3.03	4.06
110	40	254	3.60	21.3 ± 0.8	31 ± 4	35	21.3 ± 1.5	0.132 ± 0.014	0	2.79	2.78
120	40	281	1.98	21.5 ± 0.6	20 ± 2	24	22.0 ± 1.4	0.077 ± 0.008	0	2.55	2.67

Table A.3

Signal efficiency, number of expected background events, events observed in data, expected and observed limit for the one candidate (SR_1) and two candidates (SR_2) signal regions for direct slepton production.

m [GeV]	σ [fb]	$SR_1 : \varepsilon \times A$ [%]	$SR_1 : Bkg$	$SR_1 : Obs$	$SR_2 : \varepsilon \times A$ [%]	$SR_2 : Bkg$	$SR_2 : Obs$	σ_{95CLs}^{exp}	σ_{95CLs}^{obs}
191	16.69	20.0 ± 1.0	101 ± 13	89	22.3 ± 1.4	0.48 ± 0.09	1	3.78	3.60
221	7.99	23.7 ± 0.9	61 ± 8	61	23.0 ± 1.2	0.28 ± 0.05	1	3.00	3.68
251	4.26	22.0 ± 0.9	31 ± 4	35	24.3 ± 1.6	0.132 ± 0.014	0	2.96	2.45
281	2.33	20.6 ± 0.5	17 ± 2	21	24.2 ± 1.7	0.059 ± 0.006	0	2.68	2.48
312	1.35	19.6 ± 0.8	9.4 ± 1.0	10	25.2 ± 1.8	0.036 ± 0.004	0	2.40	2.17
343	0.82	19.7 ± 1.0	5.5 ± 0.6	4	25.0 ± 1.6	0.018 ± 0.003	0	2.00	1.86
373	0.46	18.1 ± 0.9	4.0 ± 0.4	3	26.1 ± 1.9	0.012 ± 0.003	0	1.96	1.82
404	0.34	17.4 ± 0.4	2.2 ± 0.3	1	25.2 ± 1.6	0.006 ± 0.001	0	1.76	1.69
435	0.21	18.0 ± 0.7	1.6 ± 0.2	1	24.3 ± 1.6	0.004 ± 0.001	0	1.69	1.75

Table A.4

Signal efficiency, number of expected background events, events observed in data, expected (with 1σ uncertainties) and observed limit for various gluino R -hadron mass hypotheses in the full-detector search.

$m_{\tilde{g}}$ [GeV]	Signal eff. [%]	Exp. bkg [events]	Obs. data [events]	Exp. limit [fb]	$+\sigma$ [fb]	$-\sigma$ [fb]	Obs. limit [fb]
200	11.3	131.2	135	89	128	65	94
300	12.6	18.7	15	19.0	27.7	13.6	14.6
400	13.8	5.2	3	9.5	14.0	6.6	6.9
500	14.4	1.8	2	6.3	9.0	4.8	6.9
600	13.6	0.6	1	4.7	6.8	4.3	6.1
700	13.4	0.3	1	4.7	6.1	4.4	6.3
800	12.6	0.1	1	4.9	5.3	4.6	6.8
900	10.9	0.2	1	5.7	6.1	5.4	7.8
1000	10.2	0.1	1	6.1	6.4	5.7	8.5
1100	9.3	0.0	1	6.7	7.0	6.2	9.3
1200	8.4	0.0	1	7.3	7.7	6.9	10.2
1300	6.9	0.0	0	8.7	9.5	7.9	8.6
1400	6.3	0.0	0	9.1	9.7	8.5	9.1

Table A.5

Signal efficiency, number of expected background events, events observed in data, expected (with 1σ uncertainties) and observed limit for various sbottom R -hadron mass hypotheses in the full-detector search.

$m_{\tilde{b}}$ [GeV]	Signal eff. [%]	Exp. bkg [events]	Obs. data [events]	Exp. limit [fb]	$+\sigma$ [fb]	$-\sigma$ [fb]	Obs. limit [fb]
200	6.8	97.1	94	114	164	80	107
300	8.9	22.0	18	29.9	43.2	20.8	23.0
400	10.1	6.3	5	14.2	20.5	9.9	12.0
500	10.2	1.4	2	8.2	11.9	6.3	9.8
600	11.0	0.9	2	6.7	9.5	5.5	9.8
700	10.8	0.3	1	5.9	7.8	5.3	7.8
800	10.9	0.3	1	5.8	7.3	5.4	7.7
900	10.8	0.2	1	5.7	7.2	5.5	7.9

Table A.6

Signal efficiency, number of expected background events, events observed in data, expected (with 1σ uncertainties) and observed limit for various stop R -hadron mass hypotheses in the full-detector search.

$m_{\tilde{t}}$ [GeV]	Signal eff. [%]	Exp. bkg [events]	Obs. data [events]	Exp. limit [fb]	$+\sigma$ [fb]	$-\sigma$ [fb]	Obs. limit [fb]
200	15.2	128.4	122	64	94	46	58
300	18.0	21.9	18	14.7	21.1	10.3	11.5
400	19.2	4.6	4	6.4	9.5	4.8	6.1
500	21.5	2.0	2	4.4	6.4	3.4	4.5
600	21.4	0.6	2	3.0	4.4	2.9	5.2
700	21.3	0.4	1	3.0	4.2	2.7	3.9
800	21.9	0.3	1	2.8	3.6	2.6	3.8
900	19.6	0.2	1	3.2	3.8	3.0	4.3

Table A.7

Signal efficiency, number of expected background events, events observed in data, expected (with 1σ uncertainties) and observed limit for various gluino R -hadron mass hypotheses in the MS-agnostic search.

$m_{\tilde{g}}$ [GeV]	Signal eff. [%]	Exp. bkg [events]	Obs. data [events]	Exp. limit [fb]	$+\sigma$ [fb]	$-\sigma$ [fb]	Obs. limit [fb]
200	3.2	45.2	47	138	199	100	146
300	5.9	22.2	17	44	59	32	33
400	6.2	2.1	0	11.7	14.4	9.5	9.3
500	7.9	0.7	0	7.9	9.8	7.0	7.1
600	7.8	0.7	0	8.0	9.3	7.0	7.4
700	8.3	1.1	0	7.6	9.7	6.5	6.6
800	8.0	0.8	0	9.5	10.9	7.4	11.2
900	7.0	0.0	0	8.2	8.7	7.8	8.2
1000	7.3	0.2	0	8.1	8.7	7.6	8.0
1100	7.0	0.4	0	8.3	9.9	7.8	8.0
1200	6.1	0.2	0	9.8	10.6	9.2	9.6
1300	5.5	0.2	0	10.6	11.4	9.7	10.5
1400	5.3	0.0	0	10.4	10.9	9.9	10.4

Table A.8

Signal efficiency, number of expected background events, events observed in data, expected (with 1σ uncertainties) and observed limit for various sbottom R -hadron mass hypotheses in the MS-agnostic search.

$m_{\tilde{b}}$ [GeV]	Signal eff. [%]	Exp. bkg [events]	Obs. data [events]	Exp. limit [fb]	$+\sigma$ [fb]	$-\sigma$ [fb]	Obs. limit [fb]
200	2.5	106.2	103	340	490	240	310
300	4.7	25.5	17	55	67	39	38
400	5.0	2.8	2	20.6	29.9	15.0	17.9
500	6.0	0.9	0	10.6	12.0	9.1	9.6
600	6.3	0.4	0	9.4	11.6	8.6	9.0
700	6.5	0.2	0	9.1	10.6	8.4	9.0
800	6.8	0.1	0	9.3	9.8	8.8	8.7
900	6.6	0.7	0	9.1	10.7	8.2	8.5

Table A.9

Signal efficiency, number of expected background events, events observed in data, expected (with 1σ uncertainties) and observed limit for various stop R -hadron mass hypotheses in the MS-agnostic search.

$m_{\tilde{t}}$ [GeV]	Signal eff. [%]	Exp. bkg [events]	Obs. data [events]	Exp. limit [fb]	$+\sigma$ [fb]	$-\sigma$ [fb]	Obs. limit [fb]
200	3.9	103.9	97	210	300	150	180
300	7.0	15.3	10	28.5	37.2	21.4	19.9
400	8.6	3.1	2	12.7	18.3	9.2	10.4
500	9.5	0.9	0	7.8	8.9	5.2	5.2
600	10.8	0.7	0	5.8	7.0	5.0	5.2
700	10.2	0.9	0	6.5	8.6	5.5	5.7
800	10.6	1.4	0	6.8	8.1	5.4	5.4
900	10.2	0.1	0	5.8	6.0	5.4	5.7

Open access

This article is published Open Access at sciencedirect.com. It is distributed under the terms of the Creative Commons Attribution License 3.0, which permits unrestricted use, distribution, and reproduction in any medium, provided the original authors and source are credited.

References

- [1] H. Miyazawa, Prog. Theor. Phys. 36 (6) (1966) 1266.
- [2] P. Ramond, Phys. Rev. D 3 (1971) 2415.
- [3] Y.A. Golfand, E.P. Likhtman, JETP Lett. 13 (1971) 323, Pisma Zh. Eksp. Teor. Fiz. 13 (1971) 452.
- [4] A. Neveu, J.H. Schwarz, Nucl. Phys. B 31 (1971) 86.
- [5] A. Neveu, J.H. Schwarz, Phys. Rev. D 4 (1971) 1109.
- [6] J. Gervais, B. Sakita, Nucl. Phys. B 34 (1971) 632.
- [7] D.V. Volkov, V.P. Akulov, Phys. Lett. B 46 (1973) 109.
- [8] J. Wess, B. Zumino, Phys. Lett. B 49 (1974) 52.
- [9] J. Wess, B. Zumino, Nucl. Phys. B 70 (1974) 39.
- [10] M. Dine, W. Fischler, Phys. Lett. B 110 (1982) 227.
- [11] L. Alvarez-Gaume, M. Claudson, M.B. Wise, Nucl. Phys. B 207 (1982) 96.
- [12] C.R. Nappi, B.A. Ovrut, Phys. Lett. B 113 (1982) 175.
- [13] M. Dine, A.E. Nelson, Phys. Rev. D 48 (1993) 1277.
- [14] M. Dine, A.E. Nelson, Y. Shirman, Phys. Rev. D 51 (1995) 1362.
- [15] M. Dine, A.E. Nelson, Y. Nir, Y. Shirman, Phys. Rev. D 53 (1996) 2658.
- [16] C.F. Kolda, Nucl. Phys. (Proc. Suppl.) 62 (1998) 266.
- [17] ALEPH Collaboration, R. Barate, et al., Phys. Lett. B 405 (1997) 379.
- [18] DELPHI Collaboration, P. Abreu, et al., Phys. Lett. B 478 (2000) 65.
- [19] L3 Collaboration, P. Achard, et al., Phys. Lett. B 517 (2001) 75.
- [20] OPAL Collaboration, G. Abbiendi, et al., Phys. Lett. B 572 (2003) 8.
- [21] H1 Collaboration, A. Aktas, et al., Eur. Phys. J. C 36 (2004) 413.
- [22] CDF Collaboration, F. Abe, et al., Phys. Rev. Lett. 63 (1989) 1447.
- [23] CDF Collaboration, F. Abe, et al., Phys. Rev. D 46 (1992) 1889.
- [24] CDF Collaboration, D. Acosta, et al., Phys. Rev. Lett. 90 (2003) 131801.
- [25] D0 Collaboration, V.M. Abazov, et al., Phys. Rev. Lett. 99 (2007) 131801.
- [26] D0 Collaboration, V. Abazov, et al., Phys. Rev. Lett. 102 (2009) 161802.
- [27] CDF Collaboration, T. Aaltonen, et al., Phys. Rev. Lett. 103 (2009) 021802.

- [28] D0 Collaboration, V.M. Abazov, et al., Phys. Rev. Lett. 108 (2012) 121802.
- [29] CMS Collaboration, Phys. Rev. Lett. 106 (2011) 011801.
- [30] CMS Collaboration, JHEP 1103 (2011) 024.
- [31] ATLAS Collaboration, Phys. Lett. B 698 (2011) 353.
- [32] ATLAS Collaboration, Phys. Lett. B 701 (2011) 1.
- [33] ATLAS Collaboration, Phys. Lett. B 703 (2011) 428.
- [34] ATLAS Collaboration, Eur. Phys. J. C 72 (2012) 1965.
- [35] CMS Collaboration, Search for heavy long-lived charged particles in pp collisions at $\sqrt{s} = 7$ TeV, CMS-EXO-11-022, CERN-PH-EP-2012-093.
- [36] G. Engelhard, J.L. Feng, I. Galon, D. Sanford, F. Yu, Comput. Phys. Commun. 181 (2010) 213.
- [37] G. Corcella, et al., JHEP 0101 (2001) 010.
- [38] T. Sjostrand, S. Mrenna, P. Skands, JHEP 0605 (2006) 026.
- [39] The source code for the dedicated R-hadron hadronisation routines can be downloaded from: <http://home.thep.lu.se/~torbjorn/pythiaaux/recent.html>.
- [40] A.C. Kraan, Eur. Phys. J. C 37 (2004) 91.
- [41] G. Farrar, R. Mackeprang, D. Milstead, J. Roberts, JHEP 1102 (2011) 018.
- [42] GEANT4 Collaboration, S. Agostinelli, et al., Nucl. Instrum. Meth. A 506 (2003) 250.
- [43] <http://r-hadrons.web.cern.ch/r-hadrons/>.
- [44] R. Mackeprang, D. Milstead, Eur. Phys. J. C 66 (2010) 493.
- [45] C. Alexa, S. Constantinescu, S. Dita, AIP Conf. Proc. 867 (2006) 463.
- [46] ATLAS Collaboration, JINST 3 (2008) S08003.
- [47] ATLAS Collaboration, dE/dx measurement in the ATLAS pixel detector and its use for particle identification, ATLAS-CONF-2011-016.
- [48] ATLAS Collaboration, Expected performance of the ATLAS experiment – detector, trigger and physics, CERN-OPEN-2008-020.
- [49] ATLAS Collaboration, Performance of the ATLAS muon trigger in 2011, ATLAS-CONF-2012-099.
- [50] ATLAS Collaboration, Eur. Phys. J. C 72 (2012) 1849.
- [51] D. Casadei, et al., The implementation of the ATLAS missing E_T triggers for the initial LHC operation, Tech. Rep., ATL-DAQ-PUB-2011-001, CERN, Geneva, 2011.
- [52] G. Cacciari, G.P. Salam, G. Soyez, JHEP 0804 (2008) 063.
- [53] H. Bichsel, Rev. Mod. Phys. 60 (1988) 663.
- [54] W. Beenakker, R. Hopker, M. Spira, P.M. Zerwas, Nucl. Phys. B 492 (1997) 51.
- [55] W. Beenakker, M. Kramer, T. Plehn, M. Spira, P.M. Zerwas, Nucl. Phys. B 515 (1998) 3.
- [56] A. Kulesza, L. Motyka, Phys. Rev. Lett. 102 (2009) 111802.
- [57] A. Kulesza, L. Motyka, Phys. Rev. D 80 (2009) 095004.
- [58] W. Beenakker, S. Brensing, M. Kramer, A. Kulesza, E. Laenen, et al., JHEP 0912 (2009) 041.
- [59] W. Beenakker, S. Brensing, M. Kramer, A. Kulesza, E. Laenen, I. Niessen, JHEP 1008 (2010) 098.
- [60] W. Beenakker, S. Brensing, M. Kramer, A. Kulesza, E. Laenen, et al., Int. J. Mod. Phys. A 26 (2011) 2637.
- [61] M. Kramer, A. Kulesza, R. van der Leeuw, M. Mangano, S. Padhi, et al., Super-symmetry production cross sections in pp collisions at $\sqrt{s} = 7$ TeV, CERN-PH-TH-2012-163.
- [62] P.Z. Skands, Phys. Rev. D 82 (2010) 074018.
- [63] ATLAS Collaboration, Jet energy measurement with the ATLAS detector in proton–proton collisions, at $\sqrt{s} = 7$ TeV.
- [64] ATLAS Collaboration, Muon reconstruction efficiency in reprocessed 2010 LHC proton–proton collision data recorded with the ATLAS detector, ATLAS-CONF-2011-063.
- [65] ATLAS Collaboration, Luminosity determination in pp collisions at $\sqrt{s} = 7$ TeV using the ATLAS detector in 2011, ATLAS-CONF-2011-116.
- [66] ATLAS Collaboration, Eur. Phys. J. C 71 (2011) 1630.
- [67] A.L. Read, J. Phys. G 28 (2002) 2693.

ATLAS Collaboration

G. Aad⁴⁸, T. Abajyan²¹, B. Abbott¹¹¹, J. Abdallah¹², S. Abdel Khalek¹¹⁵, A.A. Abdelalim⁴⁹, O. Abdinov¹¹, R. Aben¹⁰⁵, B. Abi¹¹², M. Abolins⁸⁸, O.S. AbouZeid¹⁵⁸, H. Abramowicz¹⁵³, H. Abreu¹³⁶, B.S. Acharya^{164a,164b}, L. Adamczyk³⁸, D.L. Adams²⁵, T.N. Addy⁵⁶, J. Adelman¹⁷⁶, S. Adomeit⁹⁸, P. Adragna⁷⁵, T. Adye¹²⁹, S. Aefsky²³, J.A. Aguilar-Saavedra^{124b,a}, M. Agustoni¹⁷, M. Aharrouche⁸¹, S.P. Ahlen²², F. Ahles⁴⁸, A. Ahmad¹⁴⁸, M. Ahsan⁴¹, G. Aielli^{133a,133b}, T. Akdogan^{19a}, T.P.A. Åkesson⁷⁹, G. Akimoto¹⁵⁵, A.V. Akimov⁹⁴, M.S. Alam², M.A. Alam⁷⁶, J. Albert¹⁶⁹, S. Albrand⁵⁵, M. Aleksa³⁰, I.N. Aleksandrov⁶⁴, F. Alessandria^{89a}, C. Alexa^{26a}, G. Alexander¹⁵³, G. Alexandre⁴⁹, T. Alexopoulos¹⁰, M. Alhroob^{164a,164c}, M. Aliev¹⁶, G. Alimonti^{89a}, J. Alison¹²⁰, B.M.M. Allbrooke¹⁸, P.P. Allport⁷³, S.E. Allwood-Spiers⁵³, J. Almond⁸², A. Aloisio^{102a,102b}, R. Alon¹⁷², A. Alonso⁷⁹, F. Alonso⁷⁰, A. Altheimer³⁵, B. Alvarez Gonzalez⁸⁸, M.G. Alviggi^{102a,102b}, K. Amako⁶⁵, C. Amelung²³, V.V. Ammosov^{128,*}, S.P. Amor Dos Santos^{124a}, A. Amorim^{124a,b}, N. Amram¹⁵³, C. Anastopoulos³⁰, L.S. Ancu¹⁷, N. Andari¹¹⁵, T. Andeen³⁵, C.F. Anders^{58b}, G. Anders^{58a}, K.J. Anderson³¹, A. Andreazza^{89a,89b}, V. Andrei^{58a}, M-L. Andrieux⁵⁵, X.S. Anduaga⁷⁰, P. Anger⁴⁴, A. Angerami³⁵, F. Anghinolfi³⁰, A. Anisenkov¹⁰⁷, N. Anjos^{124a}, A. Annovi⁴⁷, A. Antonaki⁹, M. Antonelli⁴⁷, A. Antonov⁹⁶, J. Antos^{144b}, F. Anulli^{132a}, M. Aoki¹⁰¹, S. Aoun⁸³, L. Aperio Bella⁵, R. Apolle^{118,c}, G. Arabidze⁸⁸, I. Aracena¹⁴³, Y. Arai⁶⁵, A.T.H. Arce⁴⁵, S. Arfaoui¹⁴⁸, J-F. Arguin¹⁵, E. Arik^{19a,*}, M. Arik^{19a}, A.J. Armbruster⁸⁷, O. Arnaez⁸¹, V. Arnal⁸⁰, C. Arnault¹¹⁵, A. Artamonov⁹⁵, G. Artoni^{132a,132b}, D. Arutinov²¹, S. Asai¹⁵⁵, R. Asfandiyarov¹⁷³, S. Ask²⁸, B. Åsman^{146a,146b}, L. Asquith⁶, K. Assamagan²⁵, A. Astbury¹⁶⁹, M. Atkinson¹⁶⁵, B. Aubert⁵, E. Auge¹¹⁵, K. Augsten¹²⁷, M. Auresseau^{145a}, G. Avolio¹⁶³, R. Avramidou¹⁰, D. Axen¹⁶⁸, G. Azuelos^{93,d}, Y. Azuma¹⁵⁵, M.A. Baak³⁰, G. Baccaglioni^{89a}, C. Bacci^{134a,134b}, A.M. Bach¹⁵, H. Bachacou¹³⁶, K. Bachas³⁰, M. Backes⁴⁹, M. Backhaus²¹, E. Badescu^{26a}, P. Bagnaia^{132a,132b}, S. Bahinipati³, Y. Bai^{33a}, D.C. Bailey¹⁵⁸, T. Bain¹⁵⁸, J.T. Baines¹²⁹, O.K. Baker¹⁷⁶, M.D. Baker²⁵, S. Baker⁷⁷, E. Banas³⁹, P. Banerjee⁹³, Sw. Banerjee¹⁷³, D. Banfi³⁰, A. Bangert¹⁵⁰, V. Bansal¹⁶⁹, H.S. Bansil¹⁸, L. Barak¹⁷², S.P. Baranov⁹⁴, A. Barbaro Galtieri¹⁵, T. Barber⁴⁸, E.L. Barberio⁸⁶, D. Barberis^{50a,50b}, M. Barbero²¹, D.Y. Bardin⁶⁴, T. Barillari⁹⁹, M. Barisonzi¹⁷⁵, T. Barklow¹⁴³, N. Barlow²⁸, B.M. Barnett¹²⁹, R.M. Barnett¹⁵, A. Baroncelli^{134a}, G. Barone⁴⁹, A.J. Barr¹¹⁸, F. Barreiro⁸⁰, J. Barreiro Guimarães da Costa⁵⁷, P. Barrillon¹¹⁵, R. Bartoldus¹⁴³, A.E. Barton⁷¹, V. Bartsch¹⁴⁹, A. Basye¹⁶⁵, R.L. Bates⁵³, L. Batkova^{144a}, J.R. Batley²⁸, A. Battaglia¹⁷, M. Battistin³⁰, F. Bauer¹³⁶, H.S. Bawa^{143,e}, S. Beale⁹⁸, T. Beau⁷⁸, P.H. Beauchemin¹⁶¹, R. Beccherle^{50a}, P. Bechtel²¹, H.P. Beck¹⁷, A.K. Becker¹⁷⁵, S. Becker⁹⁸, M. Beckingham¹³⁸, K.H. Becks¹⁷⁵, A.J. Beddall^{19c}, A. Beddall^{19c},

S. Bedikian¹⁷⁶, V.A. Bednyakov⁶⁴, C.P. Bee⁸³, L.J. Beemster¹⁰⁵, M. Begel²⁵, S. Behar Harpaz¹⁵², P.K. Behera⁶², M. Beimforde⁹⁹, C. Belanger-Champagne⁸⁵, P.J. Bell⁴⁹, W.H. Bell⁴⁹, G. Bella¹⁵³, L. Bellagamba^{20a}, F. Bellina³⁰, M. Bellomo³⁰, A. Belloni⁵⁷, O. Beloborodova^{107,f}, K. Belotskiy⁹⁶, O. Beltramello³⁰, O. Benary¹⁵³, D. Benchekroun^{135a}, K. Bendtz^{146a,146b}, N. Benekos¹⁶⁵, Y. Benhammou¹⁵³, E. Benhar Noccioli⁴⁹, J.A. Benitez Garcia^{159b}, D.P. Benjamin⁴⁵, M. Benoit¹¹⁵, J.R. Bensinger²³, K. Benslama¹³⁰, S. Bentvelsen¹⁰⁵, D. Berge³⁰, E. Bergeaas Kuutmann⁴², N. Berger⁵, F. Berghaus¹⁶⁹, E. Berglund¹⁰⁵, J. Beringer¹⁵, P. Bernat⁷⁷, R. Bernhard⁴⁸, C. Bernius²⁵, T. Berry⁷⁶, C. Bertella⁸³, A. Bertin^{20a,20b}, F. Bertolucci^{122a,122b}, M.I. Besana^{89a,89b}, G.J. Besjes¹⁰⁴, N. Besson¹³⁶, S. Bethke⁹⁹, W. Bhimji⁴⁶, R.M. Bianchi³⁰, M. Bianco^{72a,72b}, O. Biebel⁹⁸, S.P. Bieniek⁷⁷, K. Bierwagen⁵⁴, J. Biesiada¹⁵, M. Biglietti^{134a}, H. Bilokon⁴⁷, M. Bindi^{20a,20b}, S. Binet¹¹⁵, A. Bingul^{19c}, C. Bini^{132a,132b}, C. Biscarat¹⁷⁸, B. Bittner⁹⁹, K.M. Black²², R.E. Blair⁶, J.-B. Blanchard¹³⁶, G. Blanchot³⁰, T. Blazek^{144a}, I. Bloch⁴², C. Blocker²³, J. Blocki³⁹, A. Blondel⁴⁹, W. Blum⁸¹, U. Blumenschein⁵⁴, G.J. Bobbink¹⁰⁵, V.B. Bobrovnikov¹⁰⁷, S.S. Bocchetta⁷⁹, A. Bocci⁴⁵, C.R. Boddy¹¹⁸, M. Boehler⁴⁸, J. Boek¹⁷⁵, N. Boelaert³⁶, J.A. Bogaerts³⁰, A. Bogdanchikov¹⁰⁷, A. Bogouch^{90,*}, C. Bohm^{146a}, J. Bohm¹²⁵, V. Boisvert⁷⁶, T. Bold³⁸, V. Boldea^{26a}, N.M. Bolnet¹³⁶, M. Bomben⁷⁸, M. Bona⁷⁵, M. Boonekamp¹³⁶, S. Bordoni⁷⁸, C. Borer¹⁷, A. Borisov¹²⁸, G. Borissov⁷¹, I. Borjanovic^{13a}, M. Borri⁸², S. Borroni⁸⁷, V. Bortolotto^{134a,134b}, K. Bos¹⁰⁵, D. Boscherini^{20a}, M. Bosman¹², H. Boterenbrood¹⁰⁵, J. Bouchami⁹³, J. Boudreau¹²³, E.V. Bouhova-Thacker⁷¹, D. Boumediene³⁴, C. Bourdarios¹¹⁵, N. Bousson⁸³, A. Boveia³¹, J. Boyd³⁰, I.R. Boyko⁶⁴, I. Bozovic-Jelisavcic^{13b}, J. Bracinik¹⁸, P. Branchini^{134a}, G.W. Brandenburg⁵⁷, A. Brandt⁸, G. Brandt¹¹⁸, O. Brandt⁵⁴, U. Bratzler¹⁵⁶, B. Brau⁸⁴, J.E. Brau¹¹⁴, H.M. Braun^{175,*}, S.F. Brazzale^{164a,164c}, B. Brelier¹⁵⁸, J. Bremer³⁰, K. Brendlinger¹²⁰, R. Brenner¹⁶⁶, S. Bressler¹⁷², D. Britton⁵³, F.M. Brochu²⁸, I. Brock²¹, R. Brock⁸⁸, F. Broggi^{89a}, C. Bromberg⁸⁸, J. Bronner⁹⁹, G. Brooijmans³⁵, T. Brooks⁷⁶, W.K. Brooks^{32b}, G. Brown⁸², H. Brown⁸, P.A. Bruckman de Renstrom³⁹, D. Bruncko^{144b}, R. Bruneliere⁴⁸, S. Brunet⁶⁰, A. Bruni^{20a}, G. Bruni^{20a}, M. Bruschi^{20a}, T. Buanes¹⁴, Q. Buat⁵⁵, F. Bucci⁴⁹, J. Buchanan¹¹⁸, P. Buchholz¹⁴¹, R.M. Buckingham¹¹⁸, A.G. Buckley⁴⁶, S.I. Buda^{26a}, I.A. Budagov⁶⁴, B. Budick¹⁰⁸, V. Büscher⁸¹, L. Bugge¹¹⁷, O. Bulekov⁹⁶, A.C. Bundock⁷³, M. Bunse⁴³, T. Buran¹¹⁷, H. Burckhart³⁰, S. Burdin⁷³, T. Burgess¹⁴, S. Burke¹²⁹, E. Busato³⁴, P. Bussey⁵³, C.P. Buszello¹⁶⁶, B. Butler¹⁴³, J.M. Butler²², C.M. Buttar⁵³, J.M. Butterworth⁷⁷, W. Buttinger²⁸, M. Byszewski³⁰, S. Cabrera Urbán¹⁶⁷, D. Caforio^{20a,20b}, O. Cakir^{4a}, P. Calafiura¹⁵, G. Calderini⁷⁸, P. Calfayan⁹⁸, R. Calkins¹⁰⁶, L.P. Caloba^{24a}, R. Caloi^{132a,132b}, D. Calvet³⁴, S. Calvet³⁴, R. Camacho Toro³⁴, P. Camarri^{133a,133b}, D. Cameron¹¹⁷, L.M. Caminada¹⁵, R. Caminal Armadans¹², S. Campana³⁰, M. Campanelli⁷⁷, V. Canale^{102a,102b}, F. Canelli^{31,g}, A. Canepa^{159a}, J. Cantero⁸⁰, R. Cantrill⁷⁶, L. Capasso^{102a,102b}, M.D.M. Capeans Garrido³⁰, I. Caprini^{26a}, M. Caprini^{26a}, D. Capriotti⁹⁹, M. Capua^{37a,37b}, R. Caputo⁸¹, R. Cardarelli^{133a}, T. Carli³⁰, G. Carlino^{102a}, L. Carminati^{89a,89b}, B. Caron⁸⁵, S. Caron¹⁰⁴, E. Carquin^{32b}, G.D. Carrillo-Montoya¹⁷³, A.A. Carter⁷⁵, J.R. Carter²⁸, J. Carvalho^{124a,h}, D. Casadei¹⁰⁸, M.P. Casado¹², M. Cascella^{122a,122b}, C. Caso^{50a,50b,*}, A.M. Castaneda Hernandez^{173,i}, E. Castaneda-Miranda¹⁷³, V. Castillo Gimenez¹⁶⁷, N.F. Castro^{124a}, G. Cataldi^{72a}, P. Catastini⁵⁷, A. Catinaccio³⁰, J.R. Catmore³⁰, A. Cattai³⁰, G. Cattani^{133a,133b}, S. Caughron⁸⁸, V. Cavaliere¹⁶⁵, P. Cavalleri⁷⁸, D. Cavalli^{89a}, M. Cavalli-Sforza¹², V. Cavasinni^{122a,122b}, F. Ceradini^{134a,134b}, A.S. Cerqueira^{24b}, A. Cerri³⁰, L. Cerrito⁷⁵, F. Cerutti⁴⁷, S.A. Cetin^{19b}, A. Chafaq^{135a}, D. Chakraborty¹⁰⁶, I. Chalupkova¹²⁶, K. Chan³, P. Chang¹⁶⁵, B. Chapleau⁸⁵, J.D. Chapman²⁸, J.W. Chapman⁸⁷, E. Chareyre⁷⁸, D.G. Charlton¹⁸, V. Chavda⁸², C.A. Chavez Barajas³⁰, S. Cheatham⁸⁵, S. Chekanov⁶, S.V. Chekulaev^{159a}, G.A. Chelkov⁶⁴, M.A. Chelstowska¹⁰⁴, C. Chen⁶³, H. Chen²⁵, S. Chen^{33c}, X. Chen¹⁷³, Y. Chen³⁵, A. Cheplakov⁶⁴, R. Cherkaoui El Moursli^{135e}, V. Chernyatin²⁵, E. Cheu⁷, S.L. Cheung¹⁵⁸, L. Chevalier¹³⁶, G. Chiefari^{102a,102b}, L. Chikovani^{51a,*}, J.T. Childers³⁰, A. Chilingarov⁷¹, G. Chiodini^{72a}, A.S. Chisholm¹⁸, R.T. Chislett⁷⁷, A. Chitan^{26a}, M.V. Chizhov⁶⁴, G. Choudalakis³¹, S. Chouridou¹³⁷, I.A. Christidi⁷⁷, A. Christov⁴⁸, D. Chromek-Burckhart³⁰, M.L. Chu¹⁵¹, J. Chudoba¹²⁵, G. Ciapetti^{132a,132b}, A.K. Ciftci^{4a}, R. Ciftci^{4a}, D. Cinca³⁴, V. Cindro⁷⁴, C. Ciocca^{20a,20b}, A. Ciocio¹⁵, M. Cirilli⁸⁷, P. Cirkovic^{13b}, Z.H. Citron¹⁷², M. Citterio^{89a}, M. Ciubancan^{26a}, A. Clark⁴⁹, P.J. Clark⁴⁶, R.N. Clarke¹⁵, W. Cleland¹²³, J.C. Clemens⁸³, B. Clement⁵⁵, C. Clement^{146a,146b}, Y. Coadou⁸³, M. Cobal^{164a,164c}, A. Coccaro¹³⁸, J. Cochran⁶³, L. Coffey²³, J.G. Cogan¹⁴³, J. Coggeshall¹⁶⁵, E. Cogneras¹⁷⁸, J. Colas⁵, S. Cole¹⁰⁶, A.P. Colijn¹⁰⁵, N.J. Collins¹⁸, C. Collins-Tooth⁵³, J. Collot⁵⁵, T. Colombo^{119a,119b}, G. Colon⁸⁴, P. Conde Muiño^{124a},

E. Coniavitis¹¹⁸, M.C. Conidi¹², S.M. Consonni^{89a,89b}, V. Consorti⁴⁸, S. Constantinescu^{26a},
 C. Conta^{119a,119b}, G. Conti⁵⁷, F. Conventi^{102a,j}, M. Cooke¹⁵, B.D. Cooper⁷⁷, A.M. Cooper-Sarkar¹¹⁸,
 K. Copic¹⁵, T. Cornelissen¹⁷⁵, M. Corradi^{20a}, F. Corriveau^{85,k}, A. Cortes-Gonzalez¹⁶⁵, G. Cortiana⁹⁹,
 G. Costa^{89a}, M.J. Costa¹⁶⁷, D. Costanzo¹³⁹, D. Côté³⁰, L. Courneyea¹⁶⁹, G. Cowan⁷⁶, C. Cowden²⁸,
 B.E. Cox⁸², K. Cranmer¹⁰⁸, F. Crescioli^{122a,122b}, M. Cristinziani²¹, G. Crosetti^{37a,37b}, S. Crépe-Renaudin⁵⁵,
 C.-M. Cuciuc^{26a}, C. Cuenca Almenar¹⁷⁶, T. Cuhadar Donszelmann¹³⁹, M. Curatolo⁴⁷, C.J. Curtis¹⁸,
 C. Cuthbert¹⁵⁰, P. Cwetanski⁶⁰, H. Czirr¹⁴¹, P. Czodrowski⁴⁴, Z. Czyzula¹⁷⁶, S. D'Auria⁵³,
 M. D'Onofrio⁷³, A. D'Orazio^{132a,132b}, M.J. Da Cunha Sargedas De Sousa^{124a}, C. Da Via⁸²,
 W. Dabrowski³⁸, A. Dafinca¹¹⁸, T. Dai⁸⁷, C. Dallapiccola⁸⁴, M. Dam³⁶, M. Dameri^{50a,50b},
 D.S. Damiani¹³⁷, H.O. Danielsson³⁰, V. Dao⁴⁹, G. Darbo^{50a}, G.L. Darlea^{26b}, J.A. Dassoulas⁴², W. Davey²¹,
 T. Davidek¹²⁶, N. Davidson⁸⁶, R. Davidson⁷¹, E. Davies^{118,c}, M. Davies⁹³, O. Davignon⁷⁸, A.R. Davison⁷⁷,
 Y. Davygora^{58a}, E. Dawe¹⁴², I. Dawson¹³⁹, R.K. Daya-Ishmukhametova²³, K. De⁸, R. de Asmundis^{102a},
 S. De Castro^{20a,20b}, S. De Cecco⁷⁸, J. de Graat⁹⁸, N. De Groot¹⁰⁴, P. de Jong¹⁰⁵, C. De La Taille¹¹⁵,
 H. De la Torre⁸⁰, F. De Lorenzi⁶³, L. de Mora⁷¹, L. De Nooij¹⁰⁵, D. De Pedis^{132a}, A. De Salvo^{132a},
 U. De Sanctis^{164a,164c}, A. De Santo¹⁴⁹, J.B. De Vivie De Regie¹¹⁵, G. De Zorzi^{132a,132b}, W.J. Dearnaley⁷¹,
 R. Debbe²⁵, C. Debenedetti⁴⁶, B. Dechenaux⁵⁵, D.V. Dedovich⁶⁴, J. Degenhardt¹²⁰, C. Del Papa^{164a,164c},
 J. Del Peso⁸⁰, T. Del Prete^{122a,122b}, T. Delemontex⁵⁵, M. Deliyergiyev⁷⁴, A. Dell'Acqua³⁰, L. Dell'Asta²²,
 M. Della Pietra^{102a,j}, D. della Volpe^{102a,102b}, M. Delmastro⁵, P.A. Delsart⁵⁵, C. Deluca¹⁰⁵, S. Demers¹⁷⁶,
 M. Demichev⁶⁴, B. Demirköz^{12,l}, J. Deng¹⁶³, S.P. Denisov¹²⁸, D. Derendarz³⁹, J.E. Derkaoui^{135d},
 F. Derue⁷⁸, P. Dervan⁷³, K. Desch²¹, E. Devetak¹⁴⁸, P.O. Deviveiros¹⁰⁵, A. Dewhurst¹²⁹, B. DeWilde¹⁴⁸,
 S. Dhaliwal¹⁵⁸, R. Dhullipudi^{25,m}, A. Di Ciaccio^{133a,133b}, L. Di Ciaccio⁵, A. Di Girolamo³⁰,
 B. Di Girolamo³⁰, S. Di Luise^{134a,134b}, A. Di Mattia¹⁷³, B. Di Micco³⁰, R. Di Nardo⁴⁷,
 A. Di Simone^{133a,133b}, R. Di Sipio^{20a,20b}, M.A. Diaz^{32a}, E.B. Diehl⁸⁷, J. Dietrich⁴², T.A. Dietzsch^{58a},
 S. Diglio⁸⁶, K. Dindar Yagci⁴⁰, J. Dingfelder²¹, F. Dinut^{26a}, C. Dionisi^{132a,132b}, P. Dita^{26a}, S. Dita^{26a},
 F. Dittus³⁰, F. Djama⁸³, T. Djobava^{51b}, M.A.B. do Vale^{24c}, A. Do Valle Wemans^{124a,n}, T.K.O. Doan⁵,
 M. Dobbs⁸⁵, R. Dobinson^{30,*}, D. Dobos³⁰, E. Dobson^{30,o}, J. Dodd³⁵, C. Doglioni⁴⁹, T. Doherty⁵³,
 Y. Doi^{65,*}, J. Dolejsi¹²⁶, I. Dolenc⁷⁴, Z. Dolezal¹²⁶, B.A. Dolgoshein^{96,*}, T. Dohmae¹⁵⁵, M. Donadelli^{24d},
 J. Donini³⁴, J. Dopke³⁰, A. Doria^{102a}, A. Dos Anjos¹⁷³, A. Dotti^{122a,122b}, M.T. Dova⁷⁰, A.D. Doxiadis¹⁰⁵,
 A.T. Doyle⁵³, N. Dressnandt¹²⁰, M. Dris¹⁰, J. Dubbert⁹⁹, S. Dube¹⁵, E. Duchovni¹⁷², G. Duckeck⁹⁸,
 D. Duda¹⁷⁵, A. Dudarev³⁰, F. Dudziak⁶³, M. Dührssen³⁰, I.P. Duerdoth⁸², L. Duflot¹¹⁵, M.-A. Dufour⁸⁵,
 L. Duguid⁷⁶, M. Dunford³⁰, H. Duran Yildiz^{4a}, R. Duxfield¹³⁹, M. Dwuznik³⁸, F. Dydak³⁰, M. Düren⁵²,
 W.L. Ebenstein⁴⁵, J. Ebke⁹⁸, S. Eckweiler⁸¹, K. Edmonds⁸¹, W. Edson², C.A. Edwards⁷⁶, N.C. Edwards⁵³,
 W. Ehrenfeld⁴², T. Eifert¹⁴³, G. Eigen¹⁴, K. Einsweiler¹⁵, E. Eisenhandler⁷⁵, T. Ekelof¹⁶⁶,
 M. El Kacimi^{135c}, M. Ellert¹⁶⁶, S. Elles⁵, F. Ellinghaus⁸¹, K. Ellis⁷⁵, N. Ellis³⁰, J. Elmsheuser⁹⁸,
 M. Elsing³⁰, D. Emelianov¹²⁹, R. Engelmann¹⁴⁸, A. Engl⁹⁸, B. Epp⁶¹, J. Erdmann⁵⁴, A. Ereditato¹⁷,
 D. Eriksson^{146a}, J. Ernst², M. Ernst²⁵, J. Ernwein¹³⁶, D. Errede¹⁶⁵, S. Errede¹⁶⁵, E. Ertel⁸¹,
 M. Escalier¹¹⁵, H. Esch⁴³, C. Escobar¹²³, X. Espinal Curull¹², B. Esposito⁴⁷, F. Etienne⁸³, A.I. Etienvre¹³⁶,
 E. Etzion¹⁵³, D. Evangelakou⁵⁴, H. Evans⁶⁰, L. Fabbri^{20a,20b}, C. Fabre³⁰, R.M. Fakhruddinov¹²⁸,
 S. Falciano^{132a}, Y. Fang¹⁷³, M. Fanti^{89a,89b}, A. Farbin⁸, A. Farilla^{134a}, J. Farley¹⁴⁸, T. Farooque¹⁵⁸,
 S. Farrell¹⁶³, S.M. Farrington¹⁷⁰, P. Farthouat³⁰, F. Fassi¹⁶⁷, P. Fassnacht³⁰, D. Fassouliotis⁹,
 B. Fathollahzadeh¹⁵⁸, A. Favareto^{89a,89b}, L. Fayard¹¹⁵, S. Fazio^{37a,37b}, R. Febbraro³⁴, P. Federic^{144a},
 O.L. Fedin¹²¹, W. Fedorko⁸⁸, M. Fehling-Kaschek⁴⁸, L. Feligioni⁸³, D. Fellmann⁶, C. Feng^{33d}, E.J. Feng⁶,
 A.B. Fenyuk¹²⁸, J. Ferencei^{144b}, W. Fernando⁶, S. Ferrag⁵³, J. Ferrando⁵³, V. Ferrara⁴², A. Ferrari¹⁶⁶,
 P. Ferrari¹⁰⁵, R. Ferrari^{119a}, D.E. Ferreira de Lima⁵³, A. Ferrer¹⁶⁷, D. Ferrere⁴⁹, C. Ferretti⁸⁷,
 A. Ferretto Parodi^{50a,50b}, M. Fiascaris³¹, F. Fiedler⁸¹, A. Filipčič⁷⁴, F. Filthaut¹⁰⁴, M. Fincke-Keeler¹⁶⁹,
 M.C.N. Fiolhais^{124a,h}, L. Fiorini¹⁶⁷, A. Firan⁴⁰, G. Fischer⁴², M.J. Fisher¹⁰⁹, M. Flechl⁴⁸, I. Fleck¹⁴¹,
 J. Fleckner⁸¹, P. Fleischmann¹⁷⁴, S. Fleischmann¹⁷⁵, T. Flick¹⁷⁵, A. Floderus⁷⁹, L.R. Flores Castillo¹⁷³,
 M.J. Flowerdew⁹⁹, T. Fonseca Martin¹⁷, A. Formica¹³⁶, A. Forti⁸², D. Fortin^{159a}, D. Fournier¹¹⁵,
 A.J. Fowler⁴⁵, H. Fox⁷¹, P. Francavilla¹², M. Franchini^{20a,20b}, S. Franchino^{119a,119b}, D. Francis³⁰,
 T. Frank¹⁷², S. Franz³⁰, M. Fraternali^{119a,119b}, S. Fratina¹²⁰, S.T. French²⁸, C. Friedrich⁴², F. Friedrich⁴⁴,
 R. Froeschl³⁰, D. Froidevaux³⁰, J.A. Frost²⁸, C. Fukunaga¹⁵⁶, E. Fullana Torregrosa³⁰, B.G. Fulsom¹⁴³,
 J. Fuster¹⁶⁷, C. Gabaldon³⁰, O. Gabizon¹⁷², T. Gadfort²⁵, S. Gadomski⁴⁹, G. Gagliardi^{50a,50b}, P. Gagnon⁶⁰,

C. Galea⁹⁸, B. Galhardo^{124a}, E.J. Gallas¹¹⁸, V. Gallo¹⁷, B.J. Gallop¹²⁹, P. Gallus¹²⁵, K.K. Gan¹⁰⁹, Y.S. Gao^{143,e}, A. Gaponenko¹⁵, F. Garbersen¹⁷⁶, M. Garcia-Sciveres¹⁵, C. García¹⁶⁷, J.E. García Navarro¹⁶⁷, R.W. Gardner³¹, N. Garelli³⁰, H. Garitaonandia¹⁰⁵, V. Garonne³⁰, C. Gatti⁴⁷, G. Gaudio^{119a}, B. Gaur¹⁴¹, L. Gauthier¹³⁶, P. Gauzzi^{132a,132b}, I.L. Gavrilenko⁹⁴, C. Gay¹⁶⁸, G. Gaycken²¹, E.N. Gazis¹⁰, P. Ge^{33d}, Z. Gece¹⁶⁸, C.N.P. Gee¹²⁹, D.A.A. Geerts¹⁰⁵, Ch. Geich-Gimbel²¹, K. Gellerstedt^{146a,146b}, C. Gemme^{50a}, A. Gemmell⁵³, M.H. Genest⁵⁵, S. Gentile^{132a,132b}, M. George⁵⁴, S. George⁷⁶, P. Gerlach¹⁷⁵, A. Gershon¹⁵³, C. Geweniger^{58a}, H. Ghazlane^{135b}, N. Ghodbane³⁴, B. Giacobbe^{20a}, S. Giagu^{132a,132b}, V. Giakoumopoulou⁹, V. Giangiobbe¹², F. Gianotti³⁰, B. Gibbard²⁵, A. Gibson¹⁵⁸, S.M. Gibson³⁰, M. Gilchriese¹⁵, D. Gillberg²⁹, A.R. Gillman¹²⁹, D.M. Gingrich^{3,d}, J. Ginzburg¹⁵³, N. Giokaris⁹, M.P. Giordani^{164c}, R. Giordano^{102a,102b}, F.M. Giorgi¹⁶, P. Giovannini⁹⁹, P.F. Giraud¹³⁶, D. Giugni^{89a}, M. Giunta⁹³, P. Giusti^{20a}, B.K. Gjelsten¹¹⁷, L.K. Gladilin⁹⁷, C. Glasman⁸⁰, J. Glatzer⁴⁸, A. Glazov⁴², K.W. Glitza¹⁷⁵, G.L. Glonti⁶⁴, J.R. Goddard⁷⁵, J. Godfrey¹⁴², J. Godlewski³⁰, M. Goebel⁴², T. Göpfert⁴⁴, C. Goeringer⁸¹, C. Gössling⁴³, S. Goldfarb⁸⁷, T. Golling¹⁷⁶, A. Gomes^{124a,b}, L.S. Gomez Fajardo⁴², R. Gonçalo⁷⁶, J. Goncalves Pinto Firmino Da Costa⁴², L. Gonella²¹, S. González de la Hoz¹⁶⁷, G. Gonzalez Parra¹², M.L. Gonzalez Silva²⁷, S. Gonzalez-Sevilla⁴⁹, J.J. Goodson¹⁴⁸, L. Goossens³⁰, P.A. Gorbounov⁹⁵, H.A. Gordon²⁵, I. Gorelov¹⁰³, G. Gorfine¹⁷⁵, B. Gorini³⁰, E. Gorini^{72a,72b}, A. Gorišek⁷⁴, E. Gornicki³⁹, B. Gosdzik⁴², A.T. Goshaw⁶, M. Gosselink¹⁰⁵, M.I. Gostkin⁶⁴, I. Gough Eschrich¹⁶³, M. Gouighri^{135a}, D. Goujdami^{135c}, M.P. Goulette⁴⁹, A.G. Goussiou¹³⁸, C. Goy⁵, S. Gozpinar²³, I. Grabowska-Bold³⁸, P. Grafström^{20a,20b}, K-J. Grahm⁴², F. Grancagnolo^{72a}, S. Grancagnolo¹⁶, V. Grassi¹⁴⁸, V. Gratchev¹²¹, N. Grau³⁵, H.M. Gray³⁰, J.A. Gray¹⁴⁸, E. Graziani^{134a}, O.G. Grebenyuk¹²¹, T. Greenshaw⁷³, Z.D. Greenwood^{25,m}, K. Gregersen³⁶, I.M. Gregor⁴², P. Grenier¹⁴³, J. Griffiths⁸, N. Grigalashvili⁶⁴, A.A. Grillo¹³⁷, S. Grinstein¹², Ph. Gris³⁴, Y.V. Grishkevich⁹⁷, J.-F. Grivaz¹¹⁵, E. Gross¹⁷², J. Grosse-Knetter⁵⁴, J. Groth-Jensen¹⁷², K. Grybel¹⁴¹, D. Guest¹⁷⁶, C. Guicheney³⁴, E. Guido^{50a,50b}, S. Guindon⁵⁴, U. Gul⁵³, H. Guler^{85,p}, J. Gunther¹²⁵, B. Guo¹⁵⁸, J. Guo³⁵, P. Gutierrez¹¹¹, N. Guttman¹⁵³, O. Gutzwiller¹⁷³, C. Guyot¹³⁶, C. Gwenlan¹¹⁸, C.B. Gwilliam⁷³, A. Haas¹⁴³, S. Haas³⁰, C. Haber¹⁵, H.K. Hadavand⁴⁰, D.R. Hadley¹⁸, P. Haefner²¹, F. Hahn³⁰, S. Haider³⁰, Z. Hajduk³⁹, H. Hakobyan¹⁷⁷, D. Hall¹¹⁸, J. Haller⁵⁴, K. Hamacher¹⁷⁵, P. Hamal¹¹³, K. Hamano⁸⁶, M. Hamer⁵⁴, A. Hamilton^{145b,q}, S. Hamilton¹⁶¹, L. Han^{33b}, K. Hanagaki¹¹⁶, K. Hanawa¹⁶⁰, M. Hance¹⁵, C. Handel⁸¹, P. Hanke^{58a}, J.R. Hansen³⁶, J.B. Hansen³⁶, J.D. Hansen³⁶, P.H. Hansen³⁶, P. Hansson¹⁴³, K. Hara¹⁶⁰, G.A. Hare¹³⁷, T. Harenberg¹⁷⁵, S. Harkusha⁹⁰, D. Harper⁸⁷, R.D. Harrington⁴⁶, O.M. Harris¹³⁸, J. Hartert⁴⁸, F. Hartjes¹⁰⁵, T. Haruyama⁶⁵, A. Harvey⁵⁶, S. Hasegawa¹⁰¹, Y. Hasegawa¹⁴⁰, S. Hassani¹³⁶, S. Haug¹⁷, M. Hauschild³⁰, R. Hauser⁸⁸, M. Havranek²¹, C.M. Hawkes¹⁸, R.J. Hawking³⁰, A.D. Hawkins⁷⁹, T. Hayakawa⁶⁶, T. Hayashi¹⁶⁰, D. Hayden⁷⁶, C.P. Hays¹¹⁸, H.S. Hayward⁷³, S.J. Haywood¹²⁹, S.J. Head¹⁸, V. Hedberg⁷⁹, L. Heelan⁸, S. Heim⁸⁸, B. Heinemann¹⁵, S. Heisterkamp³⁶, L. Helary²², C. Heller⁹⁸, M. Heller³⁰, S. Hellman^{146a,146b}, D. Hellmich²¹, C. Helsens¹², R.C.W. Henderson⁷¹, M. Henke^{58a}, A. Henrichs⁵⁴, A.M. Henriques Correia³⁰, S. Henrot-Versille¹¹⁵, C. Hensel⁵⁴, T. Henß¹⁷⁵, C.M. Hernandez⁸, Y. Hernández Jiménez¹⁶⁷, R. Herrberg¹⁶, G. Herten⁴⁸, R. Hertenberger⁹⁸, L. Hervas³⁰, G.G. Hesketh⁷⁷, N.P. Hessey¹⁰⁵, E. Higón-Rodríguez¹⁶⁷, J.C. Hill²⁸, K.H. Hiller⁴², S. Hillert²¹, S.J. Hillier¹⁸, I. Hinchliffe¹⁵, E. Hines¹²⁰, M. Hirose¹¹⁶, F. Hirsch⁴³, D. Hirschbuehl¹⁷⁵, J. Hobbs¹⁴⁸, N. Hod¹⁵³, M.C. Hodgkinson¹³⁹, P. Hodgson¹³⁹, A. Hoecker³⁰, M.R. Hoferkamp¹⁰³, J. Hoffman⁴⁰, D. Hoffmann⁸³, M. Hohlfield⁸¹, M. Holder¹⁴¹, S.O. Holmgren^{146a}, T. Holy¹²⁷, J.L. Holzbauer⁸⁸, T.M. Hong¹²⁰, L. Hooft van Huysduynen¹⁰⁸, S. Horner⁴⁸, J.-Y. Hostachy⁵⁵, S. Hou¹⁵¹, A. Hoummada^{135a}, J. Howard¹¹⁸, J. Howarth⁸², I. Hristova¹⁶, J. Hrivnac¹¹⁵, T. Hryn'ova⁵, P.J. Hsu⁸¹, S.-C. Hsu¹⁵, D. Hu³⁵, Z. Hubacek¹²⁷, F. Hubaut⁸³, F. Huegging²¹, A. Huettmann⁴², T.B. Huffman¹¹⁸, E.W. Hughes³⁵, G. Hughes⁷¹, M. Huhtinen³⁰, M. Hurwitz¹⁵, U. Husemann⁴², N. Huseynov^{64,r}, J. Huston⁸⁸, J. Huth⁵⁷, G. Iacobucci⁴⁹, G. Iakovidis¹⁰, M. Ibbotson⁸², I. Ibragimov¹⁴¹, L. Iconomidou-Fayard¹¹⁵, J. Idarraga¹¹⁵, P. Iengo^{102a}, O. Igonkina¹⁰⁵, Y. Ikegami⁶⁵, M. Ikeno⁶⁵, D. Iliadis¹⁵⁴, N. Ilic¹⁵⁸, T. Ince²¹, J. Inigo-Golfin³⁰, P. Ioannou⁹, M. Iodice^{134a}, K. Iordanidou⁹, V. Ippolito^{132a,132b}, A. Irlles Quiles¹⁶⁷, C. Isaksson¹⁶⁶, M. Ishino⁶⁷, M. Ishitsuka¹⁵⁷, R. Ishmukhametov⁴⁰, C. Issever¹¹⁸, S. Istin^{19a}, A.V. Ivashin¹²⁸, W. Iwanski³⁹, H. Iwasaki⁶⁵, J.M. Izen⁴¹, V. Izzo^{102a}, B. Jackson¹²⁰, J.N. Jackson⁷³, P. Jackson¹, M.R. Jaekel³⁰, V. Jain⁶⁰, K. Jakobs⁴⁸, S. Jakobsen³⁶, T. Jakoubek¹²⁵, J. Jakubek¹²⁷, D.K. Jana¹¹¹, E. Jansen⁷⁷, H. Jansen³⁰,

A. Jantsch⁹⁹, M. Janus⁴⁸, G. Jarlskog⁷⁹, L. Jeanty⁵⁷, I. Jen-La Plante³¹, D. Jennens⁸⁶, P. Jenni³⁰,
 A.E. Loevschall-Jensen³⁶, P. Jež³⁶, S. Jézéquel⁵, M.K. Jha^{20a}, H. Ji¹⁷³, W. Ji⁸¹, J. Jia¹⁴⁸, Y. Jiang^{33b},
 M. Jimenez Belenguer⁴², S. Jin^{33a}, O. Jinnouchi¹⁵⁷, M.D. Joergensen³⁶, D. Joffe⁴⁰, M. Johansen^{146a,146b},
 K.E. Johansson^{146a}, P. Johansson¹³⁹, S. Johnert⁴², K.A. Johns⁷, K. Jon-And^{146a,146b}, G. Jones¹⁷⁰,
 R.W.L. Jones⁷¹, T.J. Jones⁷³, C. Joram³⁰, P.M. Jorge^{124a}, K.D. Joshi⁸², J. Jovicevic¹⁴⁷, T. Jovin^{13b}, X. Ju¹⁷³,
 C.A. Jung⁴³, R.M. Jungst³⁰, V. Juranek¹²⁵, P. Jussel⁶¹, A. Juste Rozas¹², S. Kabana¹⁷, M. Kaci¹⁶⁷,
 A. Kaczmarska³⁹, P. Kadlecik³⁶, M. Kado¹¹⁵, H. Kagan¹⁰⁹, M. Kagan⁵⁷, E. Kajomovitz¹⁵², S. Kalinin¹⁷⁵,
 L.V. Kalinovskaya⁶⁴, S. Kama⁴⁰, N. Kanaya¹⁵⁵, M. Kaneda³⁰, S. Kaneti²⁸, T. Kanno¹⁵⁷, V.A. Kantserov⁹⁶,
 J. Kanzaki⁶⁵, B. Kaplan¹⁰⁸, A. Kapliy³¹, J. Kaplon³⁰, D. Kar⁵³, M. Karagounis²¹, K. Karakostas¹⁰,
 M. Karnevskiy⁴², V. Kartvelishvili⁷¹, A.N. Karyukhin¹²⁸, L. Kashif¹⁷³, G. Kasieczka^{58b}, R.D. Kass¹⁰⁹,
 A. Kastanas¹⁴, M. Kataoka⁵, Y. Kataoka¹⁵⁵, E. Katsoufis¹⁰, J. Katzy⁴², V. Kaushik⁷, K. Kawagoe⁶⁹,
 T. Kawamoto¹⁵⁵, G. Kawamura⁸¹, M.S. Kayl¹⁰⁵, S. Kazama¹⁵⁵, V.A. Kazanin¹⁰⁷, M.Y. Kazarinov⁶⁴,
 R. Keeler¹⁶⁹, P.T. Keener¹²⁰, R. Kehoe⁴⁰, M. Keil⁵⁴, G.D. Kekelidze⁶⁴, J.S. Keller¹³⁸, M. Kenyon⁵³,
 O. Kepka¹²⁵, N. Kerschen³⁰, B.P. Kerševan⁷⁴, S. Kersten¹⁷⁵, K. Kessoku¹⁵⁵, J. Keung¹⁵⁸, F. Khalil-zada¹¹,
 H. Khandanyan^{146a,146b}, A. Khanov¹¹², D. Kharchenko⁶⁴, A. Khodinov⁹⁶, A. Khomich^{58a}, T.J. Khoo²⁸,
 G. Khorauli²¹, A. Khoroshilov¹⁷⁵, V. Khovanskiy⁹⁵, E. Khramov⁶⁴, J. Khubua^{51b}, H. Kim^{146a,146b},
 S.H. Kim¹⁶⁰, N. Kimura¹⁷¹, O. Kind¹⁶, B.T. King⁷³, M. King⁶⁶, R.S.B. King¹¹⁸, J. Kirk¹²⁹, A.E. Kiryunin⁹⁹,
 T. Kishimoto⁶⁶, D. Kisielewska³⁸, T. Kitamura⁶⁶, T. Kittelmann¹²³, K. Kiuchi¹⁶⁰, E. Kladiva^{144b},
 M. Klein⁷³, U. Klein⁷³, K. Kleinknecht⁸¹, M. Klemetti⁸⁵, A. Klier¹⁷², P. Klimek^{146a,146b}, A. Klimentov²⁵,
 R. Klingenberg⁴³, J.A. Klinger⁸², E.B. Klinkby³⁶, T. Klioutchnikova³⁰, P.F. Klok¹⁰⁴, S. Klous¹⁰⁵,
 E.-E. Kluge^{58a}, T. Kluge⁷³, P. Kluit¹⁰⁵, S. Kluth⁹⁹, N.S. Knecht¹⁵⁸, E. Kneringer⁶¹, E.B.F.G. Knoop⁸³,
 A. Knue⁵⁴, B.R. Ko⁴⁵, T. Kobayashi¹⁵⁵, M. Kobel⁴⁴, M. Kocian¹⁴³, P. Kodys¹²⁶, K. Köneke³⁰,
 A.C. König¹⁰⁴, S. Koenig⁸¹, L. Köpke⁸¹, F. Koetsveld¹⁰⁴, P. Koesvesarki²¹, T. Koffas²⁹, E. Koffeman¹⁰⁵,
 L.A. Kogan¹¹⁸, S. Kohlmann¹⁷⁵, F. Kohn⁵⁴, Z. Kohout¹²⁷, T. Kohriki⁶⁵, T. Koi¹⁴³, G.M. Kolachev^{107,*},
 H. Kolanoski¹⁶, V. Kolesnikov⁶⁴, I. Koletsou^{89a}, J. Koll⁸⁸, A.A. Komar⁹⁴, Y. Komori¹⁵⁵, T. Kondo⁶⁵,
 T. Kono^{42,s}, A.I. Kononov⁴⁸, R. Konoplich^{108,t}, N. Konstantinidis⁷⁷, S. Koperny³⁸, K. Korcyl³⁹,
 K. Kordas¹⁵⁴, A. Korn¹¹⁸, A. Korol¹⁰⁷, I. Korolkov¹², E.V. Korolkova¹³⁹, V.A. Korotkov¹²⁸, O. Kortner⁹⁹,
 S. Kortner⁹⁹, V.V. Kostyukhin²¹, S. Kotov⁹⁹, V.M. Kotov⁶⁴, A. Kotwal⁴⁵, C. Kourkoumelis⁹,
 V. Kouskoura¹⁵⁴, A. Koutsman^{159a}, R. Kowalewski¹⁶⁹, T.Z. Kowalski³⁸, W. Kozanecki¹³⁶, A.S. Kozhin¹²⁸,
 V. Kral¹²⁷, V.A. Kramarenko⁹⁷, G. Kramberger⁷⁴, M.W. Krasny⁷⁸, A. Krasznahorkay¹⁰⁸, J.K. Kraus²¹,
 S. Kreiss¹⁰⁸, F. Krejci¹²⁷, J. Kretschmar⁷³, N. Krieger⁵⁴, P. Krieger¹⁵⁸, K. Kroeninger⁵⁴, H. Kroha⁹⁹,
 J. Kroll¹²⁰, J. Kroseberg²¹, J. Krstic^{13a}, U. Kruchonak⁶⁴, H. Krüger²¹, T. Kruker¹⁷, N. Krumnack⁶³,
 Z.V. Krumshteyn⁶⁴, T. Kubota⁸⁶, S. Kuday^{4a}, S. Kuehn⁴⁸, A. Kugel^{58c}, T. Kuhl⁴², D. Kuhn⁶¹,
 V. Kukhtin⁶⁴, Y. Kulchitsky⁹⁰, S. Kuleshov^{32b}, C. Kummer⁹⁸, M. Kuna⁷⁸, J. Kunkle¹²⁰, A. Kupco¹²⁵,
 H. Kurashige⁶⁶, M. Kurata¹⁶⁰, Y.A. Kurochkin⁹⁰, V. Kus¹²⁵, E.S. Kuwertz¹⁴⁷, M. Kuze¹⁵⁷, J. Kvita¹⁴²,
 R. Kwee¹⁶, A. La Rosa⁴⁹, L. La Rotonda^{37a,37b}, L. Labarga⁸⁰, J. Labbe⁵, S. Lablak^{135a}, C. Lacasta¹⁶⁷,
 F. Lacava^{132a,132b}, H. Lacker¹⁶, D. Lacour⁷⁸, V.R. Lacuesta¹⁶⁷, E. Ladygin⁶⁴, R. Lafaye⁵, B. Laforge⁷⁸,
 T. Lagouri¹⁷⁶, S. Lai⁴⁸, E. Laisne⁵⁵, M. Lamanna³⁰, L. Lambourne⁷⁷, C.L. Lampen⁷, W. Lampl⁷,
 E. Lancon¹³⁶, U. Landgraf⁴⁸, M.P.J. Landon⁷⁵, J.L. Lane⁸², V.S. Lang^{58a}, C. Lange⁴², A.J. Lankford¹⁶³,
 F. Lanni²⁵, K. Lantsch¹⁷⁵, S. Laplace⁷⁸, C. Lapoire²¹, J.F. Laporte¹³⁶, T. Lari^{89a}, A. Larnier¹¹⁸,
 M. Lassnig³⁰, P. Laurelli⁴⁷, V. Lavorini^{37a,37b}, W. Lavrijsen¹⁵, P. Laycock⁷³, O. Le Dortz⁷⁸,
 E. Le Guirriec⁸³, E. Le Menedeu¹², T. LeCompte⁶, F. Ledroit-Guillon⁵⁵, H. Lee¹⁰⁵, J.S.H. Lee¹¹⁶,
 S.C. Lee¹⁵¹, L. Lee¹⁷⁶, M. Lefebvre¹⁶⁹, M. Legendre¹³⁶, F. Legger⁹⁸, C. Leggett¹⁵, M. Lehmacher²¹,
 G. Lehmann Miotto³⁰, X. Lei⁷, M.A.L. Leite^{24d}, R. Leitner¹²⁶, D. Lellouch¹⁷², B. Lemmer⁵⁴,
 V. Lendermann^{58a}, K.J.C. Leney^{145b}, T. Lenz¹⁰⁵, G. Lenzen¹⁷⁵, B. Lenzi³⁰, K. Leonhardt⁴⁴, S. Leontsinis¹⁰,
 F. Lepold^{58a}, C. Leroy⁹³, J.-R. Lessard¹⁶⁹, C.G. Lester²⁸, C.M. Lester¹²⁰, J. Levêque⁵, D. Levin⁸⁷,
 L.J. Levinson¹⁷², A. Lewis¹¹⁸, G.H. Lewis¹⁰⁸, A.M. Leyko²¹, M. Leyton¹⁶, B. Li⁸³, H. Li^{173,u}, S. Li^{33b,v},
 X. Li⁸⁷, Z. Liang^{118,w}, H. Liao³⁴, B. Liberti^{133a}, P. Lichard³⁰, M. Lichtnecker⁹⁸, K. Lie¹⁶⁵, W. Liebig¹⁴,
 C. Limbach²¹, A. Limosani⁸⁶, M. Limper⁶², S.C. Lin^{151,x}, F. Linde¹⁰⁵, J.T. Linnemann⁸⁸, E. Lipeles¹²⁰,
 A. Lipniacka¹⁴, T.M. Liss¹⁶⁵, D. Lissauer²⁵, A. Lister⁴⁹, A.M. Litke¹³⁷, C. Liu²⁹, D. Liu¹⁵¹, H. Liu⁸⁷,
 J.B. Liu⁸⁷, L. Liu⁸⁷, M. Liu^{33b}, Y. Liu^{33b}, M. Livan^{119a,119b}, S.S.A. Livermore¹¹⁸, A. Lleres⁵⁵,
 J. Llorente Merino⁸⁰, S.L. Lloyd⁷⁵, E. Lobodzinska⁴², P. Loch⁷, W.S. Lockman¹³⁷, T. Loddenkoetter²¹,

F.K. Loebinger⁸², A. Loginov¹⁷⁶, C.W. Loh¹⁶⁸, T. Lohse¹⁶, K. Lohwasser⁴⁸, M. Lokajicek¹²⁵, V.P. Lombardo⁵, R.E. Long⁷¹, L. Lopes^{124a}, D. Lopez Mateos⁵⁷, J. Lorenz⁹⁸, N. Lorenzo Martinez¹¹⁵, M. Losada¹⁶², P. Loscutoff¹⁵, F. Lo Sterzo^{132a,132b}, M.J. Losty^{159a,*}, X. Lou⁴¹, A. Lounis¹¹⁵, K.F. Loureiro¹⁶², J. Love⁶, P.A. Love⁷¹, A.J. Lowe^{143,e}, F. Lu^{33a}, H.J. Lubatti¹³⁸, C. Luci^{132a,132b}, A. Lucotte⁵⁵, A. Ludwig⁴⁴, D. Ludwig⁴², I. Ludwig⁴⁸, J. Ludwig⁴⁸, F. Luehring⁶⁰, G. Luijckx¹⁰⁵, W. Lukas⁶¹, L. Luminari^{132a}, E. Lund¹¹⁷, B. Lund-Jensen¹⁴⁷, B. Lundberg⁷⁹, J. Lundberg^{146a,146b}, O. Lundberg^{146a,146b}, J. Lundquist³⁶, M. Lungwitz⁸¹, D. Lynn²⁵, E. Lytken⁷⁹, H. Ma²⁵, L.L. Ma¹⁷³, G. Maccarrone⁴⁷, A. Macchiolo⁹⁹, B. Maček⁷⁴, J. Machado Miguens^{124a}, R. Mackeprang³⁶, R.J. Madaras¹⁵, H.J. Maddocks⁷¹, W.F. Mader⁴⁴, R. Maenner^{58c}, T. Maeno²⁵, P. Mättig¹⁷⁵, S. Mättig⁸¹, L. Magnoni¹⁶³, E. Magradze⁵⁴, K. Mahboubi⁴⁸, J. Mahlstedt¹⁰⁵, S. Mahmoud⁷³, G. Mahout¹⁸, C. Maiani¹³⁶, C. Maidantchik^{24a}, A. Maio^{124a,b}, S. Majewski²⁵, Y. Makida⁶⁵, N. Makovec¹¹⁵, P. Mal¹³⁶, B. Malaescu³⁰, Pa. Malecki³⁹, P. Malecki³⁹, V.P. Maleev¹²¹, F. Malek⁵⁵, U. Mallik⁶², D. Malon⁶, C. Malone¹⁴³, S. Maltezos¹⁰, V. Malyshev¹⁰⁷, S. Malyukov³⁰, R. Mameghani⁹⁸, J. Mamuzic^{13b}, A. Manabe⁶⁵, L. Mandelli^{89a}, I. Mandić⁷⁴, R. Mandrysch¹⁶, J. Maneira^{124a}, A. Manfredini⁹⁹, P.S. Mangear⁸⁸, L. Manhaes de Andrade Filho^{24b}, J.A. Manjarres Ramos¹³⁶, A. Mann⁵⁴, P.M. Manning¹³⁷, A. Manousakis-Katsikakis⁹, B. Mansoulie¹³⁶, A. Mapelli³⁰, L. Mapelli³⁰, L. March⁸⁰, J.F. Marchand²⁹, F. Marchese^{133a,133b}, G. Marchiori⁷⁸, M. Marcisovsky¹²⁵, C.P. Marino¹⁶⁹, F. Marroquim^{24a}, Z. Marshall³⁰, F.K. Martens¹⁵⁸, L.F. Marti¹⁷, S. Marti-Garcia¹⁶⁷, B. Martin³⁰, B. Martin⁸⁸, J.P. Martin⁹³, T.A. Martin¹⁸, V.J. Martin⁴⁶, B. Martin dit Latour⁴⁹, S. Martin-Haugh¹⁴⁹, M. Martinez¹², V. Martinez Outschoorn⁵⁷, A.C. Martyniuk¹⁶⁹, M. Marx⁸², F. Marzano^{132a}, A. Marzin¹¹¹, L. Masetti⁸¹, T. Mashimo¹⁵⁵, R. Mashinistov⁹⁴, J. Masik⁸², A.L. Maslennikov¹⁰⁷, I. Massa^{20a,20b}, G. Massaro¹⁰⁵, N. Massol⁵, P. Mastrandrea¹⁴⁸, A. Mastroberardino^{37a,37b}, T. Masubuchi¹⁵⁵, P. Matricon¹¹⁵, H. Matsunaga¹⁵⁵, T. Matsushita⁶⁶, C. Mattraversi^{118,c}, J. Maurer⁸³, S.J. Maxfield⁷³, A. Mayne¹³⁹, R. Mazini¹⁵¹, M. Mazur²¹, L. Mazzaferro^{133a,133b}, M. Mazzanti^{89a}, J. Mc Donald⁸⁵, S.P. Mc Kee⁸⁷, A. McCarn¹⁶⁵, R.L. McCarthy¹⁴⁸, T.G. McCarthy²⁹, N.A. McCubbin¹²⁹, K.W. McFarlane^{56,*}, J.A. McFayden¹³⁹, G. Mchedlidze^{51b}, T. Mclaughlan¹⁸, S.J. McMahon¹²⁹, R.A. McPherson^{169,k}, A. Meade⁸⁴, J. Mechnich¹⁰⁵, M. Mechtel¹⁷⁵, M. Medinnis⁴², R. Meera-Lebbai¹¹¹, T. Meguro¹¹⁶, R. Mehdiyev⁹³, S. Mehlhase³⁶, A. Mehta⁷³, K. Meier^{58a}, B. Meirose⁷⁹, C. Melachrinou³¹, B.R. Mellado Garcia¹⁷³, F. Meloni^{89a,89b}, L. Mendoza Navas¹⁶², Z. Meng^{151,u}, A. Mengarelli^{20a,20b}, S. Menke⁹⁹, E. Meoni¹⁶¹, K.M. Mercurio⁵⁷, P. Mermod⁴⁹, L. Merola^{102a,102b}, C. Meroni^{89a}, F.S. Merritt³¹, H. Merritt¹⁰⁹, A. Messina^{30,y}, J. Metcalfe²⁵, A.S. Mete¹⁶³, C. Meyer⁸¹, C. Meyer³¹, J.-P. Meyer¹³⁶, J. Meyer¹⁷⁴, J. Meyer⁵⁴, T.C. Meyer³⁰, J. Miao^{33d}, S. Michal³⁰, L. Micu^{26a}, R.P. Middleton¹²⁹, S. Migas⁷³, L. Mijović¹³⁶, G. Mikenberg¹⁷², M. Mikestikova¹²⁵, M. Mikuž⁷⁴, D.W. Miller³¹, R.J. Miller⁸⁸, W.J. Mills¹⁶⁸, C. Mills⁵⁷, A. Milov¹⁷², D.A. Milstead^{146a,146b}, D. Milstein¹⁷², A.A. Minaenko¹²⁸, M. Miñano Moya¹⁶⁷, I.A. Minashvili⁶⁴, A.I. Mincer¹⁰⁸, B. Mindur³⁸, M. Mineev⁶⁴, Y. Ming¹⁷³, L.M. Mir¹², G. Mirabelli^{132a}, J. Mitrevski¹³⁷, V.A. Mitsou¹⁶⁷, S. Mitsui⁶⁵, P.S. Miyagawa¹³⁹, J.U. Mjörnmark⁷⁹, T. Moa^{146a,146b}, V. Moeller²⁸, K. Mönig⁴², N. Möser²¹, S. Mohapatra¹⁴⁸, W. Mohr⁴⁸, R. Moles-Valls¹⁶⁷, A. Molfetas³⁰, J. Monk⁷⁷, E. Monnier⁸³, J. Montejo Berlingen¹², F. Monticelli⁷⁰, S. Monzani^{20a,20b}, R.W. Moore³, G.F. Moorhead⁸⁶, C. Mora Herrera⁴⁹, A. Moraes⁵³, N. Morange¹³⁶, J. Morel⁵⁴, G. Morello^{37a,37b}, D. Moreno⁸¹, M. Moreno Llácer¹⁶⁷, P. Morettini^{50a}, M. Morgenstern⁴⁴, M. Morii⁵⁷, A.K. Morley³⁰, G. Mornacchi³⁰, J.D. Morris⁷⁵, L. Morvaj¹⁰¹, H.G. Moser⁹⁹, M. Mosidze^{51b}, J. Moss¹⁰⁹, R. Mount¹⁴³, E. Mountricha^{10,z}, S.V. Mouraviev^{94,*}, E.J.W. Moyse⁸⁴, F. Mueller^{58a}, J. Mueller¹²³, K. Mueller²¹, T.A. Müller⁹⁸, T. Mueller⁸¹, D. Muenstermann³⁰, Y. Munwes¹⁵³, W.J. Murray¹²⁹, I. Mussche¹⁰⁵, E. Musto^{102a,102b}, A.G. Myagkov¹²⁸, M. Myska¹²⁵, J. Nadal¹², K. Nagai¹⁶⁰, R. Nagai¹⁵⁷, K. Nagano⁶⁵, A. Nagarkar¹⁰⁹, Y. Nagasaka⁵⁹, M. Nagel⁹⁹, A.M. Nairz³⁰, Y. Nakahama³⁰, K. Nakamura¹⁵⁵, T. Nakamura¹⁵⁵, I. Nakano¹¹⁰, G. Nanava²¹, A. Napier¹⁶¹, R. Narayan^{58b}, M. Nash^{77,c}, T. Nattermann²¹, T. Naumann⁴², G. Navarro¹⁶², H.A. Neal⁸⁷, P.Yu. Nechaeva⁹⁴, T.J. Neep⁸², A. Negri^{119a,119b}, G. Negri³⁰, M. Negrini^{20a}, S. Nektarijevic⁴⁹, A. Nelson¹⁶³, T.K. Nelson¹⁴³, S. Nemecek¹²⁵, P. Nemethy¹⁰⁸, A.A. Nepomuceno^{24a}, M. Nessi^{30,aa}, M.S. Neubauer¹⁶⁵, M. Neumann¹⁷⁵, A. Neusiedl⁸¹, R.M. Neves¹⁰⁸, P. Nevski²⁵, F.M. Newcomer¹²⁰, P.R. Newman¹⁸, V. Nguyen Thi Hong¹³⁶, R.B. Nickerson¹¹⁸, R. Nicolaidou¹³⁶, B. Nicquevert³⁰, F. Niedercorn¹¹⁵, J. Nielsen¹³⁷, N. Nikiforou³⁵, A. Nikiforov¹⁶, V. Nikolaenko¹²⁸, I. Nikolic-Audit⁷⁸,

K. Nikolics⁴⁹, K. Nikolopoulos¹⁸, H. Nilsen⁴⁸, P. Nilsson⁸, Y. Ninomiya¹⁵⁵, A. Nisati^{132a}, R. Nisius⁹⁹,
 T. Nobe¹⁵⁷, L. Nodulman⁶, M. Nomachi¹¹⁶, I. Nomidis¹⁵⁴, S. Norberg¹¹¹, M. Nordberg³⁰, P.R. Norton¹²⁹,
 J. Novakova¹²⁶, M. Nozaki⁶⁵, L. Nozka¹¹³, I.M. Nugent^{159a}, A.-E. Nuncio-Quiroz²¹,
 G. Nunes Hanninger⁸⁶, T. Nunnemann⁹⁸, E. Nurse⁷⁷, B.J. O'Brien⁴⁶, D.C. O'Neil¹⁴², V. O'Shea⁵³,
 L.B. Oakes⁹⁸, F.G. Oakham^{29,d}, H. Oberlack⁹⁹, J. Ocariz⁷⁸, A. Ochi⁶⁶, S. Oda⁶⁹, S. Odaka⁶⁵, J. Odier⁸³,
 H. Ogren⁶⁰, A. Oh⁸², S.H. Oh⁴⁵, C.C. Ohm³⁰, T. Ohshima¹⁰¹, H. Okawa²⁵, Y. Okumura³¹, T. Okuyama¹⁵⁵,
 A. Olariu^{26a}, A.G. Olchevski⁶⁴, S.A. Olivares Pino^{32a}, M. Oliveira^{124a,h}, D. Oliveira Damazio²⁵,
 E. Oliver Garcia¹⁶⁷, D. Olivito¹²⁰, A. Olszewski³⁹, J. Olszowska³⁹, A. Onofre^{124a,ab}, P.U.E. Onyisi³¹,
 C.J. Oram^{159a}, M.J. Oreglia³¹, Y. Oren¹⁵³, D. Orestano^{134a,134b}, N. Orlando^{72a,72b}, I. Orlov¹⁰⁷,
 C. Oropeza Barrera⁵³, R.S. Orr¹⁵⁸, B. Osculati^{50a,50b}, R. Ospanov¹²⁰, C. Osuna¹², G. Otero y Garzon²⁷,
 J.P. Ottersbach¹⁰⁵, M. Ouchrif^{135d}, E.A. Ouellette¹⁶⁹, F. Ould-Saada¹¹⁷, A. Ouraou¹³⁶, Q. Ouyang^{33a},
 A. Ovcharova¹⁵, M. Owen⁸², S. Owen¹³⁹, V.E. Ozcan^{19a}, N. Ozturk⁸, A. Pacheco Pages¹²,
 C. Padilla Aranda¹², S. Pagan Griso¹⁵, E. Paganis¹³⁹, C. Pahl⁹⁹, F. Paige²⁵, P. Pais⁸⁴, K. Pajchel¹¹⁷,
 G. Palacino^{159b}, C.P. Palestini⁷, S. Palestini³⁰, D. Pallin³⁴, A. Palma^{124a}, J.D. Palmer¹⁸, Y.B. Pan¹⁷³,
 E. Panagiotopoulou¹⁰, P. Pani¹⁰⁵, N. Panikashvili⁸⁷, S. Panitkin²⁵, D. Pantea^{26a}, A. Papadelis^{146a},
 Th.D. Papadopoulou¹⁰, A. Paramonov⁶, D. Paredes Hernandez³⁴, W. Park^{25,ac}, M.A. Parker²⁸,
 F. Parodi^{50a,50b}, J.A. Parsons³⁵, U. Parzefall⁴⁸, S. Pashapour⁵⁴, E. Pasqualucci^{132a}, S. Passaggio^{50a},
 A. Passeri^{134a}, F. Pastore^{134a,134b,*}, Fr. Pastore⁷⁶, G. Pásztor^{49,ad}, S. Pataria¹⁷⁵, N. Patel¹⁵⁰, J.R. Pater⁸²,
 S. Patricelli^{102a,102b}, T. Pauly³⁰, M. Pecsny^{144a}, S. Pedraza Lopez¹⁶⁷, M.I. Pedraza Morales¹⁷³,
 S.V. Peleganchuk¹⁰⁷, D. Pelikan¹⁶⁶, H. Peng^{33b}, B. Penning³¹, A. Penson³⁵, J. Penwell⁶⁰,
 M. Perantoni^{24a}, K. Perez^{35,ae}, T. Perez Cavalcanti⁴², E. Perez Codina^{159a}, M.T. Pérez García-Estañ¹⁶⁷,
 V. Perez Reale³⁵, L. Perini^{89a,89b}, H. Pernegger³⁰, R. Perrino^{72a}, P. Perrodo⁵, V.D. Peshekhonov⁶⁴,
 K. Peters³⁰, B.A. Petersen³⁰, J. Petersen³⁰, T.C. Petersen³⁶, E. Petit⁵, A. Petridis¹⁵⁴, C. Petridou¹⁵⁴,
 E. Petrolo^{132a}, F. Petrucci^{134a,134b}, D. Petschull⁴², M. Petteni¹⁴², R. Pezoa^{32b}, A. Phan⁸⁶, P.W. Phillips¹²⁹,
 G. Piacquadio³⁰, A. Picazio⁴⁹, E. Piccaro⁷⁵, M. Piccinini^{20a,20b}, S.M. Piec⁴², R. Piegai²⁷, D.T. Pignotti¹⁰⁹,
 J.E. Pilcher³¹, A.D. Pilkington⁸², J. Pina^{124a,b}, M. Pinamonti^{164a,164c}, A. Pinder¹¹⁸, J.L. Pinfold³,
 B. Pinto^{124a}, C. Pizio^{89a,89b}, M. Plamondon¹⁶⁹, M.-A. Pleier²⁵, E. Plotnikova⁶⁴, A. Poblaguev²⁵,
 S. Poddar^{58a}, F. Podlyski³⁴, L. Poggioli¹¹⁵, D. Pohl²¹, M. Pohl⁴⁹, G. Polesello^{119a}, A. Policicchio^{37a,37b},
 A. Polini^{20a}, J. Poll⁷⁵, V. Polychronakos²⁵, D. Pomeroy²³, K. Pommès³⁰, L. Pontecorvo^{132a}, B.G. Pope⁸⁸,
 G.A. Popeneciu^{26a}, D.S. Popovic^{13a}, A. Poppleton³⁰, X. Portell Bueso³⁰, G.E. Pospelov⁹⁹, S. Pospisil¹²⁷,
 I.N. Potrap⁹⁹, C.J. Potter¹⁴⁹, C.T. Potter¹¹⁴, G. Poulard³⁰, J. Poveda⁶⁰, V. Pozdnyakov⁶⁴, R. Prabhu⁷⁷,
 P. Pralavorio⁸³, A. Pranko¹⁵, S. Prasad³⁰, R. Pravahan²⁵, S. Prell⁶³, K. Pretzl¹⁷, D. Price⁶⁰, J. Price⁷³,
 L.E. Price⁶, D. Prieur¹²³, M. Primavera^{72a}, K. Prokofiev¹⁰⁸, F. Prokoshin^{32b}, S. Protopopescu²⁵,
 J. Proudfoot⁶, X. Prudent⁴⁴, M. Przybycien³⁸, H. Przysiezniak⁵, S. Psoroulas²¹, E. Ptacek¹¹⁴,
 E. Pueschel⁸⁴, J. Purdham⁸⁷, M. Purohit^{25,ac}, P. Puzo¹¹⁵, Y. Pylypchenko⁶², J. Qian⁸⁷, A. Quadt⁵⁴,
 D.R. Quarrie¹⁵, W.B. Quayle¹⁷³, F. Quinonez^{32a}, M. Raas¹⁰⁴, V. Radeka²⁵, V. Radescu⁴², P. Radloff¹¹⁴,
 T. Rador^{19a}, F. Ragusa^{89a,89b}, G. Rahal¹⁷⁸, A.M. Rahimi¹⁰⁹, D. Rahm²⁵, S. Rajagopalan²⁵,
 M. Rammensee⁴⁸, M. Rammes¹⁴¹, A.S. Randle-Conde⁴⁰, K. Randrianarivony²⁹, F. Rauscher⁹⁸,
 T.C. Rave⁴⁸, M. Raymond³⁰, A.L. Read¹¹⁷, D.M. Rebuzzi^{119a,119b}, A. Redelbach¹⁷⁴, G. Redlinger²⁵,
 R. Reece¹²⁰, K. Reeves⁴¹, E. Reinherz-Aronis¹⁵³, A. Reinsch¹¹⁴, I. Reisinger⁴³, C. Rembser³⁰, Z.L. Ren¹⁵¹,
 A. Renaud¹¹⁵, M. Rescigno^{132a}, S. Resconi^{89a}, B. Resende¹³⁶, P. Reznicek⁹⁸, R. Rezvani¹⁵⁸, R. Richter⁹⁹,
 E. Richter-Was^{5,af}, M. Ridel⁷⁸, M. Rijpstra¹⁰⁵, M. Rijssenbeek¹⁴⁸, A. Rimoldi^{119a,119b}, L. Rinaldi^{20a},
 R.R. Rios⁴⁰, I. Riu¹², G. Rivoltella^{89a,89b}, F. Rizatdinova¹¹², E. Rizvi⁷⁵, S.H. Robertson^{85,k},
 A. Robichaud-Veronneau¹¹⁸, D. Robinson²⁸, J.E.M. Robinson⁸², A. Robson⁵³, J.G. Rocha de Lima¹⁰⁶,
 C. Roda^{122a,122b}, D. Roda Dos Santos³⁰, A. Roe⁵⁴, S. Roe³⁰, O. Røhne¹¹⁷, S. Rolli¹⁶¹, A. Romaniouk⁹⁶,
 M. Romano^{20a,20b}, G. Romeo²⁷, E. Romero Adam¹⁶⁷, N. Rompotis¹³⁸, L. Roos⁷⁸, E. Ros¹⁶⁷, S. Rosati^{132a},
 K. Rosbach⁴⁹, A. Rose¹⁴⁹, M. Rose⁷⁶, G.A. Rosenbaum¹⁵⁸, E.I. Rosenberg⁶³, P.L. Rosendahl¹⁴,
 O. Rosenthal¹⁴¹, L. Rosselet⁴⁹, V. Rossetti¹², E. Rossi^{132a,132b}, L.P. Rossi^{50a}, M. Rotaru^{26a}, I. Roth¹⁷²,
 J. Rothberg¹³⁸, D. Rousseau¹¹⁵, C.R. Royon¹³⁶, A. Rozanov⁸³, Y. Rozen¹⁵², X. Ruan^{33a,ag}, F. Rubbo¹²,
 I. Rubinskiy⁴², N. Ruckstuhl¹⁰⁵, V.I. Rud⁹⁷, C. Rudolph⁴⁴, G. Rudolph⁶¹, F. Rühr⁷, A. Ruiz-Martinez⁶³,
 L. Rummyantsev⁶⁴, Z. Rurikova⁴⁸, N.A. Rusakovich⁶⁴, J.P. Rutherford⁷, C. Ruwiedel^{15,*}, P. Ruzicka¹²⁵,
 Y.F. Ryabov¹²¹, M. Rybar¹²⁶, G. Rybkin¹¹⁵, N.C. Ryder¹¹⁸, A.F. Saavedra¹⁵⁰, I. Sadeh¹⁵³,

H.F-W. Sadrozinski¹³⁷, R. Sadykov⁶⁴, F. Safai Tehrani^{132a}, H. Sakamoto¹⁵⁵, G. Salamanna⁷⁵,
A. Salamon^{133a}, M. Saleem¹¹¹, D. Salek³⁰, D. Salihagic⁹⁹, A. Salnikov¹⁴³, J. Salt¹⁶⁷,
B.M. Salvachua Ferrando⁶, D. Salvatore^{37a,37b}, F. Salvatore¹⁴⁹, A. Salvucci¹⁰⁴, A. Salzburger³⁰,
D. Sampsonidis¹⁵⁴, B.H. Samset¹¹⁷, A. Sanchez^{102a,102b}, V. Sanchez Martinez¹⁶⁷, H. Sandaker¹⁴,
H.G. Sander⁸¹, M.P. Sanders⁹⁸, M. Sandhoff¹⁷⁵, T. Sandoval²⁸, C. Sandoval¹⁶², R. Sandstroem⁹⁹,
D.P.C. Sankey¹²⁹, A. Sansoni⁴⁷, C. Santamarina Rios⁸⁵, C. Santoni³⁴, R. Santonico^{133a,133b}, H. Santos^{124a},
J.G. Saraiva^{124a}, T. Sarangi¹⁷³, E. Sarkisyan-Grinbaum⁸, F. Sarri^{122a,122b}, G. Sartisohn¹⁷⁵, O. Sasaki⁶⁵,
Y. Sasaki¹⁵⁵, N. Sasao⁶⁷, I. Satsounkevitch⁹⁰, G. Sauvage^{5,*}, E. Sauvan⁵, J.B. Sauvan¹¹⁵, P. Savard^{158,d},
V. Savinov¹²³, D.O. Savu³⁰, L. Sawyer^{25,m}, D.H. Saxon⁵³, J. Saxon¹²⁰, C. Sbarra^{20a}, A. Sbrizzi^{20a,20b},
D.A. Scannicchio¹⁶³, M. Scarcella¹⁵⁰, J. Schaarschmidt¹¹⁵, P. Schacht⁹⁹, D. Schaefer¹²⁰, U. Schäfer⁸¹,
S. Schaepe²¹, S. Schaetzel^{58b}, A.C. Schaffer¹¹⁵, D. Schaile⁹⁸, R.D. Schamberger¹⁴⁸, A.G. Schamov¹⁰⁷,
V. Scharf^{58a}, V.A. Schegelsky¹²¹, D. Scheirich⁸⁷, M. Schernau¹⁶³, M.I. Scherzer³⁵, C. Schiavi^{50a,50b},
J. Schieck⁹⁸, M. Schioppa^{37a,37b}, S. Schlenker³⁰, E. Schmidt⁴⁸, K. Schmieden²¹, C. Schmitt⁸¹,
S. Schmitt^{58b}, M. Schmitz²¹, B. Schneider¹⁷, U. Schnoor⁴⁴, A. Schoening^{58b}, A.L.S. Schorlemmer⁵⁴,
M. Schott³⁰, D. Schouten^{159a}, J. Schovancova¹²⁵, M. Schram⁸⁵, C. Schroeder⁸¹, N. Schroer^{58c},
M.J. Schultens²¹, J. Schultes¹⁷⁵, H.-C. Schultz-Coulon^{58a}, H. Schulz¹⁶, M. Schumacher⁴⁸,
B.A. Schumm¹³⁷, Ph. Schune¹³⁶, C. Schwanenberger⁸², A. Schwartzman¹⁴³, Ph. Schwegler⁹⁹,
Ph. Schwemling⁷⁸, R. Schwienhorst⁸⁸, R. Schwierz⁴⁴, J. Schwindling¹³⁶, T. Schwindt²¹, M. Schwoerer⁵,
G. Sciolla²³, W.G. Scott¹²⁹, J. Searcy¹¹⁴, G. Sedov⁴², E. Sedykh¹²¹, S.C. Seidel¹⁰³, A. Seiden¹³⁷,
F. Seifert⁴⁴, J.M. Seixas^{24a}, G. Sekhniaidze^{102a}, S.J. Sekula⁴⁰, K.E. Selbach⁴⁶, D.M. Seliverstov¹²¹,
B. Sellden^{146a}, G. Sellers⁷³, M. Seman^{144b}, N. Semprini-Cesari^{20a,20b}, C. Serfon⁹⁸, L. Serin¹¹⁵,
L. Serkin⁵⁴, R. Seuster⁹⁹, H. Severini¹¹¹, A. Sfyrla³⁰, E. Shabalina⁵⁴, M. Shamim¹¹⁴, L.Y. Shan^{33a},
J.T. Shank²², Q.T. Shao⁸⁶, M. Shapiro¹⁵, P.B. Shatalov⁹⁵, K. Shaw^{164a,164c}, D. Sherman¹⁷⁶, P. Sherwood⁷⁷,
S. Shimizu¹⁰¹, M. Shimojima¹⁰⁰, T. Shin⁵⁶, M. Shiyakova⁶⁴, A. Shmeleva⁹⁴, M.J. Shochet³¹, D. Short¹¹⁸,
S. Shrestha⁶³, E. Shulga⁹⁶, M.A. Shupe⁷, P. Sicho¹²⁵, A. Sidoti^{132a}, F. Siegert⁴⁸, Dj. Sijacki^{13a},
O. Silbert¹⁷², J. Silva^{124a}, Y. Silver¹⁵³, D. Silverstein¹⁴³, S.B. Silverstein^{146a}, V. Simak¹²⁷, O. Simard¹³⁶,
Lj. Simic^{13a}, S. Simion¹¹⁵, E. Simioni⁸¹, B. Simmons⁷⁷, R. Simoniello^{89a,89b}, M. Simonyan³⁶,
P. Sinervo¹⁵⁸, N.B. Sinev¹¹⁴, V. Sipica¹⁴¹, G. Siragusa¹⁷⁴, A. Sircar²⁵, A.N. Sisakyan^{64,*},
S.Yu. Sivoklov⁹⁷, J. Sjölin^{146a,146b}, T.B. Sjursen¹⁴, L.A. Skinnari¹⁵, H.P. Skottowe⁵⁷, K. Skovpen¹⁰⁷,
P. Skubic¹¹¹, M. Slater¹⁸, T. Slavicek¹²⁷, K. Sliwa¹⁶¹, V. Smakhtin¹⁷², B.H. Smart⁴⁶, L. Smestad¹¹⁷,
S.Yu. Smirnov⁹⁶, Y. Smirnov⁹⁶, L.N. Smirnova⁹⁷, O. Smirnova⁷⁹, B.C. Smith⁵⁷, D. Smith¹⁴³,
K.M. Smith⁵³, M. Smizanska⁷¹, K. Smolek¹²⁷, A.A. Snesarev⁹⁴, S.W. Snow⁸², J. Snow¹¹¹, S. Snyder²⁵,
R. Sobie^{169,k}, J. Sodomka¹²⁷, A. Soffer¹⁵³, C.A. Solans¹⁶⁷, M. Solar¹²⁷, J. Solc¹²⁷, E.Yu. Soldatov⁹⁶,
U. Soldevila¹⁶⁷, E. Solfaroli Camillocci^{132a,132b}, A.A. Solodkov¹²⁸, O.V. Solovyanov¹²⁸, V. Solovyev¹²¹,
N. Soni¹, V. Sopko¹²⁷, B. Sopko¹²⁷, M. Sosebee⁸, R. Soualah^{164a,164c}, A. Soukharev¹⁰⁷,
S. Spagnolo^{72a,72b}, F. Spanò⁷⁶, R. Spighi^{20a}, G. Spigo³⁰, R. Spiwoks³⁰, M. Spousta^{126,ah}, T. Spreitzer¹⁵⁸,
B. Spurlock⁸, R.D. St. Denis⁵³, J. Stahlman¹²⁰, R. Stamen^{58a}, E. Stanecka³⁹, R.W. Stanek⁶,
C. Stanescu^{134a}, M. Stanescu-Bellu⁴², M.M. Stanitzki⁴², S. Stapnes¹¹⁷, E.A. Starchenko¹²⁸, J. Stark⁵⁵,
P. Staroba¹²⁵, P. Starovoitov⁴², R. Staszewski³⁹, A. Staude⁹⁸, P. Stavina^{144a,*}, G. Steele⁵³, P. Steinbach⁴⁴,
P. Steinberg²⁵, I. Stekl¹²⁷, B. Stelzer¹⁴², H.J. Stelzer⁸⁸, O. Stelzer-Chilton^{159a}, H. Stenzel⁵², S. Stern⁹⁹,
G.A. Stewart³⁰, J.A. Stillings²¹, M.C. Stockton⁸⁵, K. Stoerig⁴⁸, G. Stoicea^{26a}, S. Stonjek⁹⁹, P. Strachota¹²⁶,
A.R. Stradling⁸, A. Straessner⁴⁴, J. Strandberg¹⁴⁷, S. Strandberg^{146a,146b}, A. Strandlie¹¹⁷, M. Strang¹⁰⁹,
E. Strauss¹⁴³, M. Strauss¹¹¹, P. Strizenec^{144b}, R. Ströhmer¹⁷⁴, D.M. Strom¹¹⁴, J.A. Strong^{76,*},
R. Stroynowski⁴⁰, J. Strube¹²⁹, B. Stugu¹⁴, I. Stumer^{25,*}, J. Stupak¹⁴⁸, P. Sturm¹⁷⁵, N.A. Styles⁴²,
D.A. Soh^{151,w}, D. Su¹⁴³, H.S. Subramania³, A. Succurro¹², Y. Sugaya¹¹⁶, C. Suhr¹⁰⁶, M. Suk¹²⁶,
V.V. Sulin⁹⁴, S. Sultansoy^{4d}, T. Sumida⁶⁷, X. Sun⁵⁵, J.E. Sundermann⁴⁸, K. Suruliz¹³⁹, G. Susinno^{37a,37b},
M.R. Sutton¹⁴⁹, Y. Suzuki⁶⁵, Y. Suzuki⁶⁶, M. Svatos¹²⁵, S. Swedish¹⁶⁸, I. Sykora^{144a}, T. Sykora¹²⁶,
J. Sánchez¹⁶⁷, D. Ta¹⁰⁵, K. Tackmann⁴², A. Taffard¹⁶³, R. Tafirout^{159a}, N. Taiblum¹⁵³, Y. Takahashi¹⁰¹,
H. Takai²⁵, R. Takashima⁶⁸, H. Takeda⁶⁶, T. Takeshita¹⁴⁰, Y. Takubo⁶⁵, M. Talby⁸³, A. Talyshev^{107,f},
M.C. Tamsett²⁵, K.G. Tan⁸⁶, J. Tanaka¹⁵⁵, R. Tanaka¹¹⁵, S. Tanaka¹³¹, S. Tanaka⁶⁵, A.J. Tanasijczuk¹⁴²,
K. Tani⁶⁶, N. Tannoury⁸³, S. Tapprogge⁸¹, D. Tardif¹⁵⁸, S. Tarem¹⁵², F. Tarrade²⁹, G.F. Tartarelli^{89a},
P. Tas¹²⁶, M. Tasevsky¹²⁵, E. Tassi^{37a,37b}, M. Tatarkhanov¹⁵, Y. Tayalati^{135d}, C. Taylor⁷⁷, F.E. Taylor⁹²,

G.N. Taylor⁸⁶, W. Taylor^{159b}, M. Teinturier¹¹⁵, F.A. Teischinger³⁰, M. Teixeira Dias Castanheira⁷⁵, P. Teixeira-Dias⁷⁶, K.K. Temming⁴⁸, H. Ten Kate³⁰, P.K. Teng¹⁵¹, S. Terada⁶⁵, K. Terashi¹⁵⁵, J. Terron⁸⁰, M. Testa⁴⁷, R.J. Teuscher^{158,k}, J. Therhaag²¹, T. Theveneaux-Pelzer⁷⁸, S. Thoma⁴⁸, J.P. Thomas¹⁸, E.N. Thompson³⁵, P.D. Thompson¹⁸, P.D. Thompson¹⁵⁸, A.S. Thompson⁵³, L.A. Thomsen³⁶, E. Thomson¹²⁰, M. Thomson²⁸, W.M. Thong⁸⁶, R.P. Thun⁸⁷, F. Tian³⁵, M.J. Tibbetts¹⁵, T. Tic¹²⁵, V.O. Tikhomirov⁹⁴, Y.A. Tikhonov^{107,f}, S. Timoshenko⁹⁶, P. Tipton¹⁷⁶, S. Tisserant⁸³, T. Todorov⁵, S. Todorova-Nova¹⁶¹, B. Toggerson¹⁶³, J. Tojo⁶⁹, S. Tokár^{144a}, K. Tokushuku⁶⁵, K. Tollefson⁸⁸, M. Tomoto¹⁰¹, L. Tompkins³¹, K. Toms¹⁰³, A. Tonoyan¹⁴, C. Topfel¹⁷, N.D. Topilin⁶⁴, I. Torchiani³⁰, E. Torrence¹¹⁴, H. Torres⁷⁸, E. Torr  Pastor¹⁶⁷, J. Toth^{83,ad}, F. Touchard⁸³, D.R. Tovey¹³⁹, S. Trboush¹⁵², T. Trefzger¹⁷⁴, L. Tremblet³⁰, A. Tricoli³⁰, I.M. Trigger^{159a}, S. Trincaz-Duvold⁷⁸, M.F. Tripiana⁷⁰, N. Triplett²⁵, W. Trischuk¹⁵⁸, B. Trocm ⁵⁵, C. Troncon^{89a}, M. Trottier-McDonald¹⁴², M. Trzebinski³⁹, A. Trzupek³⁹, C. Tsarouchas³⁰, J.C.-L. Tseng¹¹⁸, M. Tsiakiris¹⁰⁵, P.V. Tsiarehka⁹⁰, D. Tsiou^{5,ai}, G. Tsipolitis¹⁰, S. Tsiskaridze¹², V. Tsiskaridze⁴⁸, E.G. Tskhadadze^{51a}, I.I. Tsukerman⁹⁵, V. Tsulaia¹⁵, J.-W. Tsung²¹, S. Tsuno⁶⁵, D. Tsybychev¹⁴⁸, A. Tua¹³⁹, A. Tudorache^{26a}, V. Tudorache^{26a}, J.M. Tuggle³¹, M. Turala³⁹, D. Turecek¹²⁷, I. Turk Cakir^{4e}, E. Turlay¹⁰⁵, R. Turra^{89a,89b}, P.M. Tuts³⁵, A. Tykhonov⁷⁴, M. Tylmad^{146a,146b}, M. Tyndel¹²⁹, G. Tzanakos⁹, K. Uchida²¹, I. Ueda¹⁵⁵, R. Ueno²⁹, M. Ugland¹⁴, M. Uhlenbrock²¹, M. Uhrmacher⁵⁴, F. Ukegawa¹⁶⁰, G. Unal³⁰, A. Undrus²⁵, G. Unel¹⁶³, Y. Unno⁶⁵, D. Urbaniec³⁵, P. Urquijo²¹, G. Usai⁸, M. Uslenghi^{119a,119b}, L. Vacavant⁸³, V. Vacek¹²⁷, B. Vachon⁸⁵, S. Vahsen¹⁵, J. Valenta¹²⁵, S. Valentinetti^{20a,20b}, A. Valero¹⁶⁷, S. Valkar¹²⁶, E. Valladolid Gallego¹⁶⁷, S. Vallecorsa¹⁵², J.A. Valls Ferrer¹⁶⁷, R. Van Berg¹²⁰, P.C. Van Der Deijl¹⁰⁵, R. van der Geer¹⁰⁵, H. van der Graaf¹⁰⁵, R. Van Der Leeuw¹⁰⁵, E. van der Poel¹⁰⁵, D. van der Ster³⁰, N. van Eldik³⁰, P. van Gemmeren⁶, I. van Vulpen¹⁰⁵, M. Vanadia⁹⁹, W. Vandelli³⁰, A. Vaniachine⁶, P. Vankov⁴², F. Vannucci⁷⁸, R. Vari^{132a}, T. Varol⁸⁴, D. Varouchas¹⁵, A. Vartapetian⁸, K.E. Varvell¹⁵⁰, V.I. Vassilakopoulos⁵⁶, F. Vazeille³⁴, T. Vazquez Schroeder⁵⁴, G. Vegni^{89a,89b}, J.J. Veillet¹¹⁵, F. Veloso^{124a}, R. Veness³⁰, S. Veneziano^{132a}, A. Ventura^{72a,72b}, D. Ventura⁸⁴, M. Venturi⁴⁸, N. Venturi¹⁵⁸, V. Vercesi^{119a}, M. Verducci¹³⁸, W. Verkerke¹⁰⁵, J.C. Vermeulen¹⁰⁵, A. Vest⁴⁴, M.C. Vetterli^{142,d}, I. Vichou¹⁶⁵, T. Vickey^{145b,aj}, O.E. Vickey Boeriu^{145b}, G.H.A. Viehhauser¹¹⁸, S. Viel¹⁶⁸, M. Villa^{20a,20b}, M. Villaplana Perez¹⁶⁷, E. Vilucchi⁴⁷, M.G. Vincter²⁹, E. Vinek³⁰, V.B. Vinogradov⁶⁴, M. Virchaux^{136,*}, J. Virzi¹⁵, O. Vitells¹⁷², M. Viti⁴², I. Vivarelli⁴⁸, F. Vives Vaque³, S. Vlachos¹⁰, D. Vladoiu⁹⁸, M. Vlasak¹²⁷, A. Vogel²¹, P. Vokac¹²⁷, G. Volpi⁴⁷, M. Volpi⁸⁶, G. Volpini^{89a}, H. von der Schmitt⁹⁹, H. von Radziewski⁴⁸, E. von Toerne²¹, V. Vorobel¹²⁶, V. Vorwerk¹², M. Vos¹⁶⁷, R. Voss³⁰, T.T. Voss¹⁷⁵, J.H. Vosseveld⁷³, N. Vranjes¹³⁶, M. Vranjes Milosavljevic¹⁰⁵, V. Vrba¹²⁵, M. Vreeswijk¹⁰⁵, T. Vu Anh⁴⁸, R. Vuillermet³⁰, I. Vukotic³¹, W. Wagner¹⁷⁵, P. Wagner¹²⁰, H. Wahlen¹⁷⁵, S. Wahrenund⁴⁴, J. Wakabayashi¹⁰¹, S. Walch⁸⁷, J. Walder⁷¹, R. Walker⁹⁸, W. Walkowiak¹⁴¹, R. Wall¹⁷⁶, P. Waller⁷³, B. Walsh¹⁷⁶, C. Wang⁴⁵, H. Wang¹⁷³, H. Wang^{33b,ak}, J. Wang¹⁵¹, J. Wang⁵⁵, R. Wang¹⁰³, S.M. Wang¹⁵¹, T. Wang²¹, A. Warburton⁸⁵, C.P. Ward²⁸, M. Warsinsky⁴⁸, A. Washbrook⁴⁶, C. Wasicki⁴², I. Watanabe⁶⁶, P.M. Watkins¹⁸, A.T. Watson¹⁸, I.J. Watson¹⁵⁰, M.F. Watson¹⁸, G. Watts¹³⁸, S. Watts⁸², A.T. Waugh¹⁵⁰, B.M. Waugh⁷⁷, M.S. Weber¹⁷, P. Weber⁵⁴, A.R. Weidberg¹¹⁸, P. Weigell⁹⁹, J. Weingarten⁵⁴, C. Weiser⁴⁸, P.S. Wells³⁰, T. Wenaus²⁵, D. Wendland¹⁶, Z. Weng^{151,w}, T. Wengler³⁰, S. Wenig³⁰, N. Wermes²¹, M. Werner⁴⁸, P. Werner³⁰, M. Werth¹⁶³, M. Wessels^{58a}, J. Wetter¹⁶¹, C. Weydert⁵⁵, K. Whalen²⁹, S.J. Wheeler-Ellis¹⁶³, A. White⁸, M.J. White⁸⁶, S. White^{122a,122b}, S.R. Whitehead¹¹⁸, D. Whiteson¹⁶³, D. Whittington⁶⁰, F. Wicek¹¹⁵, D. Wicke¹⁷⁵, F.J. Wickens¹²⁹, W. Wiedenmann¹⁷³, M. Wielers¹²⁹, P. Wienemann²¹, C. Wiglesworth⁷⁵, L.A.M. Wiik-Fuchs⁴⁸, P.A. Wijeratne⁷⁷, A. Wildauer⁹⁹, M.A. Wildt^{42,s}, I. Wilhelm¹²⁶, H.G. Wilkens³⁰, J.Z. Will⁹⁸, E. Williams³⁵, H.H. Williams¹²⁰, W. Willis³⁵, S. Willocq⁸⁴, J.A. Wilson¹⁸, M.G. Wilson¹⁴³, A. Wilson⁸⁷, I. Wingerter-Seez⁵, S. Winkelmann⁴⁸, F. Winklmeier³⁰, M. Wittgen¹⁴³, S.J. Wollstadt⁸¹, M.W. Wolter³⁹, H. Wolters^{124a,h}, W.C. Wong⁴¹, G. Wooden⁸⁷, B.K. Wosiek³⁹, J. Wotschack³⁰, M.J. Woudstra⁸², K.W. Wozniak³⁹, K. Wraight⁵³, M. Wright⁵³, B. Wrona⁷³, S.L. Wu¹⁷³, X. Wu⁴⁹, Y. Wu^{33b,al}, E. Wulf³⁵, B.M. Wynne⁴⁶, S. Xella³⁶, M. Xiao¹³⁶, S. Xie⁴⁸, C. Xu^{33b,z}, D. Xu¹³⁹, B. Yabsley¹⁵⁰, S. Yacoub^{145a,am}, M. Yamada⁶⁵, H. Yamaguchi¹⁵⁵, A. Yamamoto⁶⁵, K. Yamamoto⁶³, S. Yamamoto¹⁵⁵, T. Yamamura¹⁵⁵, T. Yamanaka¹⁵⁵, J. Yamaoka⁴⁵, T. Yamazaki¹⁵⁵, Y. Yamazaki⁶⁶, Z. Yan²², H. Yang⁸⁷, U.K. Yang⁸², Y. Yang¹⁰⁹, Z. Yang^{146a,146b}, S. Yanush⁹¹, L. Yao^{33a}, Y. Yao¹⁵, Y. Yasu⁶⁵, G.V. Ybeles Smit¹³⁰, J. Ye⁴⁰,

S. Ye²⁵, M. Yilmaz^{4c}, R. Yoosofmiya¹²³, K. Yorita¹⁷¹, R. Yoshida⁶, C. Young¹⁴³, C.J. Young¹¹⁸, S. Youssef²², D. Yu²⁵, J. Yu⁸, J. Yu¹¹², L. Yuan⁶⁶, A. Yurkewicz¹⁰⁶, B. Zabinski³⁹, R. Zaidan⁶², A.M. Zaitsev¹²⁸, Z. Zajacova³⁰, L. Zanello^{132a,132b}, D. Zanzi⁹⁹, A. Zaytsev²⁵, C. Zeitnitz¹⁷⁵, M. Zeman¹²⁵, A. Zemla³⁹, C. Zender²¹, O. Zenin¹²⁸, T. Ženiš^{144a}, Z. Zinonos^{122a,122b}, S. Zenz¹⁵, D. Zerwas¹¹⁵, G. Zevi della Porta⁵⁷, Z. Zhan^{33d}, D. Zhang^{33b,ak}, H. Zhang⁸⁸, J. Zhang⁶, X. Zhang^{33d}, Z. Zhang¹¹⁵, L. Zhao¹⁰⁸, T. Zhao¹³⁸, Z. Zhao^{33b}, A. Zhemchugov⁶⁴, J. Zhong¹¹⁸, B. Zhou⁸⁷, N. Zhou¹⁶³, Y. Zhou¹⁵¹, C.G. Zhu^{33d}, H. Zhu⁴², J. Zhu⁸⁷, Y. Zhu^{33b}, X. Zhuang⁹⁸, V. Zhuravlov⁹⁹, D. Zieminska⁶⁰, N.I. Zimin⁶⁴, R. Zimmermann²¹, S. Zimmermann²¹, S. Zimmermann⁴⁸, M. Ziolkowski¹⁴¹, R. Zitoun⁵, L. Živković³⁵, V.V. Zmouchko^{128,*}, G. Zobernig¹⁷³, A. Zoccoli^{20a,20b}, M. zur Nedden¹⁶, V. Zutshi¹⁰⁶, L. Zwalinski³⁰

¹ School of Chemistry and Physics, University of Adelaide, Adelaide, Australia

² Physics Department, SUNY Albany, Albany, NY, United States

³ Department of Physics, University of Alberta, Edmonton, AB, Canada

⁴ (a) Department of Physics, Ankara University, Ankara; (b) Department of Physics, Dumlupinar University, Kutahya; (c) Department of Physics, Gazi University, Ankara; (d) Division of Physics, TOBB University of Economics and Technology, Ankara; (e) Turkish Atomic Energy Authority, Ankara, Turkey

⁵ LAPP, CNRS/IN2P3 and Université de Savoie, Annecy-le-Vieux, France

⁶ High Energy Physics Division, Argonne National Laboratory, Argonne, IL, United States

⁷ Department of Physics, University of Arizona, Tucson, AZ, United States

⁸ Department of Physics, The University of Texas at Arlington, Arlington, TX, United States

⁹ Physics Department, University of Athens, Athens, Greece

¹⁰ Physics Department, National Technical University of Athens, Zografou, Greece

¹¹ Institute of Physics, Azerbaijan Academy of Sciences, Baku, Azerbaijan

¹² Institut de Física d'Altes Energies and Departament de Física de la Universitat Autònoma de Barcelona and ICREA, Barcelona, Spain

¹³ (a) Institute of Physics, University of Belgrade, Belgrade; (b) Vinca Institute of Nuclear Sciences, University of Belgrade, Belgrade, Serbia

¹⁴ Department for Physics and Technology, University of Bergen, Bergen, Norway

¹⁵ Physics Division, Lawrence Berkeley National Laboratory and University of California, Berkeley, CA, United States

¹⁶ Department of Physics, Humboldt University, Berlin, Germany

¹⁷ Albert Einstein Center for Fundamental Physics and Laboratory for High Energy Physics, University of Bern, Bern, Switzerland

¹⁸ School of Physics and Astronomy, University of Birmingham, Birmingham, United Kingdom

¹⁹ (a) Department of Physics, Bogazici University, Istanbul; (b) Division of Physics, Dogus University, Istanbul; (c) Department of Physics Engineering, Gaziantep University, Gaziantep;

(d) Department of Physics, Istanbul Technical University, Istanbul, Turkey

²⁰ (a) INFN Sezione di Bologna; (b) Dipartimento di Fisica, Università di Bologna, Bologna, Italy

²¹ Physikalisches Institut, University of Bonn, Bonn, Germany

²² Department of Physics, Boston University, Boston, MA, United States

²³ Department of Physics, Brandeis University, Waltham, MA, United States

²⁴ (a) Universidade Federal do Rio De Janeiro COPPE/EE/IF, Rio de Janeiro; (b) Federal University of Juiz de Fora (UFJF), Juiz de Fora; (c) Federal University of Sao Joao del Rei (UFSJ), Sao Joao del Rei; (d) Instituto de Física, Universidade de Sao Paulo, Sao Paulo, Brazil

²⁵ Physics Department, Brookhaven National Laboratory, Upton, NY, United States

²⁶ (a) National Institute of Physics and Nuclear Engineering, Bucharest; (b) University Politehnica Bucharest, Bucharest; (c) West University in Timisoara, Timisoara, Romania

²⁷ Departamento de Física, Universidad de Buenos Aires, Buenos Aires, Argentina

²⁸ Cavendish Laboratory, University of Cambridge, Cambridge, United Kingdom

²⁹ Department of Physics, Carleton University, Ottawa, ON, Canada

³⁰ CERN, Geneva, Switzerland

³¹ Enrico Fermi Institute, University of Chicago, Chicago, IL, United States

³² (a) Departamento de Física, Pontificia Universidad Católica de Chile, Santiago; (b) Departamento de Física, Universidad Técnica Federico Santa María, Valparaíso, Chile

³³ (a) Institute of High Energy Physics, Chinese Academy of Sciences, Beijing; (b) Department of Modern Physics, University of Science and Technology of China, Anhui; (c) Department of Physics, Nanjing University, Jiangsu; (d) School of Physics, Shandong University, Shandong, China

³⁴ Laboratoire de Physique Corpusculaire, Clermont Université and Université Blaise Pascal and CNRS/IN2P3, Clermont-Ferrand, France

³⁵ Nevis Laboratory, Columbia University, Irvington, NY, United States

³⁶ Niels Bohr Institute, University of Copenhagen, Copenhagen, Denmark

³⁷ (a) INFN Gruppo Collegato di Cosenza; (b) Dipartimento di Fisica, Università della Calabria, Arcavacata di Rende, Italy

³⁸ AGH University of Science and Technology, Faculty of Physics and Applied Computer Science, Krakow, Poland

³⁹ The Henryk Niewodniczanski Institute of Nuclear Physics, Polish Academy of Sciences, Krakow, Poland

⁴⁰ Physics Department, Southern Methodist University, Dallas, TX, United States

⁴¹ Physics Department, University of Texas at Dallas, Richardson, TX, United States

⁴² DESY, Hamburg and Zeuthen, Germany

⁴³ Institut für Experimentelle Physik IV, Technische Universität Dortmund, Dortmund, Germany

⁴⁴ Institut für Kern- und Teilchenphysik, Technical University Dresden, Dresden, Germany

⁴⁵ Department of Physics, Duke University, Durham, NC, United States

⁴⁶ SUPA – School of Physics and Astronomy, University of Edinburgh, Edinburgh, United Kingdom

⁴⁷ INFN Laboratori Nazionali di Frascati, Frascati, Italy

⁴⁸ Fakultät für Mathematik und Physik, Albert-Ludwigs-Universität, Freiburg, Germany

⁴⁹ Section de Physique, Université de Genève, Geneva, Switzerland

⁵⁰ (a) INFN Sezione di Genova; (b) Dipartimento di Fisica, Università di Genova, Genova, Italy

⁵¹ (a) E. Andronikashvili Institute of Physics, Iv. Javakhishvili Tbilisi State University, Tbilisi; (b) High Energy Physics Institute, Tbilisi State University, Tbilisi, Georgia

⁵² II Physikalisches Institut, Justus-Liebig-Universität Giessen, Giessen, Germany

⁵³ SUPA – School of Physics and Astronomy, University of Glasgow, Glasgow, United Kingdom

⁵⁴ II Physikalisches Institut, Georg-August-Universität, Göttingen, Germany

⁵⁵ Laboratoire de Physique Subatomique et de Cosmologie, Université Joseph Fourier and CNRS/IN2P3 and Institut National Polytechnique de Grenoble, Grenoble, France

⁵⁶ Department of Physics, Hampton University, Hampton, VA, United States

⁵⁷ Laboratory for Particle Physics and Cosmology, Harvard University, Cambridge, MA, United States

⁵⁸ (a) Kirchhoff-Institut für Physik, Ruprecht-Karls-Universität Heidelberg, Heidelberg; (b) Physikalisches Institut, Ruprecht-Karls-Universität Heidelberg, Heidelberg; (c) ZITI Institut für technische Informatik, Ruprecht-Karls-Universität Heidelberg, Mannheim, Germany

⁵⁹ Faculty of Applied Information Science, Hiroshima Institute of Technology, Hiroshima, Japan

⁶⁰ Department of Physics, Indiana University, Bloomington, IN, United States

- ⁶¹ Institut für Astro- und Teilchenphysik, Leopold-Franzens-Universität, Innsbruck, Austria
⁶² University of Iowa, Iowa City, IA, United States
⁶³ Department of Physics and Astronomy, Iowa State University, Ames, IA, United States
⁶⁴ Joint Institute for Nuclear Research, JINR Dubna, Dubna, Russia
⁶⁵ KEK, High Energy Accelerator Research Organization, Tsukuba, Japan
⁶⁶ Graduate School of Science, Kobe University, Kobe, Japan
⁶⁷ Faculty of Science, Kyoto University, Kyoto, Japan
⁶⁸ Kyoto University of Education, Kyoto, Japan
⁶⁹ Department of Physics, Kyushu University, Fukuoka, Japan
⁷⁰ Instituto de Física La Plata, Universidad Nacional de La Plata and CONICET, La Plata, Argentina
⁷¹ Physics Department, Lancaster University, Lancaster, United Kingdom
⁷² ^(a) INFN Sezione di Lecce; ^(b) Dipartimento di Matematica e Fisica, Università del Salento, Lecce, Italy
⁷³ Oliver Lodge Laboratory, University of Liverpool, Liverpool, United Kingdom
⁷⁴ Department of Physics, Jožef Stefan Institute and University of Ljubljana, Ljubljana, Slovenia
⁷⁵ School of Physics and Astronomy, Queen Mary University of London, London, United Kingdom
⁷⁶ Department of Physics, Royal Holloway University of London, Surrey, United Kingdom
⁷⁷ Department of Physics and Astronomy, University College London, London, United Kingdom
⁷⁸ Laboratoire de Physique Nucléaire et de Hautes Energies, UPMC and Université Paris-Diderot and CNRS/IN2P3, Paris, France
⁷⁹ Fysiska institutionen, Lunds universitet, Lund, Sweden
⁸⁰ Departamento de Física Teórica C-15, Universidad Autónoma de Madrid, Madrid, Spain
⁸¹ Institut für Physik, Universität Mainz, Mainz, Germany
⁸² School of Physics and Astronomy, University of Manchester, Manchester, United Kingdom
⁸³ CPPM, Aix-Marseille Université and CNRS/IN2P3, Marseille, France
⁸⁴ Department of Physics, University of Massachusetts, Amherst, MA, United States
⁸⁵ Department of Physics, McGill University, Montreal, QC, Canada
⁸⁶ School of Physics, University of Melbourne, Victoria, Australia
⁸⁷ Department of Physics, The University of Michigan, Ann Arbor, MI, United States
⁸⁸ Department of Physics and Astronomy, Michigan State University, East Lansing, MI, United States
⁸⁹ ^(a) INFN Sezione di Milano; ^(b) Dipartimento di Fisica, Università di Milano, Milano, Italy
⁹⁰ B.I. Stepanov Institute of Physics, National Academy of Sciences of Belarus, Minsk, Belarus
⁹¹ National Scientific and Educational Centre for Particle and High Energy Physics, Minsk, Belarus
⁹² Department of Physics, Massachusetts Institute of Technology, Cambridge, MA, United States
⁹³ Group of Particle Physics, University of Montreal, Montreal, QC, Canada
⁹⁴ P.N. Lebedev Institute of Physics, Academy of Sciences, Moscow, Russia
⁹⁵ Institute for Theoretical and Experimental Physics (ITEP), Moscow, Russia
⁹⁶ Moscow Engineering and Physics Institute (MEPhI), Moscow, Russia
⁹⁷ Skobeltsyn Institute of Nuclear Physics, Lomonosov Moscow State University, Moscow, Russia
⁹⁸ Fakultät für Physik, Ludwig-Maximilians-Universität München, München, Germany
⁹⁹ Max-Planck-Institut für Physik (Werner-Heisenberg-Institut), München, Germany
¹⁰⁰ Nagasaki Institute of Applied Science, Nagasaki, Japan
¹⁰¹ Graduate School of Science and Kobayashi–Maskawa Institute, Nagoya University, Nagoya, Japan
¹⁰² ^(a) INFN Sezione di Napoli; ^(b) Dipartimento di Scienze Fisiche, Università di Napoli, Napoli, Italy
¹⁰³ Department of Physics and Astronomy, University of New Mexico, Albuquerque, NM, United States
¹⁰⁴ Institute for Mathematics, Astrophysics and Particle Physics, Radboud University Nijmegen/Nikhef, Nijmegen, Netherlands
¹⁰⁵ Nikhef National Institute for Subatomic Physics and University of Amsterdam, Amsterdam, Netherlands
¹⁰⁶ Department of Physics, Northern Illinois University, DeKalb, IL, United States
¹⁰⁷ Budker Institute of Nuclear Physics, SB RAS, Novosibirsk, Russia
¹⁰⁸ Department of Physics, New York University, New York, NY, United States
¹⁰⁹ Ohio State University, Columbus, OH, United States
¹¹⁰ Faculty of Science, Okayama University, Okayama, Japan
¹¹¹ Homer L. Dodge Department of Physics and Astronomy, University of Oklahoma, Norman, OK, United States
¹¹² Department of Physics, Oklahoma State University, Stillwater, OK, United States
¹¹³ Palacký University, RCPTM, Olomouc, Czech Republic
¹¹⁴ Center for High Energy Physics, University of Oregon, Eugene, OR, United States
¹¹⁵ LAL, Université Paris-Sud and CNRS/IN2P3, Orsay, France
¹¹⁶ Graduate School of Science, Osaka University, Osaka, Japan
¹¹⁷ Department of Physics, University of Oslo, Oslo, Norway
¹¹⁸ Department of Physics, Oxford University, Oxford, United Kingdom
¹¹⁹ ^(a) INFN Sezione di Pavia; ^(b) Dipartimento di Fisica, Università di Pavia, Pavia, Italy
¹²⁰ Department of Physics, University of Pennsylvania, Philadelphia, PA, United States
¹²¹ Petersburg Nuclear Physics Institute, Gatchina, Russia
¹²² ^(a) INFN Sezione di Pisa; ^(b) Dipartimento di Fisica E. Fermi, Università di Pisa, Pisa, Italy
¹²³ Department of Physics and Astronomy, University of Pittsburgh, Pittsburgh, PA, United States
¹²⁴ ^(a) Laboratório de Instrumentação e Física Experimental de Partículas – LIP, Lisboa, Portugal; ^(b) Departamento de Física Teórica y del Cosmos and CAFPE, Universidad de Granada, Granada, Spain
¹²⁵ Institute of Physics, Academy of Sciences of the Czech Republic, Praha, Czech Republic
¹²⁶ Faculty of Mathematics and Physics, Charles University in Prague, Praha, Czech Republic
¹²⁷ Czech Technical University in Prague, Praha, Czech Republic
¹²⁸ State Research Center Institute for High Energy Physics, Protvino, Russia
¹²⁹ Particle Physics Department, Rutherford Appleton Laboratory, Didcot, United Kingdom
¹³⁰ Physics Department, University of Regina, Regina, SK, Canada
¹³¹ Ritsumeikan University, Kusatsu, Shiga, Japan
¹³² ^(a) INFN Sezione di Roma I; ^(b) Dipartimento di Fisica, Università La Sapienza, Roma, Italy
¹³³ ^(a) INFN Sezione di Roma Tor Vergata; ^(b) Dipartimento di Fisica, Università di Roma Tor Vergata, Roma, Italy
¹³⁴ ^(a) INFN Sezione di Roma Tre; ^(b) Dipartimento di Fisica, Università Roma Tre, Roma, Italy
¹³⁵ ^(a) Faculté des Sciences Ain Chock, Réseau Universitaire de Physique des Hautes Energies – Université Hassan II, Casablanca; ^(b) Centre National de l’Energie des Sciences Techniques Nucleaires, Rabat; ^(c) Faculté des Sciences Semlalia, Université Cadi Ayyad, LPHEA, Marrakech; ^(d) Faculté des Sciences, Université Mohamed Premier and LPTPM, Oujda; ^(e) Faculté des sciences, Université Mohammed V-Agdal, Rabat, Morocco
¹³⁶ DSM/IRFU (Institut de Recherches sur les Lois Fondamentales de l’Univers), CEA Saclay (Commissariat à l’Energie Atomique), Gif-sur-Yvette, France

- ¹³⁷ Santa Cruz Institute for Particle Physics, University of California Santa Cruz, Santa Cruz, CA, United States
¹³⁸ Department of Physics, University of Washington, Seattle, WA, United States
¹³⁹ Department of Physics and Astronomy, University of Sheffield, Sheffield, United Kingdom
¹⁴⁰ Department of Physics, Shinshu University, Nagano, Japan
¹⁴¹ Fachbereich Physik, Universität Siegen, Siegen, Germany
¹⁴² Department of Physics, Simon Fraser University, Burnaby, BC, Canada
¹⁴³ SLAC National Accelerator Laboratory, Stanford, CA, United States
¹⁴⁴ ^(a) Faculty of Mathematics, Physics & Informatics, Comenius University, Bratislava; ^(b) Department of Subnuclear Physics, Institute of Experimental Physics of the Slovak Academy of Sciences, Kosice, Slovak Republic
¹⁴⁵ ^(a) Department of Physics, University of Johannesburg, Johannesburg; ^(b) School of Physics, University of the Witwatersrand, Johannesburg, South Africa
¹⁴⁶ ^(a) Department of Physics, Stockholm University; ^(b) The Oskar Klein Centre, Stockholm, Sweden
¹⁴⁷ Physics Department, Royal Institute of Technology, Stockholm, Sweden
¹⁴⁸ Departments of Physics & Astronomy and Chemistry, Stony Brook University, Stony Brook, NY, United States
¹⁴⁹ Department of Physics and Astronomy, University of Sussex, Brighton, United Kingdom
¹⁵⁰ School of Physics, University of Sydney, Sydney, Australia
¹⁵¹ Institute of Physics, Academia Sinica, Taipei, Taiwan
¹⁵² Department of Physics, Technion: Israel Institute of Technology, Haifa, Israel
¹⁵³ Raymond and Beverly Sackler School of Physics and Astronomy, Tel Aviv University, Tel Aviv, Israel
¹⁵⁴ Department of Physics, Aristotle University of Thessaloniki, Thessaloniki, Greece
¹⁵⁵ International Center for Elementary Particle Physics and Department of Physics, The University of Tokyo, Tokyo, Japan
¹⁵⁶ Graduate School of Science and Technology, Tokyo Metropolitan University, Tokyo, Japan
¹⁵⁷ Department of Physics, Tokyo Institute of Technology, Tokyo, Japan
¹⁵⁸ Department of Physics, University of Toronto, Toronto, ON, Canada
¹⁵⁹ ^(a) TRIUMF, Vancouver, BC; ^(b) Department of Physics and Astronomy, York University, Toronto, ON, Canada
¹⁶⁰ Faculty of Pure and Applied Sciences, University of Tsukuba, Tsukuba, Japan
¹⁶¹ Department of Physics and Astronomy, Tufts University, Medford, MA, United States
¹⁶² Centro de Investigaciones, Universidad Antonio Narino, Bogota, Colombia
¹⁶³ Department of Physics and Astronomy, University of California Irvine, Irvine, CA, United States
¹⁶⁴ ^(a) INFN Gruppo Collegato di Udine; ^(b) ICTP, Trieste; ^(c) Dipartimento di Chimica, Fisica e Ambiente, Università di Udine, Udine, Italy
¹⁶⁵ Department of Physics, University of Illinois, Urbana, IL, United States
¹⁶⁶ Department of Physics and Astronomy, University of Uppsala, Uppsala, Sweden
¹⁶⁷ Instituto de Física Corpuscular (IFIC) and Departamento de Física Atómica, Molecular y Nuclear and Departamento de Ingeniería Electrónica and Instituto de Microelectrónica de Barcelona (IMB-CNM), University of Valencia and CSIC, Valencia, Spain
¹⁶⁸ Department of Physics, University of British Columbia, Vancouver, BC, Canada
¹⁶⁹ Department of Physics and Astronomy, University of Victoria, Victoria, BC, Canada
¹⁷⁰ Department of Physics, University of Warwick, Coventry, United Kingdom
¹⁷¹ Waseda University, Tokyo, Japan
¹⁷² Department of Particle Physics, The Weizmann Institute of Science, Rehovot, Israel
¹⁷³ Department of Physics, University of Wisconsin, Madison, WI, United States
¹⁷⁴ Fakultät für Physik und Astronomie, Julius-Maximilians-Universität, Würzburg, Germany
¹⁷⁵ Fachbereich C Physik, Bergische Universität Wuppertal, Wuppertal, Germany
¹⁷⁶ Department of Physics, Yale University, New Haven, CT, United States
¹⁷⁷ Yerevan Physics Institute, Yerevan, Armenia
¹⁷⁸ Centre de Calcul de l'Institut National de Physique Nucléaire et de Physique des Particules (IN2P3), Villeurbanne, France

^a Also at Laboratório de Instrumentação e Física Experimental de Partículas – LIP, Lisboa, Portugal.

^b Also at Faculdade de Ciências and CFNUL, Universidade de Lisboa, Lisboa, Portugal.

^c Also at Particle Physics Department, Rutherford Appleton Laboratory, Didcot, United Kingdom.

^d Also at TRIUMF, Vancouver, BC, Canada.

^e Also at Department of Physics, California State University, Fresno, CA, United States.

^f Also at Novosibirsk State University, Novosibirsk, Russia.

^g Also at Fermilab, Batavia, IL, United States.

^h Also at Department of Physics, University of Coimbra, Coimbra, Portugal.

ⁱ Also at Department of Physics, UASLP, San Luis Potosi, Mexico.

^j Also at Università di Napoli Parthenope, Napoli, Italy.

^k Also at Institute of Particle Physics (IPP), Canada.

^l Also at Department of Physics, Middle East Technical University, Ankara, Turkey.

^m Also at Louisiana Tech University, Ruston, LA, United States.

ⁿ Also at Departamento de Física and CEFITEC of Faculdade de Ciências e Tecnologia, Universidade Nova de Lisboa, Caparica, Portugal.

^o Also at Department of Physics and Astronomy, University College London, London, United Kingdom.

^p Also at Group of Particle Physics, University of Montreal, Montreal, QC, Canada.

^q Also at Department of Physics, University of Cape Town, Cape Town, South Africa.

^r Also at Institute of Physics, Azerbaijan Academy of Sciences, Baku, Azerbaijan.

^s Also at Institut für Experimentalphysik, Universität Hamburg, Hamburg, Germany.

^t Also at Manhattan College, New York, NY, United States.

^u Also at School of Physics, Shandong University, Shandong, China.

^v Also at CPPM, Aix-Marseille Université and CNRS/IN2P3, Marseille, France.

^w Also at School of Physics and Engineering, Sun Yat-sen University, Guanzhou, China.

^x Also at Academia Sinica Grid Computing, Institute of Physics, Academia Sinica, Taipei, Taiwan.

^y Also at Dipartimento di Fisica, Università La Sapienza, Roma, Italy.

^z Also at DSM/IRFU (Institut de Recherches sur les Lois Fondamentales de l'Univers), CEA Saclay (Commissariat à l'Energie Atomique), Gif-sur-Yvette, France.

^{aa} Also at Section de Physique, Université de Genève, Geneva, Switzerland.

^{ab} Also at Departamento de Física, Universidade de Minho, Braga, Portugal.

^{ac} Also at Department of Physics and Astronomy, University of South Carolina, Columbia, SC, United States.

^{ad} Also at Institute for Particle and Nuclear Physics, Wigner Research Centre for Physics, Budapest, Hungary.

^{ae} Also at California Institute of Technology, Pasadena, CA, United States.

^{af} Also at Institute of Physics, Jagiellonian University, Krakow, Poland.

^{ag} Also at LAL, Université Paris-Sud and CNRS/IN2P3, Orsay, France.

^{ah} Also at Nevis Laboratory, Columbia University, Irvington, NY, United States.

^{ai} Also at Department of Physics and Astronomy, University of Sheffield, Sheffield, United Kingdom.

^{aj} Also at Department of Physics, Oxford University, Oxford, United Kingdom.

^{ak} Also at Institute of Physics, Academia Sinica, Taipei, Taiwan.

^{al} Also at Department of Physics, The University of Michigan, Ann Arbor, MI, United States.

^{am} Also at Discipline of Physics, University of KwaZulu-Natal, Durban, South Africa.

* Deceased.